

The Case for Astrons

^{1,2}Claudio Corianò, ¹Paul H. Frampton and ¹Leonardo Torcellini

¹*Dipartimento di Matematica e Fisica "Ennio De Giorgi",
Università del Salento and INFN-Lecce,
Via Arnesano, 73100 Lecce, Italy.*
²*CNR nanotec, Lecce*

Abstract

We examine a proposed population of primordial, electrically charged compact objects, which we call astrons, with fiducial parameters $M_A \sim 10^{12} M_\odot$, $Q_A \sim 4 \times 10^{32} \text{ C}$, and megaparsec-scale separations. We analyze charge generation, ordinary accretion saturation, charge persistence in an ionized medium, plasma screening, the Reissner–Nordström and Kerr–Newman geometric regimes, lensing, and the possible use of Lyman- α absorption as a probe of astron electric fields, and the cosmological interpretation of a sparse charged population. The large-charge branch is not obtained from ordinary accretion saturation; it should be treated as a primordial or early-universe charge-concentration hypothesis. A horizon-mass estimate places a $10^{12} M_\odot$ primordial object at times of order months after the Big Bang, so any relation to the early structures observed by the James Webb Space Telescope would be indirect, through later baryonic assembly around dark seeds. The main constraints are severe: plasma screening and neutralization must be avoided, the fiducial charge drives the exterior into a super-extremal regime without a Reissner–Nordström photon sphere, and the homogeneous interaction energy of a charged population scales as a^{-4} . Thus the simplest FLRW perfect-fluid reduction does not generate asymptotic late-time acceleration. Any viable cosmological role for astrons must instead come from a controlled inhomogeneous Einstein–Maxwell averaging problem beyond the homogeneous approximation.

Contents

1	Introduction	3
1.1	Picturing an astron	3
1.2	Primordial timing and early structure	4
2	Charge Generation in a Minimal Capture Model	6
3	Nonlinear Growth, Saturation and a Scaling Extrapolation	9
3.1	The Q/M extrapolation	13
4	Stability of the Charge	14
5	Screening Constraints in the Intergalactic Medium	17
6	Astrons and Naked Singularities	21
6.1	Reissner–Nordström Exteriors with Regular or Singular Interiors	22
6.2	Summary: Astrons with and without Horizons	24
6.3	Charged TOV Equations for Regular Astrons	25
7	Extension to Rotating Astrons: Kerr–Newman Geometry and Dynamics	30
8	Lensing Around an Astron Singularity	34
8.1	Schwarzschild versus extremal Reissner–Nordström lensing	35
9	Lyman-α Absorption as a Probe of Astron Electric Fields	38
10	Cosmological Implications of the Homogeneous Approximation	40
11	Backreaction Beyond the Homogeneous Approximation	44
12	Conclusions	50
A	Possible Values of the Charging Timescale	51
A.1	Astrophysical Density Benchmarks	51
A.2	Free-Fall Time for a Uniform Sphere	55
B	Origin of the Extrapolated Charge Estimate	56
C	Debye Screening	58
C.1	Debye Screening Beyond a Maxwellian Plasma	60
D	A Nonlinear and Kinetic Framework for Screening	61
E	Comparison Naked-Singularity Metrics	63
E.1	Janis–Newman–Winicour Geometry	63
E.2	Zipoy–Voorhees Geometry	63
E.3	Tomimatsu–Sato Geometry	64
F	Matching a Charged Interior to a Reissner–Nordström Exterior	64
G	Derivation of the Relativistic and Charged TOV Equations	68
H	Hamilton–Jacobi Separation in the Kerr–Newman Geometry	71

1 Introduction

The origin of the accelerated expansion of the Universe remains one of the central open problems in modern cosmology. Within the standard Λ CDM framework, the observed late-time acceleration is encoded in a cosmological constant, yet the microscopic origin of that term remains obscure. This motivates the study of alternative scenarios in which long-range interactions or collective dynamics modify cosmic expansion without introducing a fundamental vacuum component.

In this paper we revisit a framework in which the relevant degrees of freedom are primordial, electrically charged compact objects carrying charges of common sign. The present construction is closely related to earlier ideas on cosmological scenarios driven by extremely massive charged compact objects, including the electromagnetic accelerating-universe proposal and the later unified dark-matter/dark-energy model [1, 2].

Following earlier work on Primordial Extremely Massive Naked Singularities (PEMNS), we refer to these objects simply as *astrons*. The fiducial parameters usually associated with this scenario are masses $M_A \sim 10^{12} M_\odot$, charges $|Q_A| \sim 10^{32}$ C, and typical separations of order megaparsecs. If such objects exist and retain their charge over cosmological times, their mutual Coulomb interaction could in principle influence large-scale dynamics.

The conventional astrophysical expectation is that macroscopic black holes are effectively described by their mass and spin, with any residual electric charge often assumed to be negligible in realistic environments [3]. At the same time, several recent analyses have emphasized that small but non-zero charges can be generated by astrophysical processes and need not be irrelevant: even charges far below extremality can influence the motion of charged particles, shift orbital structures, and modify electromagnetic observables near compact objects [4, 5]. More generally, long-range interactions are known to have potentially large astrophysical consequences and are tightly constrained in other sectors, including dark-matter interactions with the Standard Model [12].

The present work is deliberately narrower than a full replacement of Λ CDM. Our aim is instead to determine whether the astron picture is internally consistent enough to warrant further study. Three questions are central. First, can a collapsing object acquire macroscopic charge quickly enough for charging to matter during formation? Second, once produced, can such a charge persist against accretion, plasma neutralization, and quantum discharge? Third, under what plasma conditions does Debye screening invalidate or constrain the long-range force picture?

These questions matter because each one can obstruct the entire scenario. Screening in the intergalactic medium could suppress long-range Coulomb forces, while accretion or pair production could eliminate any large charge soon after formation. Large charge-to-mass ratios also raise geometric issues, since super-extremal Reissner–Nordström configurations do not possess an event horizon. Before confronting observations, one must therefore determine which elements of the framework survive a minimal consistency analysis.

1.1 Picturing an astron

The scale GM_A/c^2 should not be interpreted as a stellar photospheric radius. It is a relativistic compactness scale. This distinction is important: for a neutral Schwarzschild object, a material surface at or below $2GM_A/c^2$ would lie at the black-hole threshold. For a charged astron the corresponding statement is more subtle, because the exterior horizon condition is the Reissner–Nordström condition controlled by Ξ , defined in Eq. (103). Thus the gravitational radius is used here mainly as a reference length for compactness and for order-of-magnitude estimates, not as a claim that the object has a luminous surface at that radius. In that sense, an astron is not expected to resemble an ordinary star, whose visible emission is produced by thermal radiation from a material outer layer. If the astron is instead modeled as an ultra-compact charged object or naked singularity, it need not possess any such radiating surface at all. Consequently, a large relativistic scale does not by itself imply that the astron would appear as a bright optical source. Significant electromagnetic emission would arise only if the object were surrounded by accreting gas or by a sufficiently dense plasma capable of producing radiation. In the absence of such an environment, the as-

tron could remain electromagnetically dim and would be more naturally probed through its gravitational influence, lensing properties, or interactions with ambient matter rather than through direct stellar-like light. For $M_A \sim 10^{12} M_\odot$, the reference angular scale associated with the compactness length is of order $R_{\text{ref}} \sim GM_A/c^2 \sim 0.05 \text{ pc}$, or $R_{\text{ref}} \sim 0.1 \text{ pc}$ if one uses $2GM_A/c^2$. The corresponding angular scale is

$$\theta_A \simeq 206265 \frac{R_{\text{ref}}(\text{pc})}{D(\text{pc})} \text{ arcsec} \simeq 0.01'' \left(\frac{R_{\text{ref}}}{0.05 \text{ pc}} \right) \left(\frac{D}{1 \text{ Mpc}} \right)^{-1}. \quad (1)$$

Thus even at a distance of 1 Mpc this reference angular scale is only of order 10^{-2} arcsec, while at 5 Mpc it falls to a few milliarcseconds. An astron would therefore not generically appear as an obvious resolved luminous disk in the sky.

It is also useful to compare this fiducial compactness scale with more familiar astrophysical systems. For $M_A \sim 10^{12} M_\odot$, the gravitational radius is

$$r_g = \frac{GM_A}{c^2} \simeq 1.5 \times 10^{15} \text{ m} \simeq 10^4 \text{ AU} \simeq 0.05 \text{ pc}, \quad (2)$$

while the corresponding Schwarzschild radius is

$$r_s = 2r_g \simeq 2 \times 10^4 \text{ AU} \simeq 0.1 \text{ pc}. \quad (3)$$

This is vastly larger than the planetary Solar System: Pluto orbits at a mean distance of about 40 AU, and the heliopause lies only at roughly 10^2 AU. At the same time, an astron remains small on galactic length scales. A sub-parsec compactness length is tiny compared with a galactic disk, whose size is typically measured in kiloparsecs. Relative to known supermassive black holes, however, the fiducial astron scale is exceptionally large. The Schwarzschild radius of Sgr A*, with $M \simeq 4 \times 10^6 M_\odot$, is only about 0.08 AU, while that of M87*, with $M \simeq 6.5 \times 10^9 M_\odot$, is about 10^2 AU. Thus an astron with $M_A \sim 10^{12} M_\odot$ would have a relativistic length scale hundreds to thousands of times larger than that of ordinary supermassive black holes, while still occupying only a sub-parsec region inside a galaxy. This comparison again refers to the compactness scale, not necessarily to a material surface. If a neutral object had $R \lesssim r_s$, it would be a black hole; in the charged case the question is instead whether the exterior lies below, at, or above the RN extremality bound. The physical radius or interior completion of a horizonless or singular astron is therefore model dependent.

1.2 Primordial timing and early structure

The fiducial large charge should not be interpreted as the natural endpoint of ordinary late-time accretion. In the minimal accretion picture discussed below, electrostatic feedback quickly limits the charge to a much smaller saturation value. Thus, if the large branch $M_A \sim 10^{12} M_\odot$, $Q_A \sim 4 \times 10^{32} \text{ C}$ exists, it should be regarded as a primordial or very early-universe charge-concentration hypothesis. The relevant question is not simply whether an already formed galaxy can accrete enough charge, but whether a rare primordial object can be born with a small charge imbalance that later survives plasma neutralization.

A useful way to locate such an object in cosmic history is to compare its mass with the horizon mass in the radiation era. For a radiation-dominated universe, up to factors of order unity,

$$H \simeq \frac{1}{2t}, \quad \rho \simeq \frac{3H^2}{8\pi G} \simeq \frac{3}{32\pi G t^2}. \quad (4)$$

Taking the causal length to be $R_H \sim 2ct$, the mass inside the horizon is

$$M_H(t) \sim \frac{4\pi}{3} \rho R_H^3 \sim \frac{c^3 t}{G}. \quad (5)$$

This is the standard order-of-magnitude estimate used in discussions of primordial black-hole formation [40]. Numerically,

$$M_H(t) \simeq 2 \times 10^5 M_\odot \left(\frac{t}{1 \text{ s}} \right), \quad (6)$$

or equivalently

$$t_A \sim \frac{GM_A}{c^3} \simeq 5 \times 10^6 \text{ s} \left(\frac{M_A}{10^{12} M_\odot} \right). \quad (7)$$

Thus the fiducial astron mass corresponds, at this crude horizon-mass level, to a time of order weeks to months after the Big Bang. This is long after the earliest Planck-era physics, but still far before recombination and far before ordinary luminous galaxies form. In this interpretation, an astron would not be an object whose birth is directly seen by galaxy surveys. It would be a dark primordial seed, already present when the later baryonic structure begins to assemble.

This point is useful in discussing the possible connection with the early structures now observed by the James Webb Space Telescope. JWST has revealed a rich population of luminous systems in the first billion years, including spectroscopically confirmed galaxies at $z \simeq 14$, roughly a few hundred million years after the Big Bang, and massive systems at $z \simeq 5 - 9$ [42–44]. These observations motivate renewed interest in early seed formation, rapid baryonic assembly and efficient black-hole growth. They do not, by themselves, imply the existence of astrons. The possible connection is more indirect: a primordial astron, if present, could act as a rare dark gravitational seed around which gas, stars or black holes later assemble.

The visible object associated with such a seed would therefore not be the singularity or compact electrovac core itself. It would be the response of the surrounding medium: infalling gas, an ionized or partially neutral plasma environment, possible screening clouds, and eventually ordinary baryonic structure. The compactness scale of the fiducial object is only $\sim 0.05\text{--}0.1$ pc, while any gaseous or plasma structure around it could be larger and more diffuse, depending on the thermal history and local environment. The observational signature would then be indirect: gravitational influence, lensing, plasma response, or unusually early baryonic collapse, rather than ordinary stellar luminosity from the compact source itself.

There is a useful numerical way to see why the charge is both small and dynamically dangerous. The number of elementary charges corresponding to the fiducial value is

$$N_Q = \frac{Q_A}{e} \simeq 2.5 \times 10^{51} \left(\frac{Q_A}{4 \times 10^{32} \text{ C}} \right). \quad (8)$$

The number of baryon masses associated with $10^{12} M_\odot$ is

$$N_b \sim \frac{M_A}{m_p} \simeq 1.2 \times 10^{69} \left(\frac{M_A}{10^{12} M_\odot} \right). \quad (9)$$

Hence the fractional charge imbalance is only

$$\epsilon_Q \equiv \frac{N_Q}{N_b} \simeq 2 \times 10^{-18} \left(\frac{Q_A}{4 \times 10^{32} \text{ C}} \right) \left(\frac{10^{12} M_\odot}{M_A} \right). \quad (10)$$

The difficulty is therefore not that the required imbalance is large as a particle-number fraction. The difficulty is that electromagnetism is so much stronger than gravity that this tiny imbalance can still correspond to $\Xi = k_e Q_A^2 / (GM_A^2)$ of order unity or larger. A primordial formation model must explain how such a small imbalance is generated and, more importantly, how it avoids being erased by the high conductivity of the early plasma.

The same distinction also clarifies the acceleration question. The original phenomenological motivation for the large charge was the possibility that long-range Coulomb repulsion among a sparse population of

massive objects could affect cosmic expansion. But if the objects are primordial, one must still ask where the effect appears in the cosmological equations. In a homogeneous FLRW reduction, the interaction energy redshifts as a^{-4} , as shown in Section 10, and therefore cannot become an asymptotic cosmological constant. Any acceleration associated with astrons would have to be either transitory in the homogeneous description or else arise from the inhomogeneous Einstein–Maxwell averaging problem discussed in Section 11. Thus the early formation question and the late-time acceleration question are logically separate: primordial seeds may affect early structure, but they do not automatically supply dark energy.

The strategy of the paper is as follows. We begin in Section 2 with a minimal capture model for charge generation during collapse and use it to estimate the characteristic charging timescale. Section 3 studies nonlinear growth and saturation of the charge, including the ordinary accretion estimate and the phenomenological Q/M extrapolation associated with the original astron proposal. Section 4 examines the stability of the charge against plasma neutralization, continued accretion, and Schwinger discharge. Section 5 turns to screening in the intergalactic medium and shows why the linear Debye analysis is both a serious constraint and, in the large-potential regime, an incomplete one. Section 6 discusses the Reissner–Nordström geometric interpretation of charged astrons, while Section 7 extends the discussion to rotating Kerr–Newman-like configurations and Section 8 considers the corresponding lensing phenomenology. Section 9 discusses Lyman- α absorption as a possible probe of astron electric fields. Section 10 analyzes the homogeneous FLRW reduction of the interaction sector and shows that, in this approximation, the astron contribution behaves like a radiation-like component rather than an accelerating one. Section 11 then revisits the cosmology beyond the homogeneous approximation, using Buchert averaging and its Einstein–Maxwell extension to formulate the backreaction problem for a discrete astron lattice. The appendices collect supporting derivations: the range of charging timescales and the free-fall time, the origin of the Frampton-type charge extrapolation, the standard Debye formula and its limitations in non-Maxwellian plasmas, and a nonlinear kinetic framework for screening.

The resulting picture is mixed but informative. The charge sector can be analyzed consistently at the level of a minimal dynamical model and points to parameter regimes in which large charges may be long-lived. By contrast, the screening problem and the cosmological reduction remain unresolved in essential respects. For that reason, the astron scenario is best viewed here as a constrained theoretical framework whose viability depends on physics beyond the simplest homogeneous approximation.

2 Charge Generation in a Minimal Capture Model

We consider a collapsing overdensity of total mass M and characteristic radius $R(t)$ embedded in an ionized plasma of number density n and temperature T . The plasma is assumed to consist of electrons and protons with equal background densities, so that the system is initially electrically neutral up to microscopic fluctuations. The purpose of this section is modest: we use a minimal capture model to estimate the timescale on which an incipient charge asymmetry can evolve and to identify its parametric dependence.

The motivation for considering such a mechanism is not purely formal. In more standard astrophysical settings, small equilibrium charges associated with proton-electron mass asymmetry, as well as induced charges generated by rotating compact objects immersed in magnetic fields, have been discussed extensively [4, 5].

The motion of a particle of species i with mass m_i and charge q_i in the field of a central object of mass M and charge Q is governed by the potential energy

$$U_i(r) = -\frac{GMm_i}{r} + \frac{k_e Q q_i}{r}. \quad (11)$$

For the capture calculation it is convenient to divide by m_i and use the potential per unit mass,

$$\phi_i(r) = -\frac{GM}{r} + \frac{k_e Q q_i}{m_i r}. \quad (12)$$

The dynamics is most conveniently described in terms of the effective potential,

$$V_{\text{eff}}(r) = \phi_i(r) + \frac{L^2}{2r^2}, \quad (13)$$

where L is the angular momentum per unit mass. For a particle incoming from infinity with velocity v_i and impact parameter b_i , one has

$$E = \frac{1}{2}v_i^2, \quad L = b_iv_i. \quad (14)$$

Capture occurs if the particle can reach the surface $r = R$, which requires that the radial kinetic energy vanishes at that point,

$$\frac{1}{2}v_i^2 = \phi_i(R) + \frac{b_i^2v_i^2}{2R^2}. \quad (15)$$

Solving for the critical impact parameter yields

$$b_i^2 = R^2 \left(1 - \frac{2\phi_i(R)}{v_i^2} \right). \quad (16)$$

The corresponding capture cross section is

$$\sigma_i = \pi b_i^2 = \pi R^2 \left(1 - \frac{2\phi_i(R)}{v_i^2} \right). \quad (17)$$

In the regime relevant for gravitational collapse, the focusing term dominates,

$$\frac{2|\phi_i(R)|}{v_i^2} \gg 1, \quad (18)$$

and the cross section simplifies to

$$\sigma_i \simeq \frac{2\pi R}{v_i^2} \left(GM - \frac{k_e Q q_i}{m_i} \right). \quad (19)$$

Assuming a thermal distribution,

$$v_i^2 = \frac{k_B T}{m_i}, \quad (20)$$

one obtains

$$\sigma_i = \frac{2\pi R}{k_B T} (GMm_i - k_e Q q_i). \quad (21)$$

The accretion rate is

$$\Gamma_i = n\sigma_i v_i = \frac{2\pi R n}{\sqrt{k_B T}} \left(GMm_i^{1/2} - k_e Q q_i m_i^{-1/2} \right). \quad (22)$$

The evolution of the net charge follows from the difference between electron and proton accretion,

$$\frac{dQ}{dt} = -e(\Gamma_e - \Gamma_p). \quad (23)$$

Substituting the explicit expressions yields

$$\frac{dQ}{dt} = -\frac{2\pi R n e}{\sqrt{k_B T}} \left[GM(m_e^{1/2} - m_p^{1/2}) + k_e Q e(m_e^{-1/2} + m_p^{-1/2}) \right]. \quad (24)$$

This equation takes the linear form

$$\frac{dQ}{dt} = C_0 + C_1 Q, \quad (25)$$

with

$$C_0 = -\frac{2\pi R n e G M}{\sqrt{k_B T}} (m_e^{1/2} - m_p^{1/2}), \quad C_1 = -\frac{2\pi R n k_e e^2}{\sqrt{k_B T}} (m_e^{-1/2} + m_p^{-1/2}). \quad (26)$$

The term C_0 encodes the asymmetry between electron and proton capture in the minimal model, while C_1 represents electric feedback. Since $m_p \gg m_e$, one has $m_e^{1/2} - m_p^{1/2} < 0$, so that $C_0 > 0$ and $C_1 < 0$ within the conventions used here.

For fixed local plasma parameters (R, n, T) , this linear equation can be solved exactly for an arbitrary initial charge $Q(0) = Q_0$. One finds

$$Q(t) = Q_{\text{eq}} + (Q_0 - Q_{\text{eq}}) e^{C_1 t}, \quad Q_{\text{eq}} = -\frac{C_0}{C_1}. \quad (27)$$

Since $C_1 < 0$, the solution tends asymptotically toward the fixed point Q_{eq} . If one starts from a neutral object, $Q_0 = 0$, then

$$Q(t) = Q_{\text{eq}} \left(1 - e^{-t/\tau}\right), \quad \tau = \frac{1}{|C_1|} = \frac{\sqrt{k_B T}}{2\pi R n k_e e^2 (m_e^{-1/2} + m_p^{-1/2})}. \quad (28)$$

At early times $Q \ll Q_{\text{eq}}$, the growth is approximately linear,

$$Q(t) \simeq C_0 t, \quad (29)$$

while at later times the electric feedback proportional to $C_1 Q$ slows the approach to the fixed point. Thus τ is simply the characteristic charging response time in the linearized model. It measures how quickly the charge moves toward Q_{eq} , but it does not by itself determine the exact equilibration time or the final nonlinear saturation value.

The charging timescale is controlled primarily by the product Rn , with only a square-root dependence on temperature. Numerically, one may rewrite it as

$$\tau \approx 2.39 \frac{\sqrt{T/\text{K}}}{R(\text{m}) n(\text{m}^{-3})} \text{ s}. \quad (30)$$

It is therefore essential to state clearly which plasma environment is being used when quoting any benchmark value for τ : the charging timescale is not a fixed number. Depending on the plasma environment and on the effective capture radius, the formal response time can range from seconds in an extremely dilute benchmark to microscopic values in dense formation regions (see Appendix A). It is therefore more informative to speak of a *range* of charging timescales than of a single benchmark. The appropriate value of τ must always be tied to a specific choice of (R, n, T) appropriate to the physical stage of the astron formation process under consideration.

The physical interpretation is straightforward. The charging time decreases when the local plasma density n increases, because a denser environment supplies more particles to the capture process. It also decreases when the effective capture radius R is larger, since a larger interaction region enhances the accretion rate. By contrast, increasing the temperature tends to lengthen the charging time, but only through a square-root dependence, so this effect is comparatively mild.

To compare this response time with the collapse time in a meaningful way, it is useful to evaluate both quantities in the same local environment. The free-fall time of a self-gravitating gas of density ρ is

$$t_{\text{ff}} = \sqrt{\frac{3\pi}{32G\rho}}. \quad (31)$$

(see appendix A). For an ionized hydrogen plasma one may take

$$\rho \simeq n m_p, \quad (32)$$

so that

$$t_{\text{ff}} = \sqrt{\frac{3\pi}{32Gm_p n}} \approx 1.62 \times 10^{18} \left(\frac{n}{\text{m}^{-3}}\right)^{-1/2} \text{ s.} \quad (33)$$

In order to illustrate the range of possibilities, we use a deliberately compact reference capture radius, normalized to the gravitational radius of a fiducial astron of mass $M \sim 10^{12} M_{\odot}$,

$$R \sim R_g = \frac{GM}{c^2} \simeq 1.48 \times 10^{15} \text{ m} \simeq 4.8 \times 10^{-2} \text{ pc} \simeq 9.9 \times 10^3 \text{ AU.} \quad (34)$$

This is a compactness benchmark, not a statement that the physical surface must sit at R_g ; for a neutral object the black-hole threshold would be set by $2R_g$, while for a charged object it is set by the RN horizon condition. The corresponding values of τ and t_{ff} then depend entirely on the local plasma environment.

For the present-day baryon density, the Particle Data Group quotes $\Omega_b h^2 \simeq 0.02237$, corresponding to a mean baryon density today of order $n_{b,0} \sim 2.5 \times 10^{-7} \text{ cm}^{-3}$ [24, 25].

By contrast, much denser environments arise in direct-collapse and supermassive-seed formation scenarios. High-velocity protogalactic collisions can produce shocked gas with $T \sim 10^6 \text{ K}$ and $n \gtrsim 10^4 \text{ cm}^{-3}$ [36]; cosmological radiation-hydrodynamics simulations of direct-collapse clouds follow the gas at least up to central densities of order 10^8 cm^{-3} [37]; and radiative-transfer calculations of the optically thick inner collapse report densities as large as $\rho \sim 10^{-6} \text{ g cm}^{-3}$, corresponding to number densities well above 10^{20} m^{-3} for ionized hydrogen [38].

Using these environments as order-of-magnitude benchmarks, one finds the values shown in Table 1 in Appendix A. In the corrected capture estimate, the formal response time is shorter than the corresponding free-fall time even for very dilute benchmark densities, and it becomes microscopic in dense formation-stage environments. This should not be overinterpreted as proof that a diffuse late-time IGM can build the large phenomenological charge: in such a medium the limiting issues are the finite charge reservoir, transport, and screening, not the local linear response coefficient. The comparison

$$\tau \ll t_{\text{ff}} \quad (35)$$

should however be interpreted with care. In the derivation of τ , the local background quantities R , n , and T are treated as fixed, whereas in an actual collapse they evolve together with the infall and with the charge itself. Moreover, as Q grows, the Coulomb force feeds back on the incoming trajectories and can slow or shut off further capture. The present comparison with t_{ff} is therefore not a self-consistent solution of the coupled collapse-plus-charging problem. Its meaning is more limited but still useful: within the assumptions of the local capture model, the charge sector adjusts much faster than the bulk hydrodynamic background changes. A fully consistent treatment would require solving simultaneously for the collapse flow, the evolving density and temperature profiles, and the charge-dependent accretion dynamics; we defer that final-radius problem to a separate analysis.

The capture asymmetry and the electric feedback define a preferred charge scale and a short response time, while the final sign and nonlinear endpoint depend on physics that is not fully encoded in the linearized equation alone. This motivates the discussion of saturation in the next section.

3 Nonlinear Growth, Saturation and a Scaling Extrapolation

The previous section identifies a short characteristic response time for the charge sector. Once the charge becomes appreciable, however, the electric contribution is no longer a perturbation, and nonlinear effects must control the subsequent evolution. We now analyze the mechanism that limits further growth.

The full evolution equation derived in Section 2,

$$\frac{dQ}{dt} = C_0 + C_1 Q, \quad (36)$$

is valid only as long as the capture cross sections remain positive for both species. As the magnitude of the charge increases, the Coulomb term modifies the effective potential differently for electrons and protons, leading to a progressive suppression of one channel and enhancement of the other. It is therefore important to keep the sign convention explicit. We take

$$q_p = +e, \quad q_e = -e, \quad (37)$$

so that a positive source charge attracts electrons and repels protons.

The neutral initial condition of the minimal model naturally moves toward the positive-charge branch, because proton capture is gravitationally focused more efficiently than electron capture. For $Q > 0$, the surface potential energies are

$$U_e(R) = -\frac{GMm_e}{R} - \frac{k_e Q e}{R}, \quad U_p(R) = -\frac{GMm_p}{R} + \frac{k_e Q e}{R}. \quad (38)$$

As Q grows, electrons are attracted more strongly, while proton capture is progressively suppressed. The proton channel shuts off when

$$GMm_p = k_e Q e. \quad (39)$$

The corresponding charge scale is

$$Q_p = \frac{GMm_p}{k_e e}. \quad (40)$$

This is not a runaway point: if Q becomes too large, electron capture reduces the positive charge, while if Q is too small the proton excess in the capture rate increases it. In the linear focusing approximation the exact fixed point is

$$Q_{\text{eq}} = \frac{GM}{k_e e} \frac{m_p^{1/2} - m_e^{1/2}}{m_p^{-1/2} + m_e^{-1/2}} \simeq \frac{GM\sqrt{m_p m_e}}{k_e e}, \quad (41)$$

and perturbations obey

$$\frac{d\delta Q}{dt} = C_1 \delta Q, \quad C_1 < 0, \quad (42)$$

so the fixed point is linearly stable.

One can also define the opposite, negative-charge branch. For $Q = -|Q| < 0$,

$$U_e(R) = -\frac{GMm_e}{R} + \frac{k_e |Q| e}{R}, \quad U_p(R) = -\frac{GMm_p}{R} - \frac{k_e |Q| e}{R}. \quad (43)$$

In that case electrons are repelled and protons are attracted. The electron channel is suppressed when

$$GMm_e = k_e |Q| e, \quad (44)$$

giving the lower charge scale

$$|Q_e| = \frac{GMm_e}{k_e e}. \quad (45)$$

Thus the ordinary accretion-limited saturation scale may be written compactly as

$$|Q|_{\text{sat}} \sim \frac{GMm_*}{k_e e}, \quad (46)$$

where $m_* = m_p$ for the natural positive branch generated by proton-dominated capture, and $m_* = m_e$ for an imposed negative branch. These ordinary accretion-limited charges are the scales dynamically selected by force balance; they should be distinguished from the much larger phenomenological Frampton-type extrapolation discussed below.

A complementary way to estimate the onset of saturation is to compare the outward stress generated by the electric field with the inward ram pressure of the infalling plasma. The electric field acts mechanically

on the surface through the Maxwell stress tensor, so its effect can be expressed as an effective electrostatic pressure.

$$P_E = n_i T_{ij} n_j = T_{rr}, \quad T_{ij} = \epsilon_0 \left(E_i E_j - \frac{1}{2} \delta_{ij} E^2 \right). \quad (47)$$

Here T_{ij} is the electrostatic Maxwell stress tensor in SI units, and the pressure is the normal component of the field stress. For a spherical charged surface the normal direction is radial, so the relevant component is T_{rr} .

$$P_E = T_{rr} = \frac{\epsilon_0 E_r^2}{2} \sim \frac{\epsilon_0}{2} \left(\frac{k_e Q}{R^2} \right)^2 = \frac{k_e Q^2}{8\pi R^4}. \quad (48)$$

In the last step we used the radial electric field at the surface of a spherically symmetric charge distribution, $E_r(R) \sim k_e Q/R^2$, which shows that the field produces an outward electrostatic pressure scaling as $k_e Q^2/R^4$.

The resulting picture is that of a fast charging stage followed by a self-regulated saturation mechanism that fixes the charge at an ordinary force-balance value on the branch under consideration. The entire process can occur on timescales much shorter than the gravitational collapse time, so that the object enters the late stages of its evolution already in a charged, near-equilibrium configuration.

The same saturation condition can be recovered in a complementary macroscopic language by comparing the outward electrostatic stress with the inward ram pressure of the accreting plasma. If the electric field becomes strong enough that its surface stress matches the momentum flux of the inflow, further accretion must cease. The inward ram pressure of the infalling plasma is

$$P_{\text{ram}} \sim \rho v^2, \quad (49)$$

where ρ is the mass density of the inflow and v its characteristic speed. The condition for continued accretion is therefore

$$P_{\text{ram}} \gtrsim P_E. \quad (50)$$

Equivalently, saturation is reached when

$$P_E \sim P_{\text{ram}}, \quad (51)$$

that is,

$$\frac{k_e Q^2}{8\pi R^4} \sim \rho v^2. \quad (52)$$

Solving for the charge gives the corresponding equilibrium scale

$$Q_{\text{sat}} \sim \sqrt{\frac{8\pi\rho v^2}{k_e}} R^2. \quad (53)$$

Beyond this point the electric stress dominates the inflow stress, so incoming charged particles are no longer able to accrete efficiently. The pressure-balance estimate should not be expected to reproduce exactly the same numerical coefficient as the microscopic force-balance criterion, since it is a coarse-grained argument. However, it does recover the same parametric saturation scale. Let m_* denote the mass of the particle species whose accretion is being suppressed at saturation. To compare the microscopic condition (46) with the pressure picture, write $|Q| = Ne$, so that the number of captured carriers is $N \sim |Q|/e$. If these occupy a region of size R , then

$$n_* \sim \frac{3|Q|}{4\pi e R^3}, \quad \rho_* \sim m_* n_* \sim \frac{3m_* |Q|}{4\pi e R^3}. \quad (54)$$

Taking the inflow speed to be of order the free-fall speed, $v^2 \sim GM/R$, the ram pressure becomes

$$P_{\text{ram}} \sim \rho_* v^2 \sim \frac{3GMm_*|Q|}{4\pi eR^4}. \quad (55)$$

Equating this with the electrostatic pressure

$$P_E \sim \frac{k_e Q^2}{8\pi R^4} \quad (56)$$

yields

$$|Q|_{\text{sat}} \sim \frac{6GMm_*}{k_e e}. \quad (57)$$

Thus the pressure formalism reproduces the same saturation scale up to a factor of order unity. The agreement is therefore parametric rather than exact, as expected for two different approximate descriptions of the same physical mechanism. For an astron of mass

$$M_A = 10^{12} M_\odot \simeq 1.99 \times 10^{42} \text{ kg}, \quad (58)$$

the ordinary accretion-limited saturation charge is obtained from

$$|Q|_{\text{sat}} \sim \frac{GM_A m_*}{k_e e}, \quad (59)$$

where m_* is the mass of the particle species whose accretion is being suppressed.

Using

$$G = 6.6743 \times 10^{-11} \text{ m}^3 \text{ kg}^{-1} \text{ s}^{-2}, \quad k_e = 8.9876 \times 10^9 \text{ N m}^2 \text{ C}^{-2}, \quad (60)$$

$$e = 1.6022 \times 10^{-19} \text{ C}, \quad m_e = 9.1094 \times 10^{-31} \text{ kg}, \quad m_p = 1.6726 \times 10^{-27} \text{ kg}, \quad (61)$$

the sign convention must be kept explicit. We define $Q = e(N_p - N_e)$, so a positive object repels protons and attracts electrons, whereas a negative object repels electrons and attracts protons. Thus the electron-limited branch is a negative-charge branch, while the proton-limited branch is a positive-charge branch. With signed charges one finds

$$Q_{\text{sat}}^{(e)} = -\frac{GM_A m_e}{k_e e} = -\frac{(6.6743 \times 10^{-11})(1.99 \times 10^{42})(9.1094 \times 10^{-31})}{(8.9876 \times 10^9)(1.6022 \times 10^{-19})} \simeq -8.4 \times 10^{10} \text{ C}, \quad (62)$$

while for proton-limited saturation

$$Q_{\text{sat}}^{(p)} = \frac{GM_A m_p}{k_e e} = \frac{(6.6743 \times 10^{-11})(1.99 \times 10^{42})(1.6726 \times 10^{-27})}{(8.9876 \times 10^9)(1.6022 \times 10^{-19})} \simeq 1.5 \times 10^{14} \text{ C}. \quad (63)$$

It is useful to distinguish these force-balance scales from the linear rate-balance value. The force-balance estimates above ask when the Coulomb force on one species is large enough to stop that species from being accreted. The linear rate-balance value asks a different question: for a fixed background, what charge makes the proton and electron capture rates equal? Starting from $Q = 0$, the strong-focusing rate is slightly larger for protons than for electrons, so the object first charges positively. A positive Q then suppresses proton capture and enhances electron capture until

$$\Gamma_p(Q_{\text{eq}}^{(+)}) = \Gamma_e(Q_{\text{eq}}^{(+)}). \quad (64)$$

Using the strong-focusing rates gives

$$Q_{\text{eq}}^{(+)} = \frac{GM_A}{k_e e} \frac{\sqrt{m_p} - \sqrt{m_e}}{m_e^{-1/2} + m_p^{-1/2}} = \frac{GM_A \sqrt{m_p m_e}}{k_e e} \frac{\sqrt{m_p} - \sqrt{m_e}}{\sqrt{m_p} + \sqrt{m_e}}. \quad (65)$$

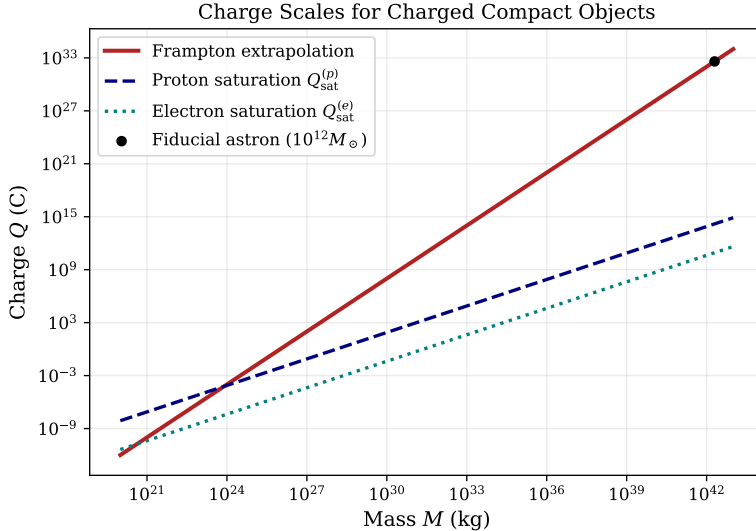


Figure 1: Numerical scan of the charge scales relevant to the astron scenario. The red curve shows the Frampton mass–charge extrapolation $Q = 10^{-52}M^2$, while the blue and teal curves show the ordinary proton- and electron-limited saturation estimates $Q_{\text{sat}} \sim GMm_*/(k_e e)$. The fiducial $10^{12}M_\odot$ astron is marked explicitly. The plot makes clear that the Frampton branch occupies a parametrically different regime from ordinary accretion-limited charging.

Since $m_p \gg m_e$, the last factor is close to one. Therefore

$$Q_{\text{eq}}^{(+)} \simeq \frac{GM_A \sqrt{m_p m_e}}{k_e e} \simeq 3.6 \times 10^{12} \text{ C}. \quad (66)$$

This value lies between the electron- and proton-limited force-balance magnitudes because $\sqrt{m_p m_e}$ is the geometric mean of m_e and m_p . It is the equilibrium charge of the linear capture equation, not a separate condition for complete shutdown of an accretion channel.

Thus, within the ordinary accretion picture, the saturation charge for an astron of mass $10^{12}M_\odot$ lies in the range

$$10^{11} \text{ C} \lesssim |Q|_{\text{sat}} \lesssim 10^{14} \text{ C}, \quad (67)$$

depending on which species sets the effective stopping condition. In the plots below the ordinary saturation curves are shown as magnitudes; the physical sign is fixed by which species is being repelled.

It is useful to summarize these scales in a single numerical scan. Although the plots that follow are not dynamical simulations, they provide a compact global view of the analytic relations derived in this section. Figure 1 compares the ordinary proton- and electron-limited saturation charges with the Frampton extrapolation $Q \propto M^2$. The qualitative separation is already clear at the level of the raw charge: the extrapolated branch grows so rapidly with M that by $M \sim 10^{12}M_\odot$ it lies many orders of magnitude above the ordinary accretion-limited values.

3.1 The Q/M extrapolation

A different estimate was proposed in Ref. [1], where the charge is not derived from a local accretion-saturation condition but from an assumed mass–charge scaling for extremely massive primordial black holes. The basic idea is to ask when the electric repulsion between two identical objects can become comparable to, or larger than, their mutual gravitational attraction.

For two objects of mass M and charge Q , the forces scale as $F_G \sim GM^2/r^2$ and $F_E \sim k_e Q^2/r^2$, so that the relevant ratio is $R \equiv F_G/F_E \sim GM^2/(k_e Q^2)$. If $R > 1$, gravity dominates, whereas if $R < 1$, Coulomb repulsion dominates.

Ref. [1] then adopts two benchmark values for the charge-to-mass ratio from the PBH-charging analysis of Ref. [35] and extends them through a log-linear ansatz, which in practice implies $Q/M \propto M$ and hence $Q \propto M^2$. Applied to the fiducial astron mass in Eq. (58), this extrapolation gives the large-charge benchmark

$$Q_A \simeq 4 \times 10^{32} \text{ C}. \quad (68)$$

This is the scale at which electromagnetic repulsion is argued to become cosmologically significant. We have reported in Appendix B details of the derivation.

Although the extrapolation used in Ref. [1] is admittedly hypothetical, the regime to which it is applied is itself far beyond any empirically controlled theory of primordial ultra-massive object formation. In that sense, the proposal should be read as an exploratory phenomenological extension.

The broader early-universe context of this assumption was discussed in Section 1.2. Recent JWST observations motivate renewed attention to early seed formation and rapid assembly, but they do not by themselves justify the large-charge extrapolation. The extrapolation should therefore be treated as a phenomenological working hypothesis whose physical consequences must be tested directly.

In the next sections we examine the physical consequences of this extrapolation, with particular attention to the issues of Debye screening and to the spacetime interpretation of such highly charged objects in the super-extremal, naked-singularity regime.

In the analysis that follows we shall assume that the characteristic inter-astron separation is of order megaparsecs. This is the physically relevant regime if astrons are to play a role in cosmological acceleration, since both the strength of their collective Coulomb interaction and the possible impact of Debye screening must be evaluated on scales comparable to the mean separation of the population.

The same numerical scan can be represented directly in the (M, Q) plane, where the geometric significance of the extrapolated charge becomes more transparent. Figure 2 shows the Frampton branch together with the Reissner–Nordström extremality line $\Xi = 1$ and the photon-sphere threshold $\Xi = 9/8$. The extrapolated branch crosses into the super-extremal regime at masses of order a few $10^{11} M_\odot$, whereas the ordinary saturation curves remain extremely far below both thresholds over the entire range shown. This anticipates the main conclusion of Section 6: the large-charge astron proposal and the ordinary accretion-saturation estimate do not correspond to nearby points in parameter space, but to qualitatively different Einstein–Maxwell regimes.

4 Stability of the Charge

The persistence of a macroscopic electric charge over cosmological timescales requires the absence of efficient discharge or neutralization mechanisms. This issue involves three conceptually distinct effects: plasma neutralization by the surrounding medium, continued accretion of opposite charges, and quantum vacuum discharge through pair production.

From the astrophysical point of view, the possibility that black holes may carry small but nonvanishing electric charges has been revisited in recent years, especially because even modest charges can affect the motion of charged particles and modify radiative signatures [4, 5]. Our purpose here is to examine whether an analogous conclusion can hold, at least parametrically, for the much more highly charged compact objects envisioned in the astron scenario.

We first consider neutralization by the intergalactic medium (IGM). For the fiducial large-charge branch in Eq. (68), the total number of elementary charges required to compensate the astron charge is

$$N_Q = \frac{Q_A}{e} \simeq \frac{4 \times 10^{32}}{1.602 \times 10^{-19}} \simeq 2.5 \times 10^{51}. \quad (69)$$

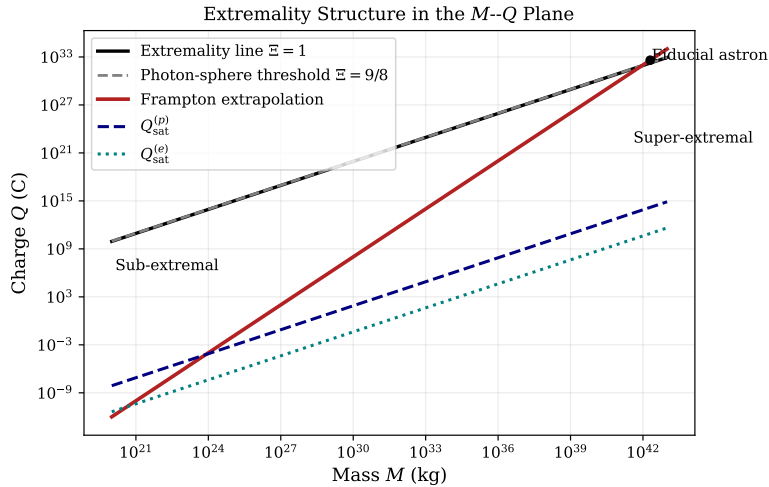


Figure 2: Extremality structure in the (M, Q) plane. The black line marks the Reissner–Nordström extremality bound $\Xi = 1$, the gray dashed line marks the photon-sphere threshold $\Xi = 9/8$, and the colored curves show the same charge prescriptions as in Fig. 1. The fiducial astron point lies deep in the super-extremal region, while the ordinary saturation branches remain many orders of magnitude below extremality.

As a representative present-day benchmark, we take the intergalactic electron density to be of order

$$n_e \sim 0.2 \text{ m}^{-3}, \quad (70)$$

consistent with the mean cosmological baryon density and standard descriptions of the low-density ionized IGM [26, 33, 34]. The number of available free charges within a sphere of radius R is

$$N_{\text{IGM}}(R) = n_e \frac{4\pi}{3} R^3. \quad (71)$$

For $R = 1 \text{ pc} = 3.086 \times 10^{16} \text{ m}$, this gives

$$N_{\text{IGM}}(1 \text{ pc}) \simeq (0.2) \frac{4\pi}{3} (3.086 \times 10^{16})^3 \simeq 2.5 \times 10^{49}. \quad (72)$$

Thus a one-parsec sphere falls short of the fiducial compensation charge by roughly two orders of magnitude. Complete neutralization would require an extended charge reservoir, with a characteristic radius of order several parsecs for this mean density. This counting argument does not replace a plasma-screening calculation, but it shows that local neutralization is not a compact near-surface process.

The remaining question is whether a large charge can subsequently be removed by quantum vacuum effects. The relevant process is the Schwinger mechanism, namely the spontaneous creation of electron–positron pairs when the electric field becomes so intense that the vacuum itself is unstable. The corresponding critical field is

$$E_{\text{crit}} = \frac{m_e^2 c^3}{e \hbar} \simeq 1.3 \times 10^{18} \text{ V/m}. \quad (73)$$

If the electric field near the charged object were to approach this value, pairs would be produced, with charges of opposite sign falling toward the source and thereby tending to reduce its net charge.

For an astron the electric field outside the source is

$$E(r) = \frac{k_e Q_A}{r^2}. \quad (74)$$

Evaluated at the reference compactness scale

$$r_A = \frac{GM_A}{c^2} \simeq 1.5 \times 10^{15} \text{ m.} \quad (75)$$

one finds

$$E(r_A) \sim 1.6 \times 10^{12} \text{ V/m,} \quad (76)$$

for the fiducial mass in Eq. (58) and the charge in Eq. (68). Hence

$$\frac{E(r_A)}{E_{\text{crit}}} \sim 1.2 \times 10^{-6}, \quad (77)$$

so the electric field at this compactness scale is many orders of magnitude below the Schwinger threshold. If a regular finite-radius realization had a larger surface radius, the exterior field at the surface would be smaller still. Since the field decreases as r^{-2} outside the source, no efficient pair creation can occur in the macroscopic region accessible to the classical description.

One may still ask whether the Schwinger threshold could be reached only at much smaller radius. Solving

$$E(r_{\text{crit}}) = E_{\text{crit}} \quad (78)$$

gives

$$r_{\text{crit}} = \sqrt{\frac{k_e Q_A}{E_{\text{crit}}}}. \quad (79)$$

For the astron parameters considered here, this radius lies many orders of magnitude below the compactness scale and deep inside the regime where the simple classical description of the compact object can no longer be trusted. For the benchmark astron charge in Eq. (68), $k_e = 8.99 \times 10^9 \text{ N m}^2 \text{ C}^{-2}$, and $E_{\text{crit}} \simeq 1.3 \times 10^{18} \text{ V/m}$, one finds

$$r_{\text{crit}} = \sqrt{\frac{k_e Q_A}{E_{\text{crit}}}} = \sqrt{\frac{(8.99 \times 10^9)(4 \times 10^{32})}{1.3 \times 10^{18}}} \simeq 1.7 \times 10^{12} \text{ m.} \quad (80)$$

For the fiducial astron mass in Eq. (58), the reference compactness scale is the one given in Eq. (75). Hence

$$\frac{r_{\text{crit}}}{r_A} \simeq 1.1 \times 10^{-3}, \quad (81)$$

so the Schwinger threshold would be reached only at radii roughly three orders of magnitude smaller than the gravitational scale of the object.

Thus, even if one formally identifies such a radius, it does not imply physically efficient pair production in the exterior region relevant to the stability of the macroscopic charge. The Schwinger mechanism is therefore not expected to play a significant role in discharging the astron.

Finally, once accretion has halted, the absence of efficient neutralization and the suppression of quantum discharge imply that the charge can evolve only through extremely weak residual interactions with the dilute intergalactic plasma. The corresponding timescale is expected to exceed the Hubble time by many orders of magnitude, so that the charge remains effectively constant over cosmological epochs.

Taken together, these considerations show that within the assumptions of the present model the astron charge can be dynamically generated, self-limited, and long-lived against both classical and quantum discharge mechanisms. In this sense, a large charge should not be viewed merely as an external input, but as a potentially stable outcome of the scenario.

5 Screening Constraints in the Intergalactic Medium

A central assumption of the astron scenario is that the electric field generated by a charged compact object can remain effective over distances comparable with the mean inter-astron separation. Since astrons are embedded in an ionized cosmic environment, this immediately raises the question of plasma screening. In an ordinary quasi-neutral electron–ion plasma, a localized charge is not felt out to arbitrarily large distances: mobile charges of the opposite sign are attracted, while charges of the same sign are repelled, producing a polarization cloud that reduces the effective field beyond a characteristic screening scale. The standard language for this phenomenon is Debye screening. This should not be confused with a gas of same-sign charges alone. If only positive charges are present, there is no ordinary Debye screening of a positive source unless a compensating negative component or neutralizing background is also introduced.

For the present problem, the main issue is not whether screening exists in some form, but whether the linear Debye picture can be applied without modification to an object as extreme as an astron. On the one hand, the intergalactic medium is very dilute, which might suggest weak screening. On the other hand, the charges postulated for astrons are so large that the electrostatic potential near the source is far from the weak-perturbation regime assumed in the usual linear Debye–Hückel treatment. The standard formulae are therefore useful as a first benchmark, but they cannot by themselves settle the question.

In this section we use the standard Debye result only as a benchmark; the derivation is given in Appendix C. For a quasi-neutral multicomponent plasma in linear response,

$$\frac{1}{\lambda_D^2} = \sum_s \frac{n_{s0} q_s^2}{\epsilon_0 k_B T_s}, \quad (82)$$

where n_{s0} , q_s , and T_s are the unperturbed density, charge, and temperature of species s . A point charge Q then produces the screened potential

$$\Phi(r) = \frac{Q}{4\pi\epsilon_0 r} e^{-r/\lambda_D}. \quad (83)$$

For a mobile electron–proton plasma with $n_e = n_p = n_0$ and $T_e = T_p = T$, Eq. (82) gives

$$\lambda_D^2 = \frac{\epsilon_0 k_B T}{2n_0 e^2}. \quad (84)$$

If instead only the electron response is retained, with the ions treated as a fixed neutralizing background, one obtains the common electron Debye length

$$\lambda_{De}^2 = \frac{\epsilon_0 k_B T}{n_e e^2}. \quad (85)$$

Thus the factor of two is not universal; it records whether both mobile species or only the electrons are included. The compact rewriting $\lambda_D^2 = \epsilon_0 k_B T / (n_{\text{tot}} e^2)$ is valid only in the quasi-neutral symmetric convention $n_{\text{tot}} = n_e + n_p = 2n_0$. It is not a general formula for an uncompensated non-neutral plasma.

Debye-type screening constraints have also been exploited in other cosmological plasma settings, for example in analyses of magnetic monopole plasmas, where the existence of large-scale magnetic fields implies strong limits on the allowed screening length [13].

The linear Debye estimate relies on two essential assumptions: (i) the perturbation is small, $|e\Phi| \ll k_B T$, and (ii) the plasma contains a sufficiently large number of mobile charges within a Debye sphere to establish local equilibrium. The first of these assumptions is clearly strained near an astron, where the potential is very large. Indeed, for the benchmark charge in Eq. (68) one has

$$\frac{e\Phi(r)}{k_B T} \gg 1 \quad (86)$$

over a broad range of distances, so the linear Debye–Hückel approximation cannot be accepted without qualification.

This point can be made explicit by evaluating the dimensionless expansion parameter of the Debye–Hückel approximation,

$$\frac{e\Phi(r)}{k_B T}. \quad (87)$$

For an astron of charge Q_A , the electrostatic potential is

$$\Phi(r) = \frac{k_e Q_A}{r}, \quad (88)$$

so that

$$\frac{e\Phi(r)}{k_B T} = \frac{k_e e Q_A}{k_B T r}. \quad (89)$$

Taking the fiducial large-charge value from Eq. (68) and $T \sim 10^6$ K, one finds

$$\frac{e\Phi(r)}{k_B T} \simeq \frac{(8.99 \times 10^9)(1.60 \times 10^{-19})(4 \times 10^{32})}{(1.38 \times 10^{-23})(10^6) r} \simeq \frac{4.2 \times 10^{40}}{r(\text{m})}. \quad (90)$$

Thus,

$$\frac{e\Phi(1 \text{ pc})}{k_B T} \simeq 1.4 \times 10^{24}, \quad \frac{e\Phi(1 \text{ Mpc})}{k_B T} \simeq 1.4 \times 10^{18}, \quad (91)$$

and even at cosmological distances the ratio remains enormously larger than unity. The condition

$$\left| \frac{e\Phi}{k_B T} \right| \ll 1 \quad (92)$$

required for the linear Debye–Hückel approximation is therefore grossly violated over the entire range of physically relevant distances. In this sense, the linear screening formula can at best be used as a rough benchmark, but not as a self-consistent description of the astron field.

Figure 3 shows this point in a compact numerical scan. The ratio $e\Phi/(k_B T)$ falls only as r^{-1} , so even at parsec and megaparsec distances it remains vastly above unity for the benchmark charge. The linear Debye regime is therefore not merely inaccurate near the source; it is absent throughout the astrophysically relevant domain.

Moreover, the standard estimate need not remain quantitatively reliable when the plasma departs strongly from local Maxwellian equilibrium. In plasmas with pronounced suprathermal tails, modeled for example by Kappa distributions, the effective Debye length can be enhanced relative to its classical value [48]. Likewise, in curved spacetime the effective screening scale acquires gravitational corrections and redshift effects, as has been shown explicitly for hot non-Abelian plasmas [14]. Although these analyses do not directly solve the astron problem, they reinforce the point that screening in an astrophysical or cosmological environment cannot always be reduced to the flat-space linear formula.

It is nevertheless useful to quote the Debye estimate as a benchmark, provided the meaning of the estimate is kept clear. The Debye length computed here is a property of the *ambient intergalactic plasma*, not of the astron itself. For representative intergalactic conditions,

$$n_e \sim 0.2 \text{ m}^{-3}, \quad T \sim 10^6 \text{ K}, \quad (93)$$

the one-species electron Debye estimate is

$$\lambda_D \approx 1.5 \times 10^5 \text{ m}, \quad (94)$$

namely about 150 km. This is extremely small compared both with a megaparsec and with the fiducial astron compactness scale $r_g \sim 1.5 \times 10^{15}$ m. Thus, if the linear Debye formula could be applied naively, it

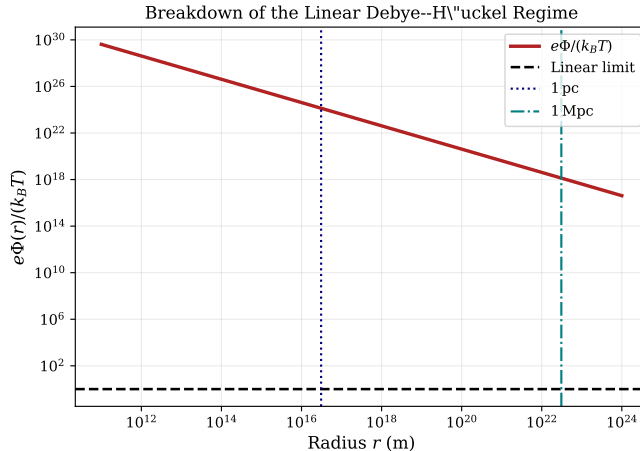


Figure 3: Numerical scan of the Debye–Hückel linearization parameter $e\Phi(r)/(k_B T)$ for the benchmark astron charge in Eq. (68) and $T = 10^6$ K. The horizontal dashed line marks the formal limit of validity of the linear approximation, while the vertical markers indicate the scales 1 pc and 1 Mpc. The plot shows that the linear regime is never reached on physically relevant scales.

would predict exponential suppression of the electric field on a scale completely negligible compared with inter-astron separations.

The number of particles in a Debye sphere,

$$N_D = \frac{4\pi}{3} n_e \lambda_D^3, \quad (95)$$

has a different meaning. It is a collectivity parameter for the background plasma: it asks how many ambient particles lie inside a volume of radius λ_D , not how many particles are needed to neutralize the astron. With the above numbers,

$$N_D \approx 3.1 \times 10^{15}. \quad (96)$$

Including both electron and proton responses changes these numbers only by factors of order unity, giving $\lambda_D \simeq 1.1 \times 10^5$ m and $N_D \simeq 1.1 \times 10^{15}$. Thus $N_D \gg 1$: the plasma is collective, and the Debye calculation is not failing because there are only order-one particles in a Debye sphere.

This should be separated from the much larger question of neutralizing the astron. The number of elementary charges corresponding to the fiducial astron charge is

$$N_Q = \frac{Q_A}{e} \simeq 2.5 \times 10^{51} \quad (97)$$

for the charge in Eq. (68). Clearly $N_Q \gg N_D$. A single Debye sphere of the unperturbed IGM does not contain enough opposite charge to compensate the astron. This is not a paradox: ordinary Debye screening is a linear polarization calculation, not the statement that one Debye sphere literally contains the full neutralizing charge of an arbitrarily large source. For the astron, however, the enormous value of N_Q is precisely a warning that the linear approximation is not self-consistent near the source.

It is therefore more transparent to ask how large a charge reservoir is needed. For the present-day benchmark density in Eq. (70), the number of ambient electrons enclosed within a sphere of radius R is

$$N_{\text{IGM}}(R) = n_e \frac{4\pi}{3} R^3. \quad (98)$$

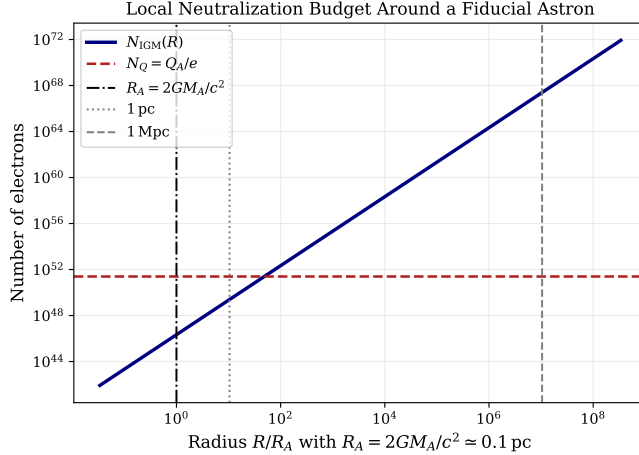


Figure 4: Comparison between the number of electrons contained in a sphere of radius R , $N_{\text{IGM}}(R) = n_e(4\pi/3)R^3$, and the number $N_Q = Q_A/e$ required to compensate the benchmark astron charge. The horizontal axis is normalized to the fiducial astron compactness scale $R_A = 2GM_A/c^2 \simeq 0.1$ pc, and the plot also marks 1 pc and 1 Mpc. It shows that complete neutralization requires a reservoir extending over many astron compactness scales even before one addresses the kinetic problem of actually transporting those charges.

Equating $N_{\text{IGM}}(R)$ with N_Q gives

$$R_Q \sim \left(\frac{3N_Q}{4\pi n_e} \right)^{1/3} \sim 1.4 \times 10^{17} \text{ m} \sim 5 \text{ pc}. \quad (99)$$

Thus a megaparsec-sized region contains vastly more than enough electrons in principle, but complete compensation of the astron charge would require drawing on a macroscopic reservoir extending over parsec scales. The real issue is therefore not a failure of plasma collectivity as measured by N_D , but the nonlinear transport and rearrangement of a very large amount of charge. Figure 4 compares this quantity with the number of electrons required to compensate the fiducial astron charge. The crossing occurs only at radii of order several parsecs, so local neutralization is not a compact near-surface phenomenon even for a realistic mean IGM density.

One may attempt to go beyond the linear regime and consider the full nonlinear Poisson–Boltzmann equation. In that case the problem becomes intrinsically kinetic and nonlocal. The timescale for transporting charge over a macroscopic distance L is controlled by diffusion or drift,

$$t_{\text{screen}} \sim \frac{L^2}{D}, \quad (100)$$

where D is the diffusion coefficient. Whether this timescale is short or long compared with cosmological evolution depends on the detailed transport model and cannot be settled by dimensional analysis alone.

A complementary way to state the issue is that the plasma may be effectively collisionless on some relevant scales, so the assumptions behind local thermodynamic equilibrium must be checked rather than assumed. This weakens the direct applicability of linear screening formulae, but it does not automatically prove the absence of screening.

The linear Debye estimate therefore has a precise role in the argument. It gives the screening scale predicted by a linear Maxwellian plasma, while the large-potential regime shows why that scale cannot by itself be promoted to a self-consistent astron solution. A reliable assessment of the screening problem requires a nonlinear or kinetic analysis. Appendix D formulates the minimal self-consistent problem in

terms of a Vlasov–Poisson or Vlasov–Fokker–Planck–Poisson description, making explicit which assumptions must be checked before one can infer either exponential screening or persistence of the long-range field.

It is useful to summarize the logic in four separate statements. First, $N_D \gg 1$ means that the intergalactic medium is a collective plasma on the linear Debye scale; it does not mean that one Debye sphere contains enough charge to neutralize an astron. Second, the value $\lambda_D \sim 150$ km is the linear Debye length of the ambient IGM plasma and is tiny compared with both the astron compactness scale and a megaparsec. Third, the charge available in one Debye sphere is $eN_D \sim 10^{-3}$ C, enormously smaller than $Q_A \sim 10^{32}$ C, so one Debye sphere cannot literally compensate the astron charge. Fourth, enough opposite charge exists only in a macroscopic reservoir, of order a few parsecs for the fiducial IGM density. Thus the screening problem for an astron is not ordinary small-perturbation Debye screening; it is a nonlinear charge-reservoir and transport problem.

6 Astrons and Naked Singularities

Because the astron scenario invokes extremely large charges for ultra-massive compact objects, it is natural to ask whether the corresponding geometry is black-hole-like, merely horizonless, or genuinely nakedly singular. In the present section we make this distinction explicit in terms of the mass M , charge Q , and physical radius R of the object. The key point is that, once spherical symmetry, vanishing rotation, and an electrovac exterior are assumed, the Einstein–Maxwell equations fix the exterior geometry from M and Q alone. The remaining ambiguity is not in the exterior metric, but in how the finite-radius interior is completed.

Under these assumptions the spacetime outside the object is necessarily of Reissner–Nordström type,

$$ds^2 = f(r)c^2 dt^2 - f(r)^{-1} dr^2 - r^2 d\Omega^2, \quad f(r) = 1 - \frac{2GM}{c^2 r} + \frac{Gk_e Q^2}{c^4 r^2}. \quad (101)$$

The potential horizons are the zeros of $f(r)$,

$$r_{\pm} = \frac{GM}{c^2} \pm \sqrt{\left(\frac{GM}{c^2}\right)^2 - \frac{Gk_e Q^2}{c^4}}, \quad (102)$$

so the outer horizon r_+ is the charged generalization of the Schwarzschild radius. Indeed, for $Q \rightarrow 0$ one recovers $r_+ \rightarrow 2GM/c^2$. For nonzero charge, however, the positive Q^2/r^2 term in $f(r)$ reduces the outer horizon radius relative to the Schwarzschild value. Equivalently, the charge appears as a subtraction inside the square root in Eq. (102): as Q increases, the square root decreases, so r_+ moves inward from $2GM/c^2$ toward GM/c^2 at extremality.

It is useful to introduce the dimensionless parameters

$$\Xi \equiv \frac{k_e Q^2}{GM^2}, \quad \eta \equiv \frac{c^2 R}{GM}. \quad (103)$$

The parameter Ξ is fixed entirely by the geometry, since Eq. (102) may be rewritten as

$$r_{\pm} = \frac{GM}{c^2} \left(1 \pm \sqrt{1 - \Xi}\right). \quad (104)$$

Equivalently, the horizon equation $f(r) = 0$ is a quadratic with discriminant

$$\Delta = \left(\frac{2GM}{c^2}\right)^2 - 4\frac{Gk_e Q^2}{c^4} = 4\left(\frac{GM}{c^2}\right)^2 (1 - \Xi). \quad (105)$$

The three cases are therefore

$$\Xi < 1 : \quad \text{sub-extremal RN with two real horizons,} \quad (106)$$

$$\Xi = 1 : \quad \text{extremal RN with } r_+ = r_- = \frac{GM}{c^2}, \quad (107)$$

$$\Xi > 1 : \quad \text{super-extremal RN with no horizon.} \quad (108)$$

This already shows that the existence or absence of a Reissner–Nordström horizon is determined entirely by the pair (M, Q) , or equivalently by the single combination Ξ . The radius R does not enter the horizon equation at all. The role of R becomes relevant only after horizons exist. If $\Xi \leq 1$, the physical question is whether the material body lies inside or outside the outer horizon r_+ . In terms of η , the condition $R < r_+$ becomes

$$\eta < 1 + \sqrt{1 - \Xi}, \quad (109)$$

whereas $R > r_+$ becomes

$$\eta > 1 + \sqrt{1 - \Xi}. \quad (110)$$

Accordingly, for $\Xi < 1$, the two radial regimes are

$$\eta < 1 + \sqrt{1 - \Xi} : \quad \text{black-hole-like object,} \quad (111)$$

$$\eta > 1 + \sqrt{1 - \Xi} : \quad \text{charged compact object with RN exterior but no horizon covering the surface.} \quad (112)$$

At extremality, $\Xi = 1$, the critical surface occurs at $\eta = 1$.

By contrast, if $\Xi > 1$, the horizon radii do not exist at all. In that regime no choice of R can restore a horizon, because there is no horizon radius with which R can be compared. The radius only fixes the size of the interior region to which the super-extremal RN exterior is matched. In this precise sense, the pair (M, Q) fixes Ξ , and Ξ fixes the RN horizon structure. The radius R instead fixes the matching of the exterior geometry to the interior, and it can be compared with r_+ only when $\Xi \leq 1$.

This still does not settle whether the object is a naked singularity, because horizonlessness and singularity are not the same notion. For the exact Reissner–Nordström solution continued all the way to $r = 0$, the center is automatically singular: in geometric units the Kretschmann scalar is

$$K = R_{\mu\nu\rho\sigma}R^{\mu\nu\rho\sigma} = \frac{48M^2}{r^6} - \frac{96MQ^2}{r^7} + \frac{56Q^4}{r^8}, \quad (113)$$

so $K \rightarrow \infty$ as $r \rightarrow 0$. Therefore an exact super-extremal Reissner–Nordström spacetime is automatically a naked singularity. However, if the same exterior geometry is interpreted only for $r > R$ and is matched to a regular finite-radius interior, one obtains instead a horizonless overcharged compact object. The distinction between these two possibilities is not in the exterior metric, but in the interior completion.

6.1 Reissner–Nordström Exteriors with Regular or Singular Interiors

The previous discussion shows that the exterior Reissner–Nordström geometry by itself does not determine whether the center is regular or singular. To make this point explicit, we use the standard curvature-coordinate form for a static, spherically symmetric charged fluid, following the charged-fluid treatment of Bekenstein and later compact-star applications [6, 7]. In these coordinates the radial coordinate is the areal radius, and the Einstein–Maxwell constraint fixes the radial metric coefficient in terms of the enclosed mass $m(r)$ and enclosed charge $q(r)$:

$$ds^2 = e^{2\Psi(r)}c^2dt^2 - \left(1 - \frac{2Gm(r)}{c^2r} + \frac{Gk_eq(r)^2}{c^4r^2}\right)^{-1} dr^2 - r^2d\Omega^2, \quad 0 \leq r < R, \quad (114)$$

Here $m(r)$ and $q(r)$ are the enclosed mass and enclosed charge functions, and $\Psi(r)$ is the gravitational redshift function. At this stage $\Psi(r)$ is left general because no microscopic equation of state or charge profile has yet been specified. It is not, however, an arbitrary physical profile in a complete interior solution. Once the matter density, pressure, and charge density are chosen, the Einstein–Maxwell equations determine $d\Psi/dr$ through the charged TOV equation, Eq. (144). The remaining additive constant in Ψ is only the normalization of the time coordinate, and is fixed by matching g_{tt} to the exterior metric at $r = R$. This is the usual charged generalization of the interior Schwarzschild/TOV parametrization; for $q(r) = 0$ it reduces to $g_{rr}^{-1} = 1 - 2Gm(r)/(c^2r)$. For $r > R$ the exterior remains

$$ds^2 = f_{\text{RN}}(r)c^2dt^2 - f_{\text{RN}}(r)^{-1}dr^2 - r^2d\Omega^2, \quad f_{\text{RN}}(r) = 1 - \frac{2GM}{c^2r} + \frac{Gk_eQ^2}{c^4r^2}. \quad (115)$$

Continuity of the metric at the matching surface $r = R$ requires

$$m(R) = M, \quad q(R) = Q, \quad e^{2\Psi(R)} = f_{\text{RN}}(R). \quad (116)$$

If one also imposes continuity of the extrinsic curvature, the matching is smooth; otherwise the jump is interpreted as a thin shell with surface stress-energy through the Israel junction conditions, as summarized in Appendix F.

Regularity at the center follows if the enclosed mass and charge behave as

$$m(r) \sim m_3r^3, \quad q(r) \sim q_3r^3, \quad \Psi(r) \rightarrow \Psi_0 \quad (r \rightarrow 0). \quad (117)$$

Indeed, under these conditions one has

$$\frac{m(r)}{r} \sim r^2, \quad \frac{q(r)^2}{r^2} \sim r^4, \quad (118)$$

so the metric coefficients remain finite at the origin. The electric field is then also regular, since

$$E(r) \sim \frac{k_eq(r)}{r^2} \sim r. \quad (119)$$

Thus an object with $R > r_+$ can perfectly well be a finite charged compact body with a regular center, in direct analogy with an ordinary star.

By contrast, singular behavior arises if the interior is chosen so that

$$m(r) \rightarrow m_0 \neq 0 \quad \text{or} \quad q(r) \rightarrow q_0 \neq 0 \quad (r \rightarrow 0), \quad (120)$$

because then the metric develops the schematic behavior

$$1 - \frac{2Gm(r)}{c^2r} + \frac{Gk_eq(r)^2}{c^4r^2} \sim 1 - \frac{2Gm_0}{c^2r} + \frac{Gk_eq_0^2}{c^4r^2}, \quad (121)$$

which is singular at $r = 0$. The exact Reissner–Nordström continuation to the center is precisely of this type.

Two simple examples illustrate the distinction. A regular thin-shell model is obtained by taking the region $r < R$ to be flat spacetime, written with a constant lapse chosen to match the exterior time normalization at the shell:

$$ds_{\text{in}}^2 = f_{\text{RN}}(R)c^2dt^2 - dr^2 - r^2d\Omega^2, \quad r < R, \quad (122)$$

where $f_{\text{RN}}(R) > 0$ is assumed so that the surface is timelike. This is flat because the constant rescaling $T = \sqrt{f_{\text{RN}}(R)}t$ brings the interior metric to the Minkowski form

$$ds_{\text{in}}^2 = c^2dT^2 - dr^2 - r^2d\Omega^2. \quad (123)$$

Thus “flat interior” means that there is no volume mass density, no volume charge density, and no electromagnetic field for $r < R$. The mass and charge are instead supported at the boundary: the charge appears as a surface charge on the shell, while the jump in extrinsic curvature is balanced by the shell stress-energy described in Appendix F. In this case the center is manifestly regular, although the matching surface is a material thin shell rather than a smooth fluid boundary. A smooth regular interior may instead be modeled by the ansatz

$$m(r) = M \left(\frac{r}{R} \right)^3, \quad q(r) = Q \left(\frac{r}{R} \right)^3, \quad (124)$$

with $\Psi(r)$ chosen regular and satisfying the matching condition at $r = R$. In a complete fluid model $\Psi(r)$ would be determined by the charged TOV equation once the equation of state and charge density are fixed; in this illustrative ansatz it is only required to remain finite at the center and to match the exterior lapse at the surface. Then

$$g_{rr}^{-1} = 1 - \frac{2GM}{c^2 R^3} r^2 + \frac{Gk_e Q^2}{c^4 R^6} r^4, \quad (125)$$

which is manifestly finite at the origin. Thus the same Reissner–Nordström exterior for $r > R$ may correspond either to a regular finite-radius charged object or to a naked singularity. The distinction is not fixed by the exterior geometry alone, but by the choice of interior completion.

6.2 Summary: Astrons with and without Horizons

It is useful to make the previous discussion even more explicit by writing the full spacetime as a piecewise metric. In the present static, spherically symmetric setting, the natural form is

$$ds^2 = \begin{cases} ds_{\text{int}}^2, & 0 \leq r < R, \\ ds_{\text{RN}}^2, & r > R, \end{cases} \quad ds_{\text{RN}}^2 = f_{\text{RN}}(r)c^2 dt^2 - f_{\text{RN}}(r)^{-1} dr^2 - r^2 d\Omega^2. \quad (126)$$

The qualitative nature of the configuration is then fixed by Ξ , defined in Eq. (103), and by the position of R relative to the outer RN horizon r_+ , whenever the latter exists.

If $\Xi < 1$, the vacuum Reissner–Nordström geometry possesses an outer horizon at

$$r_+ = \frac{GM}{c^2} \left(1 + \sqrt{1 - \Xi} \right). \quad (127)$$

This formula makes explicit why the RN outer horizon is smaller than the Schwarzschild radius: since $0 < \sqrt{1 - \Xi} < 1$ for $0 < \Xi < 1$, one has $GM/c^2 < r_+ < 2GM/c^2$. The limit $\Xi = 0$ gives the Schwarzschild value, while $\Xi = 1$ gives the extremal radius $r_+ = GM/c^2$. If in addition

$$R < r_+, \quad (128)$$

then the matching surface lies inside the outer horizon and the full spacetime is black-hole-like. Two subcases are then possible. The singular realization is the exact RN black hole,

$$ds^2 = ds_{\text{RN}}^2, \quad r > 0, \quad (129)$$

whose center is singular. The regular realization is a charged object with a regular interior,

$$ds^2 = \begin{cases} e^{2\Psi(r)} c^2 dt^2 - \left(1 - \frac{2Gm(r)}{c^2 r} + \frac{Gk_e q(r)^2}{c^4 r^2} \right)^{-1} dr^2 - r^2 d\Omega^2, & 0 \leq r < R, \\ ds_{\text{RN}}^2, & r > R, \end{cases} \quad (130)$$

with $R < r_+$. In this case the horizon is present, but the central region is regular rather than singular.

If $\Xi < 1$ but

$$R > r_+, \quad (131)$$

the situation is different. The surface of the object lies outside the radius at which the vacuum RN metric would have developed an outer horizon. Since the region $0 \leq r < R$ is not vacuum but is instead described by the interior metric ds_{int}^2 , the full spacetime need not contain any horizon at all. This is exactly analogous to the Sun: although the exterior Schwarzschild solution has a would-be horizon at $2GM/c^2$, the physical star ends long before that radius is reached, and the interior fluid solution replaces the vacuum metric. In the astron case the corresponding horizonless regular configuration is again given by Eq. (126), but now with $R > r_+$.

Finally, if $\Xi > 1$, the exterior Reissner–Nordström geometry is super-extremal and no RN horizon exists anywhere. Here again two conceptually different possibilities arise. If one takes the exact RN geometry all the way to the origin,

$$ds^2 = ds_{\text{RN}}^2, \quad r > 0, \quad \Xi > 1, \quad (132)$$

one obtains a naked singularity. If instead one matches the same exterior to a regular finite-radius interior,

$$ds^2 = \begin{cases} e^{2\Psi(r)} c^2 dt^2 - \left(1 - \frac{2Gm(r)}{c^2 r} + \frac{Gk_e q(r)^2}{c^4 r^2}\right)^{-1} dr^2 - r^2 d\Omega^2, & 0 \leq r < R, \\ ds_{\text{RN}}^2, & r > R, \end{cases} \quad \Xi > 1, \quad (133)$$

then one has a horizonless overcharged compact object rather than a naked singularity.

The four cases may therefore be summarized as follows:

$$\Xi < 1, R < r_+ : \quad \text{horizon present}, \quad (134)$$

$$\Xi < 1, R > r_+ : \quad \text{finite charged object, no horizon in the full spacetime}, \quad (135)$$

$$\Xi > 1, \text{ exact RN} : \quad \text{naked singularity}, \quad (136)$$

$$\Xi > 1, \text{ regular interior} : \quad \text{horizonless overcharged compact object}. \quad (137)$$

In this way the role of the radius R becomes completely transparent: it does not alter the exterior RN geometry, but it does determine whether the full spacetime includes only the vacuum RN region or instead replaces the central part of that geometry by a regular interior.

6.3 Charged TOV Equations for Regular Astrons

If one wishes to model an astron as a regular static charged object rather than as an exact vacuum Reissner–Nordström singularity, the appropriate interior equations are the Einstein–Maxwell generalization of the Tolman–Oppenheimer–Volkoff system. This description is meaningful for the regular configurations discussed above, namely the horizonless case $R > r_+$ and the super-extremal case $\Xi > 1$ with a regular interior. By contrast, it does not describe the exact RN naked singularity, since that solution is electrovac all the way to $r = 0$, nor is it the natural description of a fully collapsed black hole interior.

The metric form used for the interior is not an additional dynamical assumption. It is the standard parametrization of a static, spherically symmetric Einstein–Maxwell configuration in terms of the enclosed gravitational mass and the enclosed electric charge. This is the usual starting point for the Einstein–Maxwell generalization of hydrostatic equilibrium for charged fluid spheres [6, 7]. The most general static, spherically symmetric line element can first be written as

$$ds^2 = e^{2\Psi(r)} c^2 dt^2 - e^{2\Lambda(r)} dr^2 - r^2 d\Omega^2, \quad (138)$$

where the choice of r as the area radius fixes the angular part to $-r^2 d\Omega^2$. The function $\Psi(r)$ is the gravitational redshift function: it controls clock rates through $g_{tt} = e^{2\Psi} c^2$. The function $\Lambda(r)$ determines the radial geometry.

In the charged problem it is useful to introduce the charge $q(r)$ enclosed inside the sphere of area $4\pi r^2$. This definition is fixed by Maxwell's equation and gives Gauss' law in curved spacetime,

$$q(r) = 4\pi \int_0^r \rho_e(\bar{r}) e^{\Lambda(\bar{r})} \bar{r}^2 d\bar{r}. \quad (139)$$

The tt Einstein equation may then be integrated once. The result is that the radial metric coefficient can be written as

$$e^{-2\Lambda(r)} = 1 - \frac{2Gm(r)}{c^2 r} + \frac{Gk_e q(r)^2}{c^4 r^2}, \quad (140)$$

where $m(r)$ is the Misner–Sharp mass generalized to include the electromagnetic contribution. This definition is chosen so that, outside the surface where $m(r) = M$ and $q(r) = Q$, Eq. (140) reduces exactly to the exterior Reissner–Nordström metric. It also has the correct neutral limit: when $q(r) = 0$, it becomes the usual interior Schwarzschild/TOV parametrization $e^{-2\Lambda} = 1 - 2Gm/(c^2 r)$.

With these definitions the interior line element can be written as

$$ds^2 = e^{2\Psi(r)} c^2 dt^2 - \left(1 - \frac{2Gm(r)}{c^2 r} + \frac{Gk_e q(r)^2}{c^4 r^2}\right)^{-1} dr^2 - r^2 d\Omega^2, \quad 0 \leq r < R. \quad (141)$$

This is therefore a convenient rewriting of the general static spherical metric, not a separate choice of equation of state or matter model. Once this form is adopted, the Einstein–Maxwell equations reduce to a closed system for $m(r)$, $q(r)$, $\Psi(r)$, and the fluid variables $\rho(r)$ and $P(r)$.

Let the matter sector be modeled as a perfect fluid with proper energy density ρ , pressure P , and proper charge density ρ_e . Then the charge function satisfies Gauss' law in curved spacetime,

$$\frac{dq}{dr} = 4\pi r^2 \rho_e e^{\Lambda(r)}. \quad (142)$$

The Einstein equations give the mass equation

$$\frac{dm}{dr} = 4\pi r^2 \rho + \frac{k_e q}{c^2 r} \frac{dq}{dr}, \quad (143)$$

where the second term represents the contribution of the electrostatic field to the total mass function.

The remaining independent Einstein equation yields

$$\frac{d\Psi}{dr} = \frac{\frac{Gm(r)}{c^2 r^2} + \frac{4\pi G}{c^4} r P - \frac{Gk_e q(r)^2}{c^4 r^3}}{1 - \frac{2Gm(r)}{c^2 r} + \frac{Gk_e q(r)^2}{c^4 r^2}}. \quad (144)$$

Hydrostatic equilibrium is obtained from local conservation of total stress-energy, equivalently from the Euler equation with the Lorentz-force term:

$$\frac{dP}{dr} = -(\rho c^2 + P) \frac{d\Psi}{dr} + \rho_e E e^{\Lambda(r)}. \quad (145)$$

Using Eq. (142) together with $E(r) = k_e q(r)/r^2$, this may be rewritten as

$$\frac{dP}{dr} = -(\rho c^2 + P) \frac{d\Psi}{dr} + \frac{k_e q(r)}{4\pi r^4} \frac{dq}{dr}. \quad (146)$$

Substituting Eq. (144) then gives the charged TOV equation in explicit form,

$$\frac{dP}{dr} = -(\rho c^2 + P) \frac{\frac{Gm(r)}{c^2 r^2} + \frac{4\pi G}{c^4} r P - \frac{Gk_e q(r)^2}{c^4 r^3}}{1 - \frac{2Gm(r)}{c^2 r} + \frac{Gk_e q(r)^2}{c^4 r^2}} + \frac{k_e q(r)}{4\pi r^4} \frac{dq}{dr}. \quad (147)$$

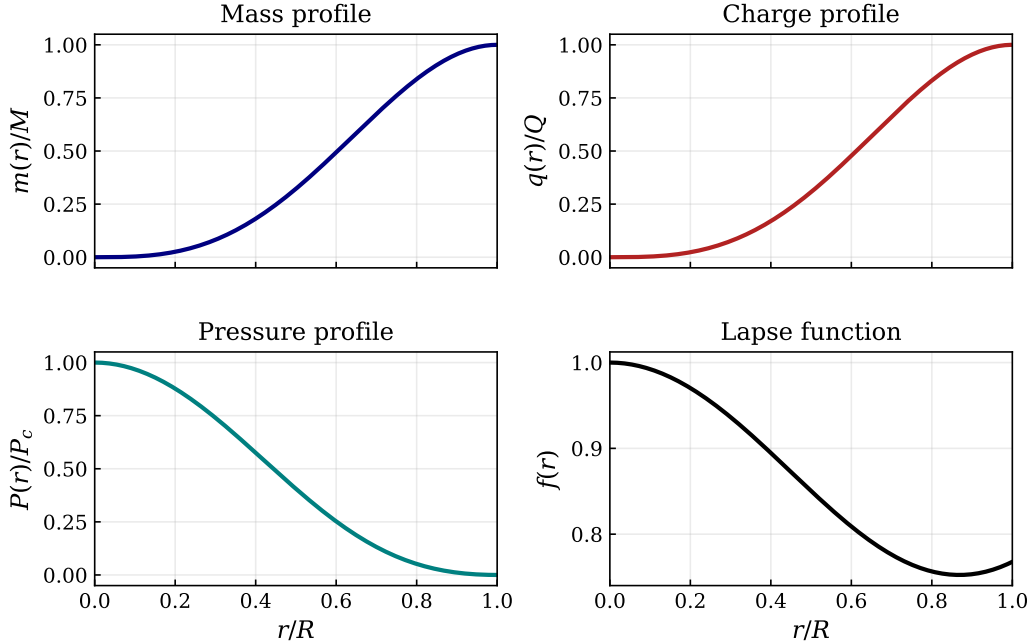


Figure 5: Single four-panel summary of an illustrative dimensionless charged-TOV integration for a regular Einstein–Maxwell interior with polytropic equation of state $P = K\rho^\Gamma$, $\Gamma = 2$, $K = 0.08$, and charge density $\rho_e = \alpha\rho$ with $\alpha = 0.08$, in units $G = c = k_e = 1$. The four panels show the normalized mass profile, charge profile, pressure profile, and lapse function. The figure is meant as a qualitative demonstration that a regular charged interior can be matched to an RN exterior without introducing a central singularity.

Equations (142), (143), and (147), supplemented by an equation of state $P = P(\rho)$ and by regularity conditions at $r = 0$, define the charged TOV problem for a regular astron interior. The boundary conditions are

$$m(0) = 0, \quad q(0) = 0, \quad P(0) = P_c, \quad (148)$$

and the surface $r = R$ is determined by

$$P(R) = 0. \quad (149)$$

The resulting solution is then matched to the exterior RN geometry with

$$m(R) = M, \quad q(R) = Q. \quad (150)$$

Thus, if astrons are interpreted as regular finite-radius charged compact objects, the Einstein–Maxwell TOV system provides the natural interior model. If instead one insists on the exact RN geometry all the way to the center, then no interior TOV description exists: one is dealing directly with a singular electrovac spacetime.

To illustrate what such a regular interior looks like, Fig. 5 shows a dimensionless charged-TOV integration for a simple polytropic equation of state $P = K\rho^\Gamma$ with $\Gamma = 2$, $K = 0.08$, and a proportional charge density $\rho_e = \alpha\rho$ with $\alpha = 0.08$, all in units $G = c = k_e = 1$. The purpose of the plot is not to present a calibrated astron model, but to make the structure of a regular Einstein–Maxwell interior explicit: the mass and charge functions rise monotonically from the center, the pressure falls smoothly to zero at the surface, and the lapse remains positive throughout the interior.

This discussion is especially transparent for the benchmark values proposed in Ref. [1]: the fiducial mass in Eq. (58) together with the charge in Eq. (68). For this branch one finds

$$\Xi_A = \frac{k_e Q_A^2}{GM_A^2} \simeq 5.4. \quad (151)$$

This is well above the extremal threshold $\Xi = 1$, so for the Frampton benchmark the horizon question is already settled by M_A and Q_A : no Reissner–Nordström horizon exists, independently of R . In this regime the radius no longer decides whether the astron is a black hole; it decides only how one interprets the interior. By contrast, the ordinary accretion-saturation charges derived in Secs. 2–4 correspond to $\Xi \ll 1$, so they lie extremely far from the super-extremal threshold.

This distinction is displayed quantitatively in Fig. 6, which shows the geometric parameter Ξ , defined in Eq. (103), for the different charge prescriptions as a function of mass. The charge is therefore not absent from the plot; rather, each curve is obtained by first choosing a mass–charge relation $Q(M)$ and then substituting it into $\Xi = k_e Q^2 / (GM^2)$. For the ordinary saturation estimates, $Q_{\text{sat}}^{(i)} \sim GMm_i / (k_e e)$, the charge scales linearly with M , so the factor of M^2 in Q^2 cancels the M^2 in the denominator of Ξ . The corresponding Ξ values are therefore essentially constant and extremely small. The Frampton branch, by contrast, uses $Q_F(M) = 10^{-52} M^2$. Substitution gives

$$\Xi_F(M) = \frac{k_e}{G} 10^{-104} M^2 = 1.35 \times 10^{-84} \left(\frac{M}{\text{kg}} \right)^2. \quad (152)$$

Equivalently, in solar-mass units,

$$\Xi_F(M) = 5.32 \times 10^{-24} \left(\frac{M}{M_\odot} \right)^2. \quad (153)$$

Thus the fiducial value $M_A = 10^{12} M_\odot$ gives

$$\Xi_F(M_A) \simeq 5.32. \quad (154)$$

The two relevant thresholds are reached at

$$\Xi_F = 1 : \quad M \simeq 8.62 \times 10^{41} \text{ kg} \simeq 4.33 \times 10^{11} M_\odot, \quad (155)$$

and

$$\Xi_F = \frac{9}{8} : \quad M \simeq 9.14 \times 10^{41} \text{ kg} \simeq 4.60 \times 10^{11} M_\odot. \quad (156)$$

For comparison, the ordinary saturation branches give the mass-independent values. In SI units the corresponding charge laws are

$$Q_{\text{sat}}^{(p)} \simeq 7.75 \times 10^{-29} \left(\frac{M}{\text{kg}} \right) \text{ C}, \quad Q_{\text{sat}}^{(e)} \simeq 4.22 \times 10^{-32} \left(\frac{M}{\text{kg}} \right) \text{ C}. \quad (157)$$

Substitution into Ξ gives

$$\Xi_{\text{sat}}^{(p)} = \frac{Gm_p^2}{k_e e^2} \simeq 8.09 \times 10^{-37}, \quad \Xi_{\text{sat}}^{(e)} = \frac{Gm_e^2}{k_e e^2} \simeq 2.40 \times 10^{-43}. \quad (158)$$

These numbers explain the visual structure of the plot: the ordinary saturation curves are horizontal and many orders of magnitude below extremality, whereas the Frampton curve rises as M^2 , appearing as a straight line of slope two on the log–log plot. It crosses both the extremality bound $\Xi = 1$ and the photon-sphere threshold $\Xi = 9/8$ in the range relevant to the fiducial astron benchmark. In this sense the

Geometric Charge Parameter Across Mass Scales

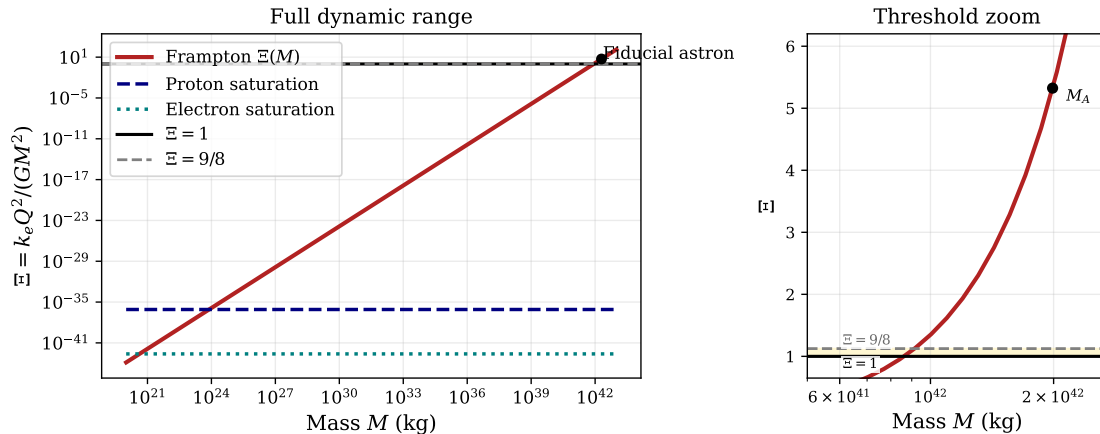


Figure 6: The dimensionless geometric charge parameter $\Xi = k_e Q^2 / (GM^2)$, defined in Eq. (103), as a function of mass after imposing a charge prescription $Q = Q(M)$. Thus Q is included implicitly in each curve. The Frampton extrapolation uses $Q_F = 10^{-52} M^2$, giving $\Xi_F \propto M^2$, while the ordinary proton- and electron-limited saturation charges scale as $Q_{\text{sat}} \propto M$, giving nearly constant Ξ . The left panel shows the full dynamic range, while the right panel zooms into the threshold region where the extremality line $\Xi = 1$, the photon-sphere threshold $\Xi = 9/8$, and the Frampton fiducial point would otherwise be compressed together on the logarithmic scale. The figure shows directly that ordinary saturation remains sub-extremal by an enormous margin, whereas the Frampton branch enters the super-extremal regime in the mass range of interest for astrons.

figure makes explicit that the “large-charge” astron proposal is not a small deformation of an ordinary charged compact object, but a transition into a different geometric sector of the Einstein–Maxwell system.

It is also useful to display separately the roles of the dimensionless parameters Ξ and η , defined in Eq. (103). Figure 7 shows the resulting classification in the (Ξ, η) plane. For $\Xi < 1$, the boundary $\eta = 1 + \sqrt{1 - \Xi}$ separates objects whose surfaces lie inside the outer RN horizon from those whose surfaces lie outside it. Once $\Xi > 1$, however, no Reissner–Nordström horizon exists at all, and varying R cannot restore one. This is precisely the sense in which (M, Q) control the horizon structure, while R controls only the interior matching whenever a horizon exists.

This point also clarifies how astrons relate to other classes of horizonless compact objects. A first relevant comparison is with gravastar-type models in the sense of Mazur and Mottola [49]. A gravastar replaces the central singularity by a regular interior, typically of de Sitter type, matched through a shell to an exterior Schwarzschild geometry; charged generalizations can likewise be matched to a Reissner–Nordström exterior. Gravastars therefore show explicitly that a horizonless object need not be singular. For astrons, this is conceptually useful because the same super-extremal RN exterior can be interpreted either as a naked singularity or as the exterior field of a regular finite-radius object.

If rotation is included, the relevant comparison shifts from Reissner–Nordström to Kerr and Kerr–Newman. In those spacetimes horizons disappear if the spin or the combined spin–charge parameters exceed their extremal limits, so over-rotating Kerr and over-extremal Kerr–Newman solutions are also naked singularities [52, 53]. These are close in spirit to the astron picture because Kerr–Newman shares the same Einstein–Maxwell origin as Reissner–Nordström while adding angular momentum. The static RN discussion given here should therefore be read as the simplest charge-dominated limit of a more general charged and rotating compact object.

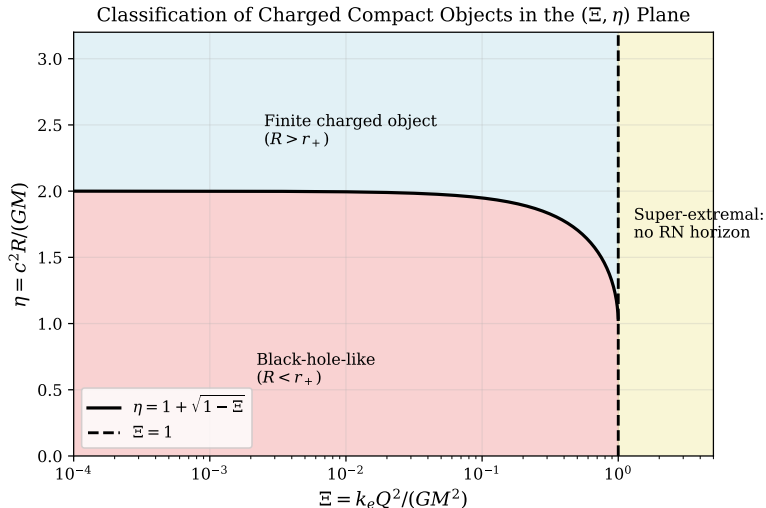


Figure 7: Classification of charged compact objects in the (Ξ, η) plane, with both parameters defined in Eq. (103). For $\Xi < 1$, the solid curve $\eta = 1 + \sqrt{1 - \Xi}$ separates black-hole-like configurations ($R < r_+$) from finite charged objects with surfaces outside the outer RN horizon ($R > r_+$). For $\Xi > 1$, the spacetime is super-extremal and no RN horizon exists, independently of the value of R .

For completeness, Appendix E records several standard naked-singularity metrics often used as comparison geometries, including the Janis–Newman–Winicour solution, the Zipoy–Voorhees metric, and the Tomimatsu–Sato family. They are useful mathematical reference points, but they are not the mechanism at work in the astron model: JNW is sourced by a scalar field, while Zipoy–Voorhees and Tomimatsu–Sato are vacuum multipole geometries rather than electrically charged compact-object exteriors.

The main lesson is therefore simple. Under spherical symmetry, no rotation, and an electrovac exterior, an astron is necessarily described outside the source by Reissner–Nordström geometry, and the control parameter is Ξ as defined in Eq. (103). Once Ξ is fixed, the radius R tells us whether a sub-extremal object lies inside or outside its outer horizon; in the super-extremal case it cannot change the absence of horizons. Accordingly, if one adopts the large Frampton charge, the astron is naturally driven into the super-extremal Einstein–Maxwell regime. Whether one then calls it a naked singularity or a horizonless overcharged compact object depends on whether the interior is taken to be singular or regular. In that precise sense, the astron scenario sits at the intersection between the Reissner–Nordström branch of naked singularities and the wider class of horizonless compact alternatives, including gravastar-like completions.

7 Extension to Rotating Astrons: Kerr–Newman Geometry and Dynamics

The analysis presented so far has been restricted to static, spherically symmetric configurations, for which the exterior geometry is of Reissner–Nordström type. A realistic astrophysical or primordial compact object, however, is expected to carry angular momentum. The natural generalization is therefore to stationary, axisymmetric configurations described by the Kerr–Newman solution of the Einstein–Maxwell equations. This extension is not merely technical: rotation modifies the extremality condition, the capture dynamics, and the stability properties of the charge sector in a qualitatively nontrivial way.

The Kerr–Newman metric in Boyer–Lindquist coordinates is

$$ds^2 = \frac{\Delta}{\Sigma} (c dt - a \sin^2 \theta d\phi)^2 - \frac{\Sigma}{\Delta} dr^2 - \Sigma d\theta^2 - \frac{\sin^2 \theta}{\Sigma} [(r^2 + a^2)d\phi - ac dt]^2, \quad (159)$$

where

$$\Sigma = r^2 + a^2 \cos^2 \theta, \quad \Delta = r^2 - \frac{2GM}{c^2} r + \frac{Gk_e Q^2}{c^4} + a^2, \quad (160)$$

and the rotation parameter is defined as

$$a = \frac{J}{Mc}. \quad (161)$$

The electromagnetic potential is correspondingly given by

$$A_\mu dx^\mu = -\frac{k_e Q r}{\Sigma} (c dt - a \sin^2 \theta d\phi). \quad (162)$$

The horizon structure is determined by the zeros of Δ ,

$$r_\pm = \frac{GM}{c^2} \pm \sqrt{\left(\frac{GM}{c^2}\right)^2 - \left(a^2 + \frac{Gk_e Q^2}{c^4}\right)}. \quad (163)$$

The condition for the existence of horizons is therefore

$$\left(\frac{GM}{c^2}\right)^2 \geq a^2 + \frac{Gk_e Q^2}{c^4}. \quad (164)$$

It is convenient to introduce the dimensionless parameters

$$\Xi_Q \equiv \frac{k_e Q^2}{GM^2}, \quad \Xi_J \equiv \frac{c^2 J^2}{G^2 M^4}, \quad (165)$$

in terms of which the extremality condition becomes

$$\Xi_Q + \Xi_J \leq 1. \quad (166)$$

This result generalizes the static Reissner–Nordström classification. In particular,

$$\Xi_Q + \Xi_J < 1: \quad \text{sub-extremal configuration with horizons,} \quad (167)$$

$$\Xi_Q + \Xi_J = 1: \quad \text{extremal configuration,} \quad (168)$$

$$\Xi_Q + \Xi_J > 1: \quad \text{super-extremal configuration without horizons.} \quad (169)$$

Thus rotation and charge compete in determining the global structure of the spacetime. For fixed mass, the presence of angular momentum reduces the maximal charge compatible with a horizon. In particular, the large-charge branch discussed in the static case is driven even more deeply into the super-extremal regime once rotation is included.

This structure is summarized in Fig. 8, which displays the Kerr–Newman extremality condition in the (Ξ_Q, Ξ_J) plane. The boundary $\Xi_Q + \Xi_J = 1$ separates the sub-extremal sector from the horizonless one. The static Reissner–Nordström analysis corresponds to the axis $\Xi_J = 0$; once rotation is added, the admissible charge compatible with a horizon is reduced still further. In this sense the rotating extension does not weaken the super-extremality problem of the large-charge branch, but sharpens it.

A second qualitative effect of rotation concerns the electromagnetic sector itself. A rotating compact object immersed in an external magnetic field develops an induced charge through the Wald mechanism. Parametrically,

$$Q_{\text{ind}} \sim 2BJ, \quad (170)$$

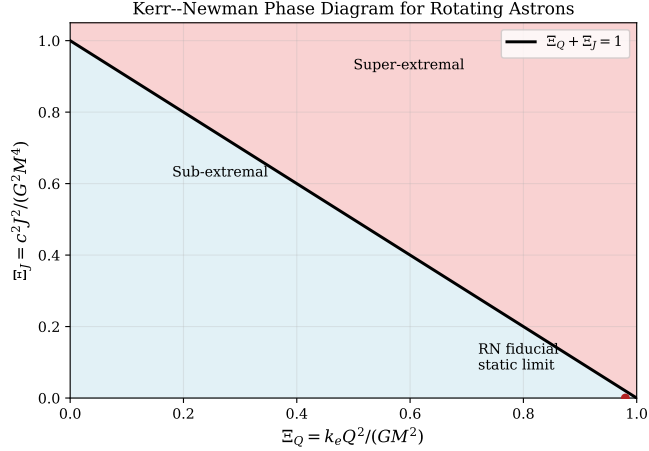


Figure 8: Kerr–Newman extremality diagram in terms of the dimensionless charge and spin parameters $\Xi_Q = k_e Q^2 / (GM^2)$ and $\Xi_J = c^2 J^2 / (G^2 M^4)$. The line $\Xi_Q + \Xi_J = 1$ separates sub-extremal configurations with horizons from super-extremal horizonless configurations. The static RN limit lies on the $\Xi_J = 0$ axis. The figure makes explicit that angular momentum further reduces the maximal charge compatible with a horizon.

where B is the characteristic magnetic field strength. This provides a dynamical mechanism for generating a nonzero charge even if the initial configuration is neutral. More importantly, it introduces a direct coupling between the evolution of the charge and that of the angular momentum. In the minimal capture model, the evolution equation for the charge is therefore modified to

$$\frac{dQ}{dt} = C_0 + C_1 Q + C_J J, \quad (171)$$

where the additional term encodes the rotationally induced contribution. This term can bias the sign of the charge and may therefore provide a microscopic mechanism for selecting a preferred branch of the evolution.

The capture process itself is also modified. In the static case, particle motion is governed by a central effective potential depending only on r . In the Kerr–Newman geometry the motion is axisymmetric rather than central: the energy and the axial angular momentum are conserved, but the total angular momentum is not. The relevant equations follow from the Hamilton–Jacobi separation found by Carter [54]. To make the structure transparent, we use geometrized units $G = c = k_e = 1$ in this paragraph; the derivation is given in Appendix H. For a massive species i , define the specific conserved quantities

$$\varepsilon_i \equiv \frac{E_i}{m_i}, \quad \ell_i \equiv \frac{L_{z,i}}{m_i}, \quad \alpha_i \equiv \frac{q_i}{m_i}, \quad (172)$$

where q_i is the particle charge. The Hamilton–Jacobi action may be written in separated form as

$$S_i = -\varepsilon_i t + \ell_i \phi + S_{r,i}(r) + S_{\theta,i}(\theta), \quad (173)$$

with the electromagnetic coupling included through $\partial_\mu S_i - \alpha_i A_\mu$. The separated equations are

$$\Sigma^2 \dot{r}^2 = \mathcal{R}_i(r), \quad \Sigma^2 \dot{\theta}^2 = \Theta_i(\theta), \quad (174)$$

where the overdot denotes differentiation with respect to proper time for a massive particle. The radial potential is

$$\mathcal{R}_i(r) = [(r^2 + a^2)\varepsilon_i - a\ell_i - \alpha_i Q r]^2 - \Delta [r^2 + (\ell_i - a\varepsilon_i)^2 + \mathcal{K}_i], \quad (175)$$

and the polar potential is

$$\Theta_i(\theta) = \mathcal{K}_i - \cos^2 \theta \left[a^2(1 - \varepsilon_i^2) + \frac{\ell_i^2}{\sin^2 \theta} \right]. \quad (176)$$

Here \mathcal{K}_i is the Carter constant. In the equatorial plane $\theta = \pi/2$, one has $\mathcal{K}_i = 0$. For neutral particles $\alpha_i = 0$; for a nonrotating source $a = 0$, the dependence on the orientation of L_z disappears and one recovers the central RN problem.

Equation (175) displays the three effects relevant for capture. The combination $(r^2 + a^2)\varepsilon_i - a\ell_i$ is the usual Kerr frame-dragging combination. It distinguishes co-rotating orbits ($a\ell_i > 0$) from counter-rotating orbits ($a\ell_i < 0$). The term $-\alpha_i Q r$ is the electromagnetic work term and has opposite sign for oppositely charged species. Finally, the Δ -term contains the rest-mass and angular barriers.

The turning points of the radial motion are the zeros of $\mathcal{R}_i(r)$. A particle arriving from large radius is captured if there is no outer turning point outside the surface of the object, or outside the outer horizon when a horizon exists. The boundary between scattering and capture is obtained from an unstable spherical orbit,

$$\mathcal{R}_i(r_c) = 0, \quad \frac{d\mathcal{R}_i}{dr}(r_c) = 0, \quad \frac{d^2\mathcal{R}_i}{dr^2}(r_c) < 0. \quad (177)$$

Solving these equations gives the critical values of ℓ_i and \mathcal{K}_i , hence the critical impact parameters of the incoming particle. Because the result depends separately on ℓ_i , \mathcal{K}_i , a , and the sign of $\alpha_i Q$, the capture cross section is no longer a single central quantity. Schematically,

$$\sigma_i = \sigma_i(\varepsilon_i, \ell_i, \mathcal{K}_i; a, Q), \quad (178)$$

and it is generally enhanced for co-rotating trajectories while being suppressed for counter-rotating trajectories. Charge further splits the electron and proton capture domains through the sign of $\alpha_i Q$.

This modification propagates into the saturation mechanism. In the static analysis, saturation occurs when Coulomb repulsion balances gravitational attraction for the species with the same sign as the object's charge, namely the species whose infall is being shut off. For the natural positive branch this species is the proton; for an imposed negative branch it is the electron. The corresponding force-balance condition may therefore be written as

$$GMm_* \sim k_e |Q| e, \quad (179)$$

with $m_* = m_p$ on the positive proton-limited branch and $m_* = m_e$ on the negative electron-limited branch. In the rotating case, the effective radial force includes an additional centrifugal contribution, leading schematically to

$$\frac{GMm_*}{R^2} \sim \frac{k_e |Q| e}{R^2} + \frac{J^2}{M^2 R^3}. \quad (180)$$

Thus rotation reduces the maximal charge attainable before accretion shuts off. To leading order, one may express this effect as a suppression of the saturation scale relative to the static value,

$$Q_{\max}(J) \simeq Q_{\max}(0) \left(1 - \frac{\Xi_J}{1 - \Xi_Q} \right), \quad (181)$$

showing explicitly that fast rotation stabilizes the system against further charge growth.

Rotation also introduces an ergoregion defined by the condition $g_{tt} > 0$, within which no static observers exist. This region allows for energy extraction processes analogous to the Penrose mechanism and may provide additional channels for dissipating angular momentum or redistributing energy in the surrounding plasma. In the absence of a horizon, the presence of an ergoregion can lead to dynamical instabilities, which are absent in the purely static case.

Finally, the optical properties are qualitatively modified. The notion of a photon sphere generalizes to a photon region, and the resulting lensing is no longer spherically symmetric. Frame dragging introduces

asymmetries in deflection angles and can distort the apparent shadow of the object. In strongly super-extremal configurations, the absence of a photon region leads to a suppression of strong-field lensing, reinforcing the conclusions obtained in the static analysis.

Taken together, these results show that the rotating extension of the astron scenario is governed by a two-parameter family (Ξ_Q, Ξ_J) rather than a single charge parameter. Rotation provides both a mechanism for generating charge and an additional constraint on its maximal value. It also strengthens the conclusion that the large-charge branch corresponds to a deeply super-extremal regime, whose physical realization depends sensitively on the interior completion and on the stability of horizonless configurations. In this sense, the static Reissner–Nordström analysis should be regarded as a limiting case of a more general Kerr–Newman framework in which charge and rotation are intrinsically coupled.

8 Lensing Around an Astron Singularity

If astrons are described by highly charged compact objects whose exterior geometry is of Reissner–Nordström type, then their lensing properties are controlled by null geodesics in the metric below. This discussion is purely geometrical, but it is closely related to the radiative lens-equation and post-Newtonian analyses of photon and neutrino lensing in black-hole backgrounds, as well as to electroweak corrections to photon scattering and polarization in a gravitational field [55, 56].

$$ds^2 = f(r)c^2 dt^2 - f(r)^{-1} dr^2 - r^2 d\Omega^2, \quad f(r) = 1 - \frac{2GM_A}{c^2 r} + \frac{Gk_e Q_A^2}{c^4 r^2}. \quad (182)$$

In the equatorial plane, $\theta = \pi/2$, the null geodesics satisfy

$$\dot{r}^2 + V_{\text{eff}}(r) = E^2, \quad V_{\text{eff}}(r) = \frac{L^2}{r^2} f(r), \quad (183)$$

where E and L are the conserved photon energy and angular momentum. The bending angle is therefore determined by the effective potential V_{eff} , exactly as in the Schwarzschild case, but now modified by the charge term Q_A^2/r^2 .

A first important difference from Schwarzschild appears in the existence of a photon sphere. Circular null orbits satisfy

$$\frac{d}{dr} \left(\frac{f(r)}{r^2} \right) = 0, \quad (184)$$

which gives

$$r^2 - 3 \frac{GM_A}{c^2} r + 2 \frac{Gk_e Q_A^2}{c^4} = 0. \quad (185)$$

Hence the photon-sphere radii are

$$r_{\text{ph}}^{\pm} = \frac{GM_A}{2c^2} \left(3 \pm \sqrt{9 - 8\Xi} \right). \quad (186)$$

Here Ξ is the parameter defined in Eq. (103), evaluated for M_A and Q_A . Real photon spheres therefore exist only if

$$\Xi \leq \frac{9}{8}. \quad (187)$$

By contrast, horizons exist only for

$$\Xi \leq 1. \quad (188)$$

This leads to three qualitatively different regimes:

$$\Xi < 1 : \text{ charged black hole with horizon and photon sphere,} \quad (189)$$

$$1 < \Xi \leq \frac{9}{8} : \text{ naked singularity, but still with a photon sphere,} \quad (190)$$

$$\Xi > \frac{9}{8} : \text{ naked singularity without a photon sphere.} \quad (191)$$

The geometry behind these three regimes is shown explicitly in Fig. 9. As Ξ increases from the Schwarzschild limit, the outer and inner RN horizons move toward each other and merge at $\Xi = 1$. The outer photon-sphere radius persists slightly beyond extremality and disappears only at $\Xi = 9/8$. The interval $1 < \Xi \leq 9/8$ is therefore special: it corresponds to a horizonless configuration that still retains a photon sphere and can consequently mimic part of the strong-lensing structure of a black hole. Once $\Xi > 9/8$, even this last remnant of black-hole-like optics is lost.

Here the phrase photon sphere has a precise meaning: it denotes the unstable circular null orbit, or in a rotating geometry the corresponding photon region, that underlies the usual black-hole shadow, photon ring and logarithmic strong-deflection behaviour. Its absence should not be confused with the absence of gravitational lensing. A massive astron still deflects light through the ordinary gravitational field, and in the weak-field regime the leading Schwarzschild-like bending term remains present. What is lost when the photon sphere disappears is the black-hole-like strong-lensing structure associated with light orbiting the compact object many times before escaping.

8.1 Schwarzschild versus extremal Reissner–Nordström lensing

A useful elementary comparison is obtained by fixing the mass and comparing the Schwarzschild metric with the extremal Reissner–Nordström metric. In geometrized units, $G = c = k_e = 1$, the line element is

$$ds^2 = f(r)dt^2 - f(r)^{-1}dr^2 - r^2d\Omega^2, \quad f(r) = 1 - \frac{2M}{r} + \frac{Q^2}{r^2}. \quad (192)$$

Schwarzschild corresponds to $Q = 0$, while extremal RN corresponds to $Q^2 = M^2$, namely

$$f_{\text{Schw}}(r) = 1 - \frac{2M}{r}, \quad f_{\text{ext}}(r) = 1 - \frac{2M}{r} + \frac{M^2}{r^2} = \left(1 - \frac{M}{r}\right)^2. \quad (193)$$

The two metrics have the same $1/r$ term, but differ at order $1/r^2$. This already shows why their lensing can agree at leading weak-field order while being different beyond leading order.

For equatorial null geodesics, the conserved energy and angular momentum are

$$E = f(r)\dot{t}, \quad L = r^2\dot{\phi}, \quad (194)$$

and the null condition gives

$$\dot{r}^2 = E^2 - \frac{L^2}{r^2}f(r). \quad (195)$$

Equivalently, with impact parameter $b = L/E$, the distance of closest approach r_0 satisfies

$$b^2 = \frac{r_0^2}{f(r_0)}. \quad (196)$$

The bending angle is therefore

$$\hat{\alpha}(b) = 2 \int_{r_0}^{\infty} \frac{b dr}{r^2 \sqrt{1 - b^2 f(r)/r^2}} - \pi. \quad (197)$$

Expanding this integral for $M/b \ll 1$ and $Q^2/b^2 \ll 1$ gives

$$\hat{\alpha}_{\text{RN}}(b) = \frac{4M}{b} + \frac{\pi}{4b^2} (15M^2 - 3Q^2) + O(b^{-3}). \quad (198)$$

Thus the leading term is identical for Schwarzschild and extremal RN,

$$\hat{\alpha}_{\text{Schw}}(b) = \frac{4M}{b} + \frac{15\pi M^2}{4b^2} + O(b^{-3}), \quad (199)$$

whereas

$$\hat{\alpha}_{\text{ext}}(b) = \frac{4M}{b} + \frac{3\pi M^2}{b^2} + O(b^{-3}). \quad (200)$$

The equality is therefore only a leading weak-field equality. The charge term reduces the next-to-leading focusing correction.

The strong-lensing difference is even clearer from the photon sphere. Circular null orbits are extrema of $f(r)/r^2$, so

$$\frac{d}{dr} \left(\frac{f(r)}{r^2} \right) = 0. \quad (201)$$

This condition gives

$$r^2 - 3Mr + 2Q^2 = 0. \quad (202)$$

For Schwarzschild this gives the usual photon sphere. The critical impact parameter follows from the same radial equation. At a circular null orbit one has $\dot{r} = 0$, and therefore

$$E^2 = \frac{L^2}{r_{\text{ph}}^2} f(r_{\text{ph}}). \quad (203)$$

Since the impact parameter is $b = L/E$, Eq. (203) immediately gives

$$b_c^2 = \frac{r_{\text{ph}}^2}{f(r_{\text{ph}})}, \quad b_c = \frac{r_{\text{ph}}}{\sqrt{f(r_{\text{ph}})}}. \quad (204)$$

For Schwarzschild this gives

$$r_{\text{ph}}^{\text{Schw}} = 3M, \quad b_c^{\text{Schw}} = \frac{r_{\text{ph}}}{\sqrt{f(r_{\text{ph}})}} = 3\sqrt{3} M. \quad (205)$$

For extremal RN, $Q^2 = M^2$, the roots are $r = M$ and $r = 2M$. The external unstable photon sphere is

$$r_{\text{ph}}^{\text{ext}} = 2M, \quad b_c^{\text{ext}} = \frac{2M}{\sqrt{f_{\text{ext}}(2M)}} = 4M. \quad (206)$$

Thus the critical impact parameter, and hence the shadow scale in this spherically symmetric comparison, is smaller for extremal RN than for Schwarzschild at the same mass. The two spacetimes therefore do not have identical lensing: they agree only in the leading asymptotic weak-field term.

This classification is crucial for lensing. If a photon sphere exists, then the spacetime can support strong-field lensing with large deflection angles and the usual sequence of relativistic images associated with photons that loop around the compact object many times. In that case, a naked singularity can mimic several of the optical features often associated with black holes. If no photon sphere exists, however, the lensing structure changes qualitatively: the logarithmic strong-deflection regime disappears, there is no infinite sequence of relativistic images, and the object does not possess the standard photon-sphere shadow characteristic of Schwarzschild or Kerr black holes. For the benchmark astron parameters one finds the value in Eq. (151), namely $\Xi_A \simeq 5.4$. This is far above both the horizon threshold $\Xi = 1$ and the photon-sphere threshold $\Xi = 9/8$. Thus, if one adopts this large-charge benchmark literally, the corresponding astron would be a strongly super-extremal naked singularity with no photon sphere. In that regime one should not expect the standard strong-lensing phenomenology of a black hole. This statement is not a claim of optical invisibility: the astron mass still produces gravitational deflection. The lensing

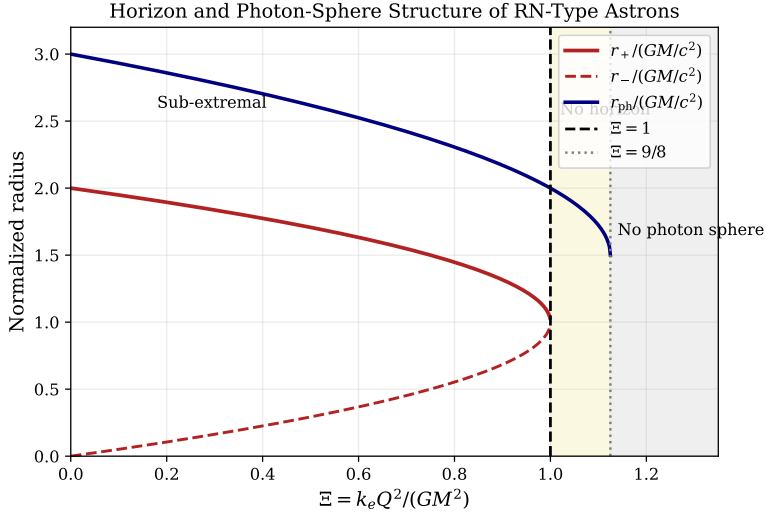


Figure 9: Normalized Reissner–Nordström characteristic radii as functions of Ξ , defined in Eq. (103). The outer and inner horizons r_{\pm} exist only for $\Xi \leq 1$, where they merge at extremality. The outer photon-sphere radius survives into the mildly super-extremal regime and disappears only at $\Xi = 9/8$. This figure makes transparent why the interval $1 < \Xi \leq 9/8$ is lensing-relevant: the object is already horizonless, but it still possesses a photon sphere.

would instead be dominated by ordinary weak-field deflection, with charge corrections that tend to reduce the total bending angle.

Indeed, in the weak-field regime the deflection angle for a Reissner–Nordström lens can be expanded as

$$\hat{\alpha}(b) \simeq \frac{4GM_A}{c^2 b} + \frac{3\pi}{4b^2} \left(5 \frac{G^2 M_A^2}{c^4} - \frac{G k_e Q_A^2}{c^4} \right), \quad (207)$$

where b is the impact parameter. The first term is the usual Schwarzschild bending, while the charge contribution enters with the opposite sign at the next order and therefore weakens the focusing effect. In this sense, electric charge acts against gravitational lensing rather than enhancing it.

This suppression can be displayed directly by isolating the coefficient of the b^{-2} term. Relative to Schwarzschild, the corresponding RN correction is reduced by the factor $(5 - \Xi)/5$, which decreases linearly with Ξ and changes sign for sufficiently large charge. Figure 10 shows this normalized coefficient together with the extremality threshold, the photon-sphere threshold, and the fiducial astron value. The main message is not that the weak-field expansion remains quantitatively trustworthy arbitrarily close to the source, but that already at the level of the analytic correction term the trend is monotonic: increasing charge weakens the second-order focusing effect.

It is useful to compare this behaviour with other naked-singularity families. The Janis–Newman–Winicour spacetime provides a scalar-field example in which, depending on the scalar charge, a photon sphere may or may not exist. In this respect the astron singularity resembles JNW geometries at the level of lensing phenomenology: both may fall either into a black-hole-like strong-lensing class or into a weakly focusing class without a photon sphere. The physical origin, however, is different. In the astron case the suppression of lensing is driven by electric charge in the Einstein–Maxwell sector, whereas in JNW it is driven by a scalar field.

The main conclusion is therefore simple. If the astron charge is large enough to make the object only mildly super-extremal, then strong lensing similar to that of a black hole may still survive. If, however, one adopts the much larger charge benchmark in Eq. (68), then the object lies deep in the regime $\Xi > 9/8$,

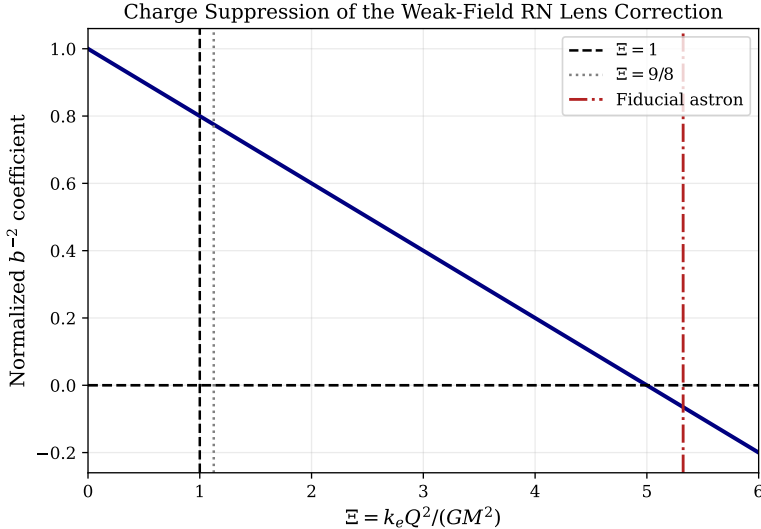


Figure 10: Normalized coefficient of the b^{-2} correction in the weak-field Reissner–Nordström bending angle, relative to its Schwarzschild value. The coefficient decreases linearly with Ξ , showing that electric charge weakens the next-to-leading focusing term. The vertical markers indicate the extremality threshold, the photon-sphere threshold, and the fiducial astron value.

where the photon sphere disappears and the standard black-hole-like lensing structure is lost. Thus lensing directly measures how far into the super-extremal regime the astron hypothesis is being pushed.

9 Lyman- α Absorption as a Probe of Astron Electric Fields

The lensing discussion probes the metric produced by an astron. A different kind of observable would probe the electric field itself. The natural astrophysical system to consider is neutral hydrogen, since the spectra of high-redshift quasars contain many intervening Lyman- α absorption features. The Lyman- α forest is produced when quasar light crosses neutral hydrogen clouds at different redshifts. The rest-frame transition is the $1s \rightarrow 2p$ absorption line of hydrogen,

$$\lambda_\alpha = 1215.67 \text{ \AA}, \quad (208)$$

so an absorber at redshift z_{abs} produces a line at

$$\lambda_{\text{obs}} = \lambda_\alpha (1 + z_{\text{abs}}). \quad (209)$$

Many absorbers along the same line of sight generate the forest of absorption features observed blueward of the quasar Lyman- α emission line [27, 29]. Denser neutral systems, such as Lyman-limit systems and damped Lyman- α absorbers, provide related probes of neutral hydrogen with larger column densities and more complicated astrophysical environments.

The possible connection with astrons is conceptually simple. Neutral hydrogen does not experience a net Coulomb acceleration as a charged particle would, but it is polarizable. For an absorber i , the observed line would be schematically

$$\lambda_{\text{obs},i,\alpha} = (1 + z_i) \left[\lambda_\alpha^{(0)} + \Delta\lambda_\alpha(E_i) \right], \quad E_i = E(r_i; Q_A, \lambda_D, \text{environment}), \quad (210)$$

where α labels a possible Stark component. The field-dependent part is therefore absorber-dependent rather than a universal shift of the whole forest.

For hydrogen, an external electric field perturbs the atomic Hamiltonian by

$$H_{\text{Stark}} = e \mathbf{E} \cdot \mathbf{r}, \quad (211)$$

or $H_{\text{Stark}} = eEz$ if the field is chosen along the z -axis. In the ideal Coulomb problem, the $n = 2$ level contains $2n^2 = 8$ spin states, and the $2s$ state mixes linearly with the $2p, m = 0$ state. The two shifted linear combinations have

$$\Delta E_{2,\pm} = \pm 3ea_0E, \quad (212)$$

while the ground state has no linear Stark shift in the same approximation. More generally, in parabolic quantum numbers,

$$\Delta E_{n,k} = \frac{3}{2} n k ea_0E, \quad (213)$$

where a_0 is the Bohr radius, $E = |\mathbf{E}|$, and k is the parabolic quantum-number difference. Since Lyman- α absorption involves the $n = 2$ level, the characteristic frequency scale is therefore

$$\Delta\nu_2 \sim \frac{3ea_0E}{h}. \quad (214)$$

Equivalently, using $E_{21} \simeq 10.2 \text{ eV}$,

$$\left| \frac{\Delta\lambda}{\lambda} \right| \simeq \frac{3ea_0E}{E_{21}} \simeq 1.6 \times 10^{-11} \left(\frac{E}{1 \text{ V m}^{-1}} \right), \quad (215)$$

or

$$\Delta v \simeq 4.7 \times 10^{-3} \left(\frac{E}{1 \text{ V m}^{-1}} \right) \text{ m s}^{-1}. \quad (216)$$

An unscreened astron electric field could therefore in principle induce Stark shifts, line splittings or excess broadening of neutral-hydrogen absorption features, but the required field scale is large.

For an isolated astron with charge Q_A , the unscreened field is

$$E_A(r) = \frac{k_e Q_A}{r^2}. \quad (217)$$

At a megaparsec this gives

$$E_A(1 \text{ Mpc}) \simeq 3.8 \times 10^{-3} \text{ V m}^{-1} \left(\frac{Q_A}{4 \times 10^{32} \text{ C}} \right). \quad (218)$$

Substituting this value into Eq. (214) gives only

$$\Delta\nu_2 \sim 1.5 \times 10^2 \text{ Hz} \left(\frac{E_A}{4 \times 10^{-3} \text{ V m}^{-1}} \right), \quad (219)$$

or a velocity-equivalent shift

$$\Delta v \sim c \frac{\Delta\nu_2}{\nu_\alpha} \sim 2 \times 10^{-5} \text{ m s}^{-1}. \quad (220)$$

This is completely negligible compared with ordinary thermal and turbulent line widths in the intergalactic medium. For example, a hydrogen cloud at $T \sim 10^4 \text{ K}$ has a thermal Doppler parameter

$$b_{\text{th}} = \left(\frac{2k_B T}{m_H} \right)^{1/2} \simeq 13 \text{ km s}^{-1}. \quad (221)$$

Thus a megaparsec-scale unscreened field would not produce a directly resolvable Stark splitting in an ordinary Lyman- α forest line.

One can invert the estimate to see what field would be needed. Requiring a frequency shift comparable to a Doppler width b gives

$$E_{\text{req}} \sim \frac{h\nu_\alpha}{3ea_0} \frac{b}{c} \simeq 2 \times 10^6 \text{ V m}^{-1} \left(\frac{b}{10 \text{ km s}^{-1}} \right). \quad (222)$$

For the fiducial charge this unscreened field occurs only within

$$r_{\text{req}} \sim \left(\frac{k_e Q_A}{E_{\text{req}}} \right)^{1/2} \simeq 40 \text{ pc} \left(\frac{Q_A}{4 \times 10^{32} \text{ C}} \right)^{1/2} \left(\frac{10 \text{ km s}^{-1}}{b} \right)^{1/2}. \quad (223)$$

This is much smaller than the typical inter-astron separation and lies in a region where the gas may be ionized, dynamically disturbed, or otherwise different from the diffuse neutral absorbers responsible for the usual forest. The more promising targets would therefore not be generic forest lines far from the source, but unusually neutral gas associated with the astron environment, such as high-column-density absorbers or extended gas clouds in which some neutral fraction survives.

The calculation above gives the natural scale of the effect in the ideal hydrogen problem. In realistic absorbers the $n = 2$ degeneracy is already split by fine structure, hyperfine structure and the Lamb shift, while the observed Lyman- α profile is shaped by thermal broadening, peculiar velocities, Hubble flow across the absorber, saturation, radiative transfer and instrumental resolution [27, 28]. For a megaparsec-distance fiducial astron field, the Stark scale is far below these astrophysical widths. The useful conclusion is therefore qualitative: generic forest lines are not expected to resolve a far-field splitting, whereas neutral gas much closer to an unscreened source could in principle probe the survival of the electric field.

Screening introduces a further suppression. If the field is Yukawa screened on a scale λ_D , the electrostatic potential is approximately

$$\Phi(r) \simeq \frac{k_e Q_A}{r} e^{-r/\lambda_D}, \quad (224)$$

and the radial field becomes

$$E(r) \simeq \frac{k_e Q_A}{r^2} \left(1 + \frac{r}{\lambda_D} \right) e^{-r/\lambda_D}. \quad (225)$$

Thus if $\lambda_D \ll r$, the neutral hydrogen sees essentially no long-range electric field. A Lyman- α Stark signal would therefore be a direct probe not only of the charge but also of the survival of the electric field through the surrounding plasma. Conversely, the absence of such a signal in systems expected to pass close to an astron environment would bound the combination of Q_A , λ_D , and the neutral-gas geometry.

The observational role of Lyman- α absorption is consequently best understood as a way to constrain the model rather than as an immediate discovery channel. A positive signal would require a rare alignment in which neutral hydrogen lies sufficiently close to an unscreened astron field while remaining cool and neutral enough to produce identifiable absorption. A null result, especially in high-column-density neutral systems near candidate massive dark seeds, could instead bound the combination of charge, screening length and neutral gas geometry. In this sense, Lyman- α absorption complements lensing: lensing tests the metric and photon-sphere structure, while Lyman- α spectroscopy tests whether the electric field itself survives into regions containing neutral hydrogen.

10 Cosmological Implications of the Homogeneous Approximation

The large-scale dynamics of the Universe in the presence of an astron population must first be compared with the standard homogeneous FLRW framework. In units $c = 1$, the metric is

$$ds^2 = dt^2 - a(t)^2 \left[\frac{dr^2}{1 - kr^2} + r^2 d\Omega^2 \right]. \quad (226)$$

For this metric the Einstein tensor has the components

$$G_{00} = 3 \left(H^2 + \frac{k}{a^2} \right), \quad G^i_j = \left(2 \frac{\ddot{a}}{a} + H^2 + \frac{k}{a^2} \right) \delta^i_j, \quad (227)$$

where $H = \dot{a}/a$. A homogeneous and isotropic source is a perfect fluid,

$$T_{\mu\nu} = (\rho + p)u_\mu u_\nu - pg_{\mu\nu}, \quad u^\mu = (1, 0, 0, 0). \quad (228)$$

Substituting these expressions into Einstein's equations gives the Friedmann equations

$$H^2 \equiv \left(\frac{\dot{a}}{a} \right)^2 = \frac{8\pi G}{3} \rho_{\text{tot}} - \frac{k}{a^2}, \quad (229)$$

$$\frac{\ddot{a}}{a} = -\frac{4\pi G}{3} (\rho_{\text{tot}} + 3p_{\text{tot}}). \quad (230)$$

The Bianchi identity gives the continuity equation

$$\dot{\rho} + 3H(\rho + p) = 0. \quad (231)$$

Thus a component with $p = w\rho$ scales as

$$\rho(a) = \rho_0 a^{-3(1+w)}. \quad (232)$$

Matter, radiation, and a cosmological constant therefore scale as

$$\rho_m \propto a^{-3}, \quad \rho_r \propto a^{-4}, \quad \rho_\Lambda = \text{const.} \quad (233)$$

In the traditional Λ CDM analysis, the observed acceleration is produced by the last component: $\rho_\Lambda = \text{const.}$, $p_\Lambda = -\rho_\Lambda$, so that $\rho_\Lambda + 3p_\Lambda = -2\rho_\Lambda < 0$. The question for the astron scenario is whether the charged population can generate an analogous late-time source, or whether it merely adds ordinary matter and radiation-like terms.

It is useful to compare this homogeneous treatment with exact Einstein–Maxwell constructions in which multiple charged black holes are embedded in a cosmological geometry. Such solutions show explicitly that electric charge can modify the size of the cosmological region and contribute to backreaction effects, while still allowing well-defined charged black-hole cosmologies [15]. They therefore support the broader idea that charged compact objects can be incorporated consistently into cosmological settings, even if they do not by themselves provide late-time acceleration.

In a homogeneous reduction the astron sector has two conceptually different pieces. The first is the rest-mass density of the compact objects. If the comoving number density is conserved, then

$$n_A(a) = n_{A0} a^{-3}, \quad \rho_{M,A} = M_A n_A \propto a^{-3}, \quad (234)$$

so the astron rest mass behaves like dust. The second is the electromagnetic interaction energy of the charged population. Thus, schematically,

$$\rho_{\text{tot}} = \rho_m + \rho_{M,A} + \rho_C, \quad (235)$$

where ρ_m denotes the non-astron matter sector and ρ_C denotes the coarse-grained Coulomb interaction energy.

At this stage it is important to state clearly what this homogeneous treatment can and cannot establish. If one wishes to reproduce a genuine cosmological-constant sector within FLRW, one needs an effectively constant energy density,

$$\rho_\Lambda = \text{const.}, \quad p_\Lambda = -\rho_\Lambda, \quad w_\Lambda = -1. \quad (236)$$

In that case the Friedmann equation acquires an additive constant term and the late-time expansion approaches de Sitter behavior. The question addressed in this section is therefore whether the simplest homogeneous reduction of the astron interaction sector produces anything of that type. As we now show, it does not.

The matter component evolves as usual,

$$\rho_m = \rho_{m0} a^{-3}. \quad (237)$$

The homogeneous Coulomb contribution follows from a simple scaling argument. If the typical physical separation is $L(a) = aL_c$, then a pairwise Coulomb energy scales as

$$V_C(L) \sim \frac{k_e Q_A^2}{L} \propto a^{-1}. \quad (238)$$

Since $n_A \propto a^{-3}$, the interaction energy density scales as

$$\rho_C \sim n_A V_C \propto a^{-4}. \quad (239)$$

Equivalently, in a comoving volume $V \propto a^3$, the total Coulomb energy scales as $U_C = \rho_C V \propto a^{-1}$. The work relation $dU_C = -p_C dV$ then gives

$$p_C = \frac{1}{3} \rho_C. \quad (240)$$

The modified Friedmann equation therefore takes the form

$$H^2 = \frac{8\pi G}{3} (\rho_{m0} a^{-3} + \rho_{M,A0} a^{-3} + \rho_{C0} a^{-4}). \quad (241)$$

This scaling law implies that the astron contribution behaves formally as a radiation-like component at the level of the continuity equation. Its microscopic origin is different from that of ordinary radiation, but its homogeneous redshift behaviour is the same. In particular, the interaction term is not constant in time. For that reason alone it cannot be identified with a cosmological constant in the strict FLRW sense.

To characterize the effective equation of state, one considers the conservation equation

$$\dot{\rho}_C + 3H(\rho_C + p_C) = 0. \quad (242)$$

Substituting $\rho_C \propto a^{-4}$ yields

$$p_C = \frac{1}{3} \rho_C. \quad (243)$$

At the level of the homogeneous background, the astron contribution therefore corresponds to an effective equation-of-state parameter

$$w_C = \frac{1}{3}. \quad (244)$$

This result is already highly constraining. Although the Coulomb interaction is repulsive, the associated homogeneous energy density redshifts as a^{-4} and therefore does not mimic a cosmological constant. In particular, it does not generate a constant source term in the Friedmann equation and does not provide a de Sitter-like late-time solution. This is the precise sense in which the homogeneous astron sector does not, by itself, justify the cosmological constant.

To make contact with observations, it is useful to rewrite the Friedmann equation in terms of redshift $z = a^{-1} - 1$,

$$H^2(z) = H_0^2 [\Omega_{m0}^{\text{eff}} (1+z)^3 + \Omega_{C0} (1+z)^4], \quad (245)$$

where Ω_{m0}^{eff} includes ordinary nonrelativistic matter and the astron rest-mass contribution.

This should be compared with the standard Λ CDM expression,

$$H_{\Lambda\text{CDM}}^2(z) = H_0^2 [\Omega_{m0}(1+z)^3 + \Omega_\Lambda]. \quad (246)$$

The two models differ sharply in their late-time behaviour. In Λ CDM, the constant term Ω_Λ dominates asymptotically, leading to exponential expansion,

$$a(t) \sim e^{H_\Lambda t}. \quad (247)$$

In contrast, in the homogeneous astron approximation the interaction term decays as $(1+z)^4$, implying that it becomes subdominant at sufficiently late times. The expansion therefore returns asymptotically to matter domination,

$$a(t) \propto t^{2/3}. \quad (248)$$

This distinction is not merely quantitative but qualitative. A radiation-like term may temporarily contribute to the energy budget, but it cannot act as a constant vacuum component. Therefore, even if one normalizes ρ_A so that it is comparable to the matter density at some epoch, the model still lacks the constant late-time driver that characterizes Λ CDM.

Equivalently, the homogeneous astron interaction cannot provide an asymptotic acceleration era. A component with $\rho_C \propto a^{-4}$ becomes less important relative to matter as the universe expands and cannot approach a de Sitter fixed point. Thus, even in a phenomenological interpretation in which the charged sector affects the expansion over some finite interval, that effect is transitory unless additional physics beyond the homogeneous perfect-fluid reduction is supplied.

The present epoch may correspond to a regime in which the Coulomb contribution is comparable to the matter density,

$$\rho_C \sim \rho_m, \quad (249)$$

but that fact alone does not imply acceleration.

The deceleration parameter is

$$q = -\frac{\ddot{a}}{aH^2} = \frac{1}{2} \left(1 + 3 \frac{p_{\text{tot}}}{\rho_{\text{tot}}} \right). \quad (250)$$

Substituting the components yields

$$q(z) = \frac{1}{2} \frac{\Omega_{m0}^{\text{eff}}(1+z)^3 + 2\Omega_{C0}(1+z)^4}{\Omega_{m0}^{\text{eff}}(1+z)^3 + \Omega_{C0}(1+z)^4}. \quad (251)$$

For positive densities, the expression above is always positive. The homogeneous perfect-fluid reduction presented here therefore does *not* generate accelerated expansion, and in particular it cannot generate asymptotically late-time acceleration. Instead, it shows that the simplest FLRW treatment of the astron interaction sector behaves like an additional radiation-like component. This is the most direct way to formulate the limitation emphasized above: within homogeneous FLRW, astrons do not produce a constant solution and therefore do not reproduce dark energy in the form of a cosmological constant. Any acceleration era associated with the homogeneous interaction energy would have to be a finite-epoch effect, not a de Sitter asymptote.

This observation should be read as a limitation, not as a failure of the broader idea. A cosmological implementation based on discrete charged objects may require physics beyond a homogeneous perfect-fluid description, for example genuinely inhomogeneous dynamics, non-perturbative backreaction, or a different coarse-graining prescription. However, none of those effects is derived in the present paper. What can be stated firmly is that the simplest background treatment is insufficient to replace Λ CDM, and that any stronger cosmological claim must rely on physics beyond the homogeneous approximation.

11 Backreaction Beyond the Homogeneous Approximation

The failure of the homogeneous FLRW reduction does not automatically rule out the astron framework. It does, however, identify the central open problem. The astron scenario is intrinsically one of a sparse population of discrete, extremely massive, charged compact objects interacting through long-range gravitational and electromagnetic fields. Such a system is not obviously equivalent to a homogeneous perfect fluid, and reducing it to one may erase precisely the effects one would hope to retain. The natural place to revisit the cosmology is therefore the backreaction problem: whether averaging the Einstein–Maxwell dynamics of an inhomogeneous astron population can lead to an effective large-scale evolution that differs significantly from the naive FLRW result.

In cosmology, backreaction refers to the fact that averaging and time evolution need not commute in a nonlinear theory such as general relativity. This issue has been discussed extensively in the literature, both from the point of view of constructive averaging formalisms and from the point of view of mathematically controlled limitations [16,18]. The central question is whether small- or intermediate-scale inhomogeneities can feed back into the effective expansion of the Universe strongly enough to mimic, enhance, or otherwise modify the role that would conventionally be assigned to dark energy.

The simplest formal framework in which to express this idea is Buchert averaging, originally developed for irrotational dust cosmologies [16]. For a scalar quantity S , the spatial average over a domain \mathcal{D} is defined by

$$\langle S \rangle_{\mathcal{D}} = \frac{1}{V_{\mathcal{D}}} \int_{\mathcal{D}} S \sqrt{h} d^3x, \quad V_{\mathcal{D}}(t) = \int_{\mathcal{D}} \sqrt{h} d^3x, \quad (252)$$

where h is the determinant of the induced spatial metric. The effective scale factor associated with the domain is

$$a_{\mathcal{D}}(t) \equiv \left(\frac{V_{\mathcal{D}}(t)}{V_{\mathcal{D}}(t_0)} \right)^{1/3}. \quad (253)$$

Since the volume element evolves according to

$$\partial_t \sqrt{h} = \theta \sqrt{h}, \quad (254)$$

where θ is the local expansion scalar, one obtains

$$\frac{\dot{a}_{\mathcal{D}}}{a_{\mathcal{D}}} = \frac{1}{3} \langle \theta \rangle_{\mathcal{D}}. \quad (255)$$

For irrotational dust, the two scalar local equations are the Hamiltonian constraint and the Raychaudhuri equation,

$$\frac{1}{3} \theta^2 = 8\pi G \rho - \frac{1}{2} \mathcal{R} + \sigma^2 + \Lambda, \quad (256)$$

$$\dot{\theta} = -\frac{1}{3} \theta^2 - 2\sigma^2 - 4\pi G \rho + \Lambda. \quad (257)$$

Here \mathcal{R} is the spatial Ricci scalar and σ^2 is the shear scalar. Averaging the Hamiltonian constraint and using $\langle \theta \rangle_{\mathcal{D}} = 3\dot{a}_{\mathcal{D}}/a_{\mathcal{D}}$ gives

$$3 \left(\frac{\dot{a}_{\mathcal{D}}}{a_{\mathcal{D}}} \right)^2 = 8\pi G \langle \rho \rangle_{\mathcal{D}} - \frac{1}{2} \langle \mathcal{R} \rangle_{\mathcal{D}} - \frac{1}{2} Q_{\mathcal{D}} + \Lambda, \quad (258)$$

where the kinematical backreaction term is

$$Q_{\mathcal{D}} = \frac{2}{3} (\langle \theta^2 \rangle_{\mathcal{D}} - \langle \theta \rangle_{\mathcal{D}}^2) - 2 \langle \sigma^2 \rangle_{\mathcal{D}}. \quad (259)$$

The acceleration equation follows by averaging the Raychaudhuri equation. Equivalently, one uses the Buchert commutation rule

$$\partial_t \langle S \rangle_{\mathcal{D}} - \langle \partial_t S \rangle_{\mathcal{D}} = \langle S \theta \rangle_{\mathcal{D}} - \langle S \rangle_{\mathcal{D}} \langle \theta \rangle_{\mathcal{D}}, \quad (260)$$

with $S = \theta$. This gives

$$3\frac{\ddot{a}_{\mathcal{D}}}{a_{\mathcal{D}}} = -4\pi G\langle\rho\rangle_{\mathcal{D}} + Q_{\mathcal{D}} + \Lambda. \quad (261)$$

These equations show immediately what would be required for backreaction to matter dynamically: the variance of the local expansion must be sufficiently large and positive, and it must not be cancelled by equally large shear contributions.

The astron problem is not, however, a pure dust problem. The correct microscopic system is Einstein–Maxwell with charged compact sources. In units $c = 1$, the field equations are

$$G_{\mu\nu} + \Lambda g_{\mu\nu} = 8\pi G \left(T_{\mu\nu}^{(A)} + T_{\mu\nu}^{(\text{EM})} \right), \quad (262)$$

together with

$$\nabla_{\nu} F^{\mu\nu} = \mu_0 J^{\mu}, \quad \nabla_{[\alpha} F_{\beta\gamma]} = 0. \quad (263)$$

The electromagnetic stress tensor is

$$T_{\mu\nu}^{(\text{EM})} = \frac{1}{\mu_0} \left(F_{\mu\alpha} F_{\nu}^{\alpha} - \frac{1}{4} g_{\mu\nu} F_{\alpha\beta} F^{\alpha\beta} \right), \quad (264)$$

up to the sign convention used for the metric. What is invariant is that it is traceless and anisotropic. In a local orthonormal frame its energy density is

$$\rho_{\text{EM}} = \frac{1}{2} \left(\epsilon_0 E^2 + \frac{B^2}{\mu_0} \right), \quad (265)$$

and its traceless anisotropic part contains terms of the form

$$\pi_{ij}^{(\text{EM})} \sim \epsilon_0 \left(E_i E_j - \frac{1}{3} E^2 \delta_{ij} \right) + \frac{1}{\mu_0} \left(B_i B_j - \frac{1}{3} B^2 \delta_{ij} \right). \quad (266)$$

This is the first place where the discrete nature of the astron system enters: the inter-astron field is a vector field with preferred directions, not a scalar fluid pressure.

The total stress tensor is conserved, but the matter and electromagnetic parts are not separately conserved:

$$\nabla_{\mu} T_{(A)}^{\mu\nu} = F^{\nu\lambda} J^{\lambda}, \quad \nabla_{\mu} T_{(\text{EM})}^{\mu\nu} = -F^{\nu\lambda} J^{\lambda}. \quad (267)$$

Thus the compact sources are not geodesic dust particles. For a pressureless charged component with mass density ρ_M , charge density ρ_q , and four-velocity u^{μ} , one has schematically

$$u^{\nu} \nabla_{\nu} u^{\mu} \equiv a^{\mu} = \frac{\rho_q}{\rho_M} F^{\mu}{}_{\nu} u^{\nu}. \quad (268)$$

In nonrelativistic language this is just the Lorentz force density

$$\mathbf{f} = \rho_q \mathbf{E} + \mathbf{J} \times \mathbf{B}. \quad (269)$$

Therefore the relevant averaging problem is not only the averaging of an energy density, but also the averaging of directed forces, Maxwell stresses, shear, and curvature.

The scalar equations can be generalized in a form that makes the new terms explicit. Let u^{μ} be the congruence used to define the averaging domain, and assume vanishing vorticity for simplicity. The Hamiltonian constraint becomes

$$\frac{1}{3}\theta^2 = 8\pi G (\rho_M + \rho_{\text{EM}}) - \frac{1}{2}\mathcal{R} + \sigma^2 + \Lambda, \quad (270)$$

while the Raychaudhuri equation contains both the electromagnetic energy density and the non-geodesic acceleration of the charged congruence:

$$\dot{\theta} = -\frac{1}{3}\theta^2 - 2\sigma^2 - 4\pi G\rho_M - 8\pi G\rho_{\text{EM}} + \Lambda + \nabla_\mu a^\mu. \quad (271)$$

The factor multiplying ρ_{EM} is different from the dust term because the Maxwell stress tensor is traceless; equivalently, an isotropically averaged electromagnetic field has $p_{\text{EM}} = \rho_{\text{EM}}/3$.

Averaging these scalar equations gives the Einstein–Maxwell analogue of the dust averaged equation:

$$3\left(\frac{\dot{a}_{\mathcal{D}}}{a_{\mathcal{D}}}\right)^2 = 8\pi G\langle\rho_M + \rho_{\text{EM}}\rangle_{\mathcal{D}} - \frac{1}{2}\langle\mathcal{R}\rangle_{\mathcal{D}} - \frac{1}{2}Q_{\mathcal{D}} + \Lambda, \quad (272)$$

and

$$3\frac{\ddot{a}_{\mathcal{D}}}{a_{\mathcal{D}}} = -4\pi G\langle\rho_M\rangle_{\mathcal{D}} - 8\pi G\langle\rho_{\text{EM}}\rangle_{\mathcal{D}} + Q_{\mathcal{D}} + A_{\mathcal{D}} + \Lambda, \quad (273)$$

where

$$A_{\mathcal{D}} \equiv \langle\nabla_\mu a^\mu\rangle_{\mathcal{D}} \quad (274)$$

is a boundary-sensitive acceleration term generated by the Lorentz force on the charged sources. Unlike $Q_{\mathcal{D}}$, this is not a standard Buchert dust variable; it is our shorthand for the additional non-geodesic acceleration term that appears in the Einstein–Maxwell extension. For a compact domain it may be written schematically as a flux through the boundary,

$$A_{\mathcal{D}} \sim \frac{1}{V_{\mathcal{D}}} \int_{\partial\mathcal{D}} a^i n_i dS. \quad (275)$$

Thus, in the absence of a cosmological constant, the condition for averaged acceleration is not the dust condition alone but rather

$$Q_{\mathcal{D}} + A_{\mathcal{D}} > 4\pi G\langle\rho_M\rangle_{\mathcal{D}} + 8\pi G\langle\rho_{\text{EM}}\rangle_{\mathcal{D}}. \quad (276)$$

This equation is the analytic target for the astron scenario. The homogeneous fluid approximation effectively sets $A_{\mathcal{D}} = 0$, suppresses the anisotropic Maxwell stresses, and replaces vector correlations by a scalar radiation-like energy density. A discrete Einstein–Maxwell treatment keeps these terms.

To make the connection concrete, imagine placing astrons on a cubic lattice with comoving spacing L_c . The physical separation is

$$L(t) = a_{\mathcal{D}}(t)L_c. \quad (277)$$

If a domain contains N lattice cells, then

$$V_{\mathcal{D}}(t) \simeq Na_{\mathcal{D}}^3 L_c^3, \quad n_A(t) = \frac{N}{V_{\mathcal{D}}(t)} = \frac{1}{a_{\mathcal{D}}^3 L_c^3}. \quad (278)$$

The rest-mass density of the astron lattice therefore behaves as dust,

$$\langle\rho_M\rangle_{\mathcal{D}} = M_A n_A = \frac{M_A}{L_c^3} a_{\mathcal{D}}^{-3}. \quad (279)$$

The Coulomb contribution is obtained by summing the pairwise interaction energy,

$$U_C(\mathcal{D}) = \frac{1}{2} \sum_{i \neq j \in \mathcal{D}} \frac{k_e Q_A^2}{r_{ij}}, \quad r_{ij} = a_{\mathcal{D}} L_c |\mathbf{n}_i - \mathbf{n}_j|. \quad (280)$$

Equivalently,

$$U_C(\mathcal{D}) = \frac{k_e Q_A^2}{a_{\mathcal{D}} L_c} \mathcal{S}_{\mathcal{D}}, \quad (281)$$

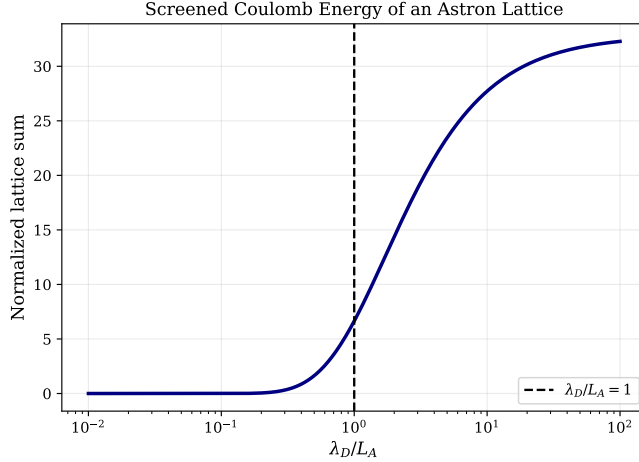


Figure 11: Shell-truncated cubic-lattice sum for a Yukawa-screened inter-astron interaction, shown as a function of λ_D/L_A . For $\lambda_D \ll L_A$ the interaction is strongly suppressed, while for $\lambda_D \gtrsim L_A$ an extended lattice contribution survives. The figure therefore provides a simple numerical proxy for the interplay between screening and the backreaction problem.

where $\mathcal{S}_{\mathcal{D}}$ is the dimensionless lattice sum. For a finite domain, or for a physically screened or otherwise regularized lattice, $\mathcal{S}_{\mathcal{D}}$ is proportional to the number of cells N . In that case

$$\rho_C(\mathcal{D}) = \frac{U_C(\mathcal{D})}{V_{\mathcal{D}}} \propto a_{\mathcal{D}}^{-4}. \quad (282)$$

Thus a perfectly homogeneous or regularly coarse-grained lattice reproduces the radiation-like scaling found in the previous section. The lattice picture therefore does not by itself solve the acceleration problem.

The role of screening in this lattice picture can be illustrated by replacing the bare Coulomb interaction by a Yukawa form and evaluating a shell-truncated cubic lattice sum. Figure 11 shows the resulting normalized interaction energy as a function of λ_D/L_A , where L_A is the lattice spacing. For $\lambda_D \ll L_A$ the interaction is strongly suppressed and the lattice behaves effectively locally, whereas long-range correlations survive only once $\lambda_D \gtrsim L_A$. This is a compact way to visualize why the screening problem and the backreaction problem are inseparable: if the Debye length is too short compared with the inter-astron separation, the long-range lattice interaction needed for any collective cosmological effect is removed from the start.

The possible new effect is instead contained in the combination $Q_{\mathcal{D}} + A_{\mathcal{D}}$. If the lattice cells have local expansion rates H_i , then schematically

$$\theta_i \simeq 3H_i, \quad (283)$$

and a coarse cell average gives

$$Q_{\mathcal{D}} \simeq 6 (\langle H_i^2 \rangle_{\mathcal{D}} - \langle H_i \rangle_{\mathcal{D}}^2) - 2 \langle \sigma_i^2 \rangle_{\mathcal{D}}. \quad (284)$$

For a perfectly regular isotropic lattice, all cells expand in the same way,

$$H_i = H_{\mathcal{D}}, \quad \sigma_i^2 \simeq 0, \quad A_{\mathcal{D}} \simeq 0, \quad (285)$$

and therefore

$$Q_{\mathcal{D}} \simeq 0. \quad (286)$$

The lattice then reduces to the homogeneous result. By contrast, if the discrete Einstein–Maxwell dynamics produces large cell-to-cell variations in expansion, or large curvature, shear, and Lorentz-force boundary terms that do not average away, then the combination $Q_{\mathcal{D}} + A_{\mathcal{D}}$ may become dynamically relevant. Setting $\Lambda = 0$, averaged acceleration would require

$$Q_{\mathcal{D}} + A_{\mathcal{D}} > 4\pi G \langle \rho_M \rangle_{\mathcal{D}} + 8\pi G \langle \rho_{\text{EM}} \rangle_{\mathcal{D}}. \quad (287)$$

This inequality is the concrete target for any astron-lattice realization of backreaction-driven acceleration.

This is also the precise sense in which the astron proposal is different from simply assigning a scalar pressure to a homogeneous fluid. In a fluid description the interaction is compressed into ρ and p . In the discrete Einstein–Maxwell description one must instead keep the vector Lorentz force, the traceless Maxwell stress, and the domain dependence of the fields. A further complication is that an infinite same-sign Coulomb lattice is not globally well defined without a screening prescription, a finite-domain prescription, or some compensating background. This is another way in which the screening problem and the cosmological backreaction problem are intertwined.

Let us now apply these estimates to a fiducial astron lattice using the mass in Eq. (58) and the charge in Eq. (68). Denote the present physical lattice spacing by L_A . The number density is

$$n_A = L_A^{-3} \simeq 3.4 \times 10^{-68} \left(\frac{L_A}{1 \text{ Mpc}} \right)^{-3} \text{ m}^{-3}. \quad (288)$$

The corresponding mass density is

$$\rho_M = M_A n_A \simeq 6.8 \times 10^{-26} \left(\frac{M_A}{10^{12} M_{\odot}} \right) \left(\frac{L_A}{1 \text{ Mpc}} \right)^{-3} \text{ kg m}^{-3}. \quad (289)$$

Using $H_0 \simeq 67.4 \text{ km s}^{-1} \text{ Mpc}^{-1}$, this corresponds to

$$\Omega_A = \frac{\rho_M}{\rho_{\text{crit}}} \simeq 7.9 \left(\frac{M_A}{10^{12} M_{\odot}} \right) \left(\frac{L_A}{1 \text{ Mpc}} \right)^{-3}. \quad (290)$$

Thus a literal spacing $L_A \simeq 1 \text{ Mpc}$ would overclose the Universe. If one wants the astron rest mass to be of order the matter abundance, $\Omega_A \sim 0.3$, the corresponding spacing is instead

$$L_A \simeq 3 \text{ Mpc} \left(\frac{M_A}{10^{12} M_{\odot}} \right)^{1/3} \left(\frac{0.3}{\Omega_A} \right)^{1/3}. \quad (291)$$

For a sparser population, such as $N_A \sim 10^{11}$ objects in a Hubble-scale volume of radius 14 Gpc, the mean separation is of order

$$L_A \simeq 5 \text{ Mpc}, \quad (292)$$

corresponding to $\Omega_A \sim 0.07$.

The charge benchmark is large enough that the electromagnetic force between two astrons exceeds their mutual Newtonian attraction, as clear from (151).

This number is independent of the lattice spacing. The acceleration of one astron due to a single nearest neighbour is instead scale dependent:

$$a_{\text{pair}} \sim \frac{k_e Q_A^2 - G M_A^2}{M_A L_A^2} \simeq 6.2 \times 10^{-13} \left(\frac{L_A}{1 \text{ Mpc}} \right)^{-2} \text{ m s}^{-2}. \quad (293)$$

This estimate should not be confused with a cosmological acceleration, since a symmetric lattice cancels most vector forces by symmetry. Its role is only to show the local scale of the inter-astron repulsion.

The same point appears at the level of the interaction energy. A nearest-neighbour estimate gives

$$\rho_C \sim \frac{k_e Q_A^2 / L_A}{L_A^3} \simeq 1.6 \times 10^{-15} \left(\frac{Q_A}{4 \times 10^{32} \text{ C}} \right)^2 \left(\frac{L_A}{1 \text{ Mpc}} \right)^{-4} \text{ J m}^{-3}. \quad (294)$$

Compared with the rest-mass energy density,

$$\rho_M c^2 \simeq 6.1 \times 10^{-9} \left(\frac{M_A}{10^{12} M_\odot} \right) \left(\frac{L_A}{1 \text{ Mpc}} \right)^{-3} \text{ J m}^{-3}, \quad (295)$$

one obtains

$$\frac{\rho_C}{\rho_M c^2} \sim 2.6 \times 10^{-7} \left(\frac{Q_A}{4 \times 10^{32} \text{ C}} \right)^2 \left(\frac{M_A}{10^{12} M_\odot} \right)^{-1} \left(\frac{L_A}{1 \text{ Mpc}} \right)^{-1}. \quad (296)$$

Therefore, if the Coulomb sum is effectively local or screened, its energy density is much too small to act as a dark-energy component. More generally, a screened lattice would involve the replacement

$$U_C(\mathcal{D}; \lambda_D) = \frac{1}{2} \sum_{i \neq j \in \mathcal{D}} \frac{k_e Q_A^2}{r_{ij}} e^{-r_{ij}/\lambda_D}. \quad (297)$$

If $\lambda_D \ll L_A$, inter-cell correlations are exponentially suppressed and the backreaction problem becomes essentially local. If instead $\lambda_D \gtrsim L_A$, the fields correlate many lattice cells and the averaging domain $V_{\mathcal{D}}$ must be chosen large enough to contain the relevant nonlocal electromagnetic stresses. If the same-sign Coulomb field is assumed to remain unscreened across many lattice cells, the lattice sum is no longer a simple local quantity and a global prescription is needed. This is precisely why the screening problem cannot be separated from the cosmological backreaction problem.

Finally, the Einstein–Maxwell acceleration condition gives a useful target scale. With $\Lambda = 0$, acceleration requires

$$Q_{\mathcal{D}} + A_{\mathcal{D}} > 4\pi G \rho_M + 8\pi G \rho_{\text{EM}}. \quad (298)$$

For a local or screened Coulomb estimate, ρ_{EM} is much smaller than $\rho_M c^2$, so the leading target scale is still set by

$$4\pi G \rho_M \simeq 5.7 \times 10^{-35} \left(\frac{M_A}{10^{12} M_\odot} \right) \left(\frac{L_A}{1 \text{ Mpc}} \right)^{-3} \text{ s}^{-2}. \quad (299)$$

Equivalently,

$$\frac{Q_{\mathcal{D}} + A_{\mathcal{D}}}{H_0^2} > \frac{3}{2} \Omega_A. \quad (300)$$

Thus, if astrons make up a matter-like abundance $\Omega_A \sim 0.3$, the required backreaction is not a small correction: one needs $Q_{\mathcal{D}} + A_{\mathcal{D}}$ of order $0.5 H_0^2$. This gives a concrete criterion for the astron proposal. A viable astron-lattice cosmology must show that the discrete Einstein–Maxwell dynamics generates a positive effective backreaction of approximately this size, without being cancelled by shear, by the positive focusing of electromagnetic energy, or by plasma screening.

This criterion is the useful outcome of the averaging analysis. It shows that the homogeneous result $\rho_A \propto a^{-4}$ is not the end of the cosmological question, because the homogeneous reduction has erased the discreteness of the sources, the anisotropic Maxwell stresses and the non-geodesic Lorentz-force contribution $A_{\mathcal{D}}$. These are precisely the terms through which a charged astron lattice can depart from a perfect-fluid description.

The connection with the general backreaction literature is then quite concrete. Green and Wald have shown that, under their weak-limit assumptions, the effective stress-energy generated by small-scale inhomogeneities is traceless and satisfies the weak energy condition, so it does not behave as a cosmological constant [18]. This is relevant because the Maxwell stress tensor is also traceless. At the same time, the astron problem is not the standard dust backreaction problem: the sources are rare, extremely massive

charged compact objects, the inter-source fields are long-ranged, and the averaged equations contain the additional Einstein–Maxwell structures $Q_{\mathcal{D}}$, $A_{\mathcal{D}}$, and the anisotropic electromagnetic stress. The analysis above therefore turns the cosmological part of the proposal into a definite calculation rather than a general appeal to inhomogeneity.

Several routes can implement this calculation. One may extend Buchert averaging to an Einstein–Maxwell system with compact charged sources, construct charged black-hole or statistically homogeneous charged lattices in the spirit of known exact charged cosmologies [15], or develop a post-Newtonian coarse-graining scheme in which the discrete Coulomb and gravitational interactions are retained. In each case the relevant observable is not simply an effective fluid equation of state, but the expansion, shear and curvature of a domain that contains a finite population of astrons. The positive result of the present section is that the homogeneous a^{-4} scaling has been isolated from the genuinely inhomogeneous Einstein–Maxwell problem, and the size of the required backreaction has been reduced to the explicit target $Q_{\mathcal{D}} + A_{\mathcal{D}} \sim H_0^2$ for a cosmologically significant astron abundance.

12 Conclusions

The analysis leads to a clear picture of the astron proposal and separates several issues that had been intertwined. A minimal capture model shows that charge separation can occur on timescales shorter than gravitational collapse, and the ordinary accretion branch saturates at a charge proportional to M . This gives a controlled sub-extremal sector of charged compact objects with well-defined local dynamics. The large-charge branch used in the original phenomenological proposal is a different regime: the extrapolated $Q \propto M^2$ charge places a fiducial $10^{12}M_{\odot}$ astron deep in the super-extremal Einstein–Maxwell domain.

This separation is one of the main results of the paper. The exterior geometry is controlled by the dimensionless charge and spin parameters, while the physical radius determines the interior completion. The same exterior data can therefore describe either a singular spacetime or a regular horizonless charged compact object, and the charged-TOV scans show explicitly that regular Einstein–Maxwell interiors are available. The lensing analysis gives an independent observable consequence: the fiducial large-charge branch lies beyond the photon-sphere threshold, so it is not expected to reproduce the strong black-hole-like sequence of relativistic images even though it still lenses weakly through its mass.

The cosmological analysis also gives a definite result. In a homogeneous FLRW reduction the interaction energy of the charged population scales as a^{-4} , so that sector behaves like radiation rather than like a cosmological constant. The relevant cosmological question is therefore not whether the Coulomb energy can be renamed as a dark-energy fluid, but whether the discrete Einstein–Maxwell system produces a different averaged evolution through $Q_{\mathcal{D}}$, $A_{\mathcal{D}}$, anisotropic Maxwell stress and long-range inter-source correlations. The paper formulates this problem explicitly and identifies the required scale, $Q_{\mathcal{D}} + A_{\mathcal{D}} \sim H_0^2$, for a cosmologically significant astron population.

Screening remains the central physical input controlling that possibility. The linear Debye estimate is an important benchmark, but the large-potential regime of the fiducial charge lies outside the assumptions of linear Debye–Hückel theory. The numerical estimates given here show both the enormous size of $e\Phi/(k_B T)$ and the macroscopic reservoir needed for charge compensation, thereby motivating the nonlinear kinetic formulation developed in the appendices. The resulting picture is not a dismissal of the astron scenario; it is a sharper version of it. Astrons define a calculable Einstein–Maxwell framework in which charge generation, compact-object geometry, lensing, screening and cosmological averaging become linked tests of the same large-charge hypothesis.

Acknowledgements

This work is partially supported by INFN, iniziativa specifica *QG-sky*. C.C. thanks the Yang Institute for Theoretical Physics and the Simons Center at Stony Brook for hospitality while completing the project.

A Possible Values of the Charging Timescale

The characteristic charging timescale in the linearized capture model was defined in Eq. (28). That expression shows immediately that τ is controlled mainly by the product Rn , while the dependence on temperature is only through \sqrt{T} . It is therefore misleading to speak of a single preferred value of τ without specifying the local plasma environment and the characteristic capture radius.

The corresponding numerical form is Eq. (30). Hence

$$\tau \propto \frac{\sqrt{T}}{Rn}. \quad (301)$$

For orientation, it is useful to normalize the estimate to the gravitational scale of a fiducial astron of mass

$$M \sim 10^{12} M_{\odot}, \quad (302)$$

for which

$$R_g = \frac{GM}{c^2} \approx 1.48 \times 10^{15} \text{ m}. \quad (303)$$

If one takes $R \sim R_g$, then Eq. (30) becomes

$$\tau \approx 1.6 \times 10^1 \left(\frac{T}{10^6 \text{ K}} \right)^{1/2} \left(\frac{R}{1.48 \times 10^{15} \text{ m}} \right)^{-1} \left(\frac{n}{10^{-13} \text{ m}^{-3}} \right)^{-1} \text{ s}. \quad (304)$$

This form makes the environmental dependence transparent.

A.1 Astrophysical Density Benchmarks

The charging times reported in Table 1 should be read as order-of-magnitude environmental benchmarks rather than as the prediction of a single formation model. Since the quantity τ scales mainly as $(Rn)^{-1}$, the physically important input is the local baryon density in the region where the compact object forms or accretes. It is therefore useful to make explicit the range of densities that is astrophysically plausible in the various contexts relevant to the astron scenario.

At the lowest-density end, a natural cosmological reference is the present-day mean baryon density. The Particle Data Group quotes

$$\Omega_b h^2 \simeq 0.02237, \quad (305)$$

which for $h \simeq 0.67$ implies

$$\Omega_b = \frac{\Omega_b h^2}{h^2} \simeq \frac{0.02237}{0.67^2} \simeq 0.049. \quad (306)$$

Using

$$\Omega_b \equiv \frac{\rho_{b,0}}{\rho_{c,0}}, \quad \rho_{c,0} = \frac{3H_0^2}{8\pi G}, \quad H_0 = 100 h \text{ km s}^{-1} \text{ Mpc}^{-1}, \quad (307)$$

one finds for the present critical density

$$\rho_{c,0} \simeq 8.4 \times 10^{-30} \text{ g cm}^{-3}, \quad (308)$$

and therefore for the mean baryon mass density

$$\rho_{b,0} = \Omega_b \rho_{c,0} \simeq (0.049)(8.4 \times 10^{-30}) \simeq 4 \times 10^{-31} \text{ g cm}^{-3}. \quad (309)$$

Dividing by the proton mass gives a present-day mean baryon number density

$$n_{b,0} \sim \frac{\rho_{b,0}}{m_p} \sim 2.5 \times 10^{-7} \text{ cm}^{-3} \sim 0.25 \text{ m}^{-3}, \quad (310)$$

consistent with standard cosmological parameter summaries [24, 25]. This value is many orders of magnitude above the extreme low-density benchmark $n \sim 10^{-13} \text{ m}^{-3}$ used below only as a conservative dilute limit, but it remains extremely small compared with the densities encountered in collapse scenarios.

Moving to denser environments, direct-collapse and massive-seed formation models probe gas far from the present cosmic mean. In the high-velocity protogalactic collision scenario of Ref. [36], the shocked layer reaches approximately

$$T \sim 10^6 \text{ K}, \quad n \gtrsim 10^4 \text{ cm}^{-3} \sim 10^{10} \text{ m}^{-3}, \quad (311)$$

providing a useful benchmark for hot, compressed gas in a pre-collapse stage. Radiation-hydrodynamics simulations of direct-collapse clouds follow the central gas at least up to

$$n \sim 10^8 \text{ cm}^{-3} \sim 10^{14} \text{ m}^{-3}, \quad (312)$$

[37], which is already sufficient to drive the charging time far below the free-fall time in the linearized estimate. Finally, radiative transfer studies of the optically thick inner collapse report densities as large as

$$\rho \sim 10^{-6} \text{ g cm}^{-3} = 10^{-3} \text{ kg m}^{-3}, \quad (313)$$

which for ionized hydrogen correspond to

$$n \sim \frac{\rho}{m_p} \sim 6 \times 10^{23} \text{ m}^{-3}, \quad (314)$$

well above 10^{20} m^{-3} [38]. Such values should not be interpreted as a unique “astron density,” but rather as markers of the broad dynamical range that realistic collapse calculations already explore.

The entries in Table 1 are chosen to span this hierarchy, from very dilute late-time environments through atomic-cooling and direct-collapse gas to extremely dense local collapse regions. The purpose of the table is therefore comparative: it shows how sensitively the charging time responds to the ambient density. Once the formal value of τ falls below microscopic plasma response times, such as the inverse electron plasma frequency $\omega_{pe}^{-1} = (\epsilon_0 m_e / n_e e^2)^{1/2}$, the numbers should not be interpreted literally; they only indicate that the local linear capture coefficient is not the macroscopic bottleneck. For an ionized hydrogen plasma with $n_e \simeq n$, both the electron plasma time and the free-fall time scale as $n^{-1/2}$. Their ratio is density independent,

$$\frac{\omega_{pe}^{-1}}{t_{\text{ff}}} = \left(\frac{32G\epsilon_0 m_e m_p}{3\pi e^2} \right)^{1/2} \simeq 4.5 \times 10^{-19}.$$

Thus collective plasma rearrangement is microscopic compared with gravitational collapse at any density for which the single-fluid estimates apply.

Diffuse Late-Time Intergalactic Plasma This benchmark is meant to represent the most rarefied ionized gas in the present-day intergalactic medium, far from collapsed halos or actively accreting structures [29, 30]. The temperature

$$T \sim 10^6 \text{ K}, \quad (315)$$

is typical of a hot, highly ionized plasma, while the density

$$n \sim 10^{-13} \text{ m}^{-3}, \quad (316)$$

is chosen as an intentionally extreme dilute limit within the broad warm-hot intergalactic medium range discussed in the literature [31]. In this case

$$\tau \sim 1.6 \times 10^1 \text{ s}. \quad (317)$$

This formal response time is short compared with the corresponding free-fall time. The diffuse IGM is nevertheless not a realistic environment for generating the large phenomenological astron charge, because the assumptions of a local reservoir, steady supply, and negligible screening are precisely the assumptions under question.

Environment	T (K)	n (m^{-3})	τ (s)	t_{ff} (s)	τ/t_{ff}
Diffuse late-time IGM	10^6	10^{-13}	1.6×10^1	5.1×10^{24}	3.1×10^{-24}
Tenuous halo gas	10^6	10^6	1.6×10^{-18}	1.6×10^{15}	9.9×10^{-34}
Atomic-cooling gas	10^4	10^{10}	1.6×10^{-23}	1.6×10^{13}	9.9×10^{-37}
Moderately dense collapse gas	10^4	10^{12}	1.6×10^{-25}	1.6×10^{12}	9.9×10^{-38}
Dense collapse gas	10^4	10^{14}	1.6×10^{-27}	1.6×10^{11}	9.9×10^{-39}
Homogeneous early background	10^6	10^{17}	1.6×10^{-29}	5.1×10^9	3.1×10^{-39}
Local collapse region	10^6	10^{20}	1.6×10^{-32}	1.6×10^8	9.9×10^{-41}
Local collapse region	10^6	10^{21}	1.6×10^{-33}	5.1×10^7	3.1×10^{-41}
Local collapse region	10^6	10^{22}	1.6×10^{-34}	1.6×10^7	9.9×10^{-42}

Table 1: Representative charging and free-fall times for different plasma environments, computed with the reference compactness scale $R = GM/c^2$ for $M = 10^{12}M_{\odot}$. This choice normalizes the capture estimate and should not be read as an asserted material surface radius. The densities are intended only as order-of-magnitude benchmarks. Extremely small formal values of τ should be read as a breakdown of the macroscopic frozen-background approximation, not as literal sub-plasma microphysics.

Tenuous Halo or Circumgalactic Gas This case is intended to mimic hot gas in galactic halos or in the circumgalactic medium, where virial heating or feedback can maintain temperatures near

$$T \sim 10^6 \text{ K}, \quad (318)$$

while the density remains low compared with star-forming or collapsing regions [32]. For a representative value

$$n \sim 10^6 \text{ m}^{-3}, \quad (319)$$

one finds

$$\tau \sim 1.6 \times 10^{-18} \text{ s}, \quad (320)$$

Such a value is already below ordinary macroscopic plasma timescales. It should therefore be read only as saying that the local linear response has ceased to be the slow variable in the problem.

Atomic-Cooling or Moderately Dense Collapse Gas These entries represent gas that has already condensed into an atomic-cooling or early direct-collapse cloud [36, 37]. The characteristic temperature

$$T \sim 10^4 \text{ K}. \quad (321)$$

is natural because hydrogen line cooling keeps the gas near 10^4 K over a broad range of densities. Taking first

$$n \sim 10^{10} \text{ m}^{-3}, \quad (322)$$

one obtains

$$\tau \sim 1.6 \times 10^{-23} \text{ s}, \quad (323)$$

If the density increases further to

$$n \sim 10^{12} \text{ m}^{-3}, \quad (324)$$

with the same temperature, then

$$\tau \sim 1.6 \times 10^{-25} \text{ s}, \quad (325)$$

At

$$n \sim 10^{14} \text{ m}^{-3}, \quad (326)$$

the timescale falls to

$$\tau \sim 1.6 \times 10^{-27} \text{ s}. \quad (327)$$

These examples show that once the gas enters the atomic-cooling or early collapse regime, the formal charging response becomes effectively instantaneous on dynamical timescales. The numerical values themselves should not be extrapolated below the microscopic domain of validity of the capture model.

Homogeneous Early-Universe Background This benchmark should be read as a schematic dense ionized background rather than as a detailed thermal-history model. The density

$$n \sim 10^{17} \text{ m}^{-3}$$

is not associated with a unique physical transition; it is chosen as an order-of-magnitude reference point for a very early homogeneous plasma. Its meaning can be made explicit by extrapolating the present mean baryon density backward with the standard FLRW scaling

$$n_b(z) = n_{b,0}(1+z)^3, \quad (328)$$

starting from

$$n_{b,0} \simeq 0.25 \text{ m}^{-3} \quad (329)$$

as derived above [19–21]. Setting

$$n_b(z) \sim 10^{17} \text{ m}^{-3} \quad (330)$$

corresponds to

$$1+z \sim \left(\frac{10^{17}}{0.25} \right)^{1/3} \sim 7 \times 10^5. \quad (331)$$

At such a redshift the radiation temperature, estimated from

$$T_\gamma(z) = T_{\gamma,0}(1+z), \quad T_{\gamma,0} \simeq 2.725 \text{ K}, \quad (332)$$

is

$$T_\gamma \sim 2 \times 10^6 \text{ K}. \quad (333)$$

Thus the benchmark pair

$$T \sim 10^6 \text{ K}, \quad n \sim 10^{17} \text{ m}^{-3}, \quad (334)$$

is internally consistent as a rough early-Universe ionized-plasma reference point.

This entry is not meant to describe a local direct-collapse environment, nor is 10^{17} m^{-3} a special threshold. Its purpose is only to show how the formal charging response behaves when the cosmic mean plasma density is extrapolated to very early epochs. With the parameters above, Eq. (30) gives

$$\tau \sim 1.6 \times 10^{-29} \text{ s}. \quad (335)$$

Such a value is far below microscopic plasma response times and should not be interpreted literally. It indicates only that, in this dense homogeneous benchmark, the local linear capture coefficient is not the macroscopic bottleneck; a kinetic plasma treatment would be required to assign a physical response time.

Dense Local Collapse Region The shortest values of τ arise in the immediate neighborhood of the collapsing object, where radiation-hydrodynamics and optically thick inner-core calculations indicate very large densities [37, 38]. The temperature

$$T \sim 10^6 \text{ K}, \quad (336)$$

is appropriate for shock-heated or strongly ionized gas. For

$$n \sim 10^{20} \text{ m}^{-3}, \quad (337)$$

one finds

$$\tau \sim 1.6 \times 10^{-32} \text{ s.} \quad (338)$$

For

$$n \sim 10^{21} \text{ m}^{-3}, \quad (339)$$

this becomes

$$\tau \sim 1.6 \times 10^{-33} \text{ s,} \quad (340)$$

and for

$$n \sim 10^{22} \text{ m}^{-3}, \quad (341)$$

one obtains

$$\tau \sim 1.6 \times 10^{-34} \text{ s.} \quad (342)$$

Thus the dense local-collapse entries should be interpreted qualitatively: the charge sector adjusts essentially instantaneously relative to the bulk collapse, while a more microscopic kinetic treatment is needed to assign literal sub-plasma times. All of the numerical examples above were quoted for

$$R \sim 1.48 \times 10^{15} \text{ m} \simeq 9.9 \times 10^3 \text{ AU} \simeq 10^4 \text{ AU.} \quad (343)$$

which corresponds to R_g for a fiducial $10^{12} M_\odot$ astron. If the actual capture radius is smaller than this, then τ increases in inverse proportion. For example, reducing R by a factor of 10^3 increases τ by a factor of 10^3 . Conversely, a larger effective capture radius shortens the charging time.

This sensitivity is physically important. The quantity R in the capture model is not a universal constant, but the radius at which the capture cross section is being evaluated. Different assumptions about the collapse geometry or about the effective capture zone therefore map directly into different values of τ .

A.2 Free-Fall Time for a Uniform Sphere

We consider a pressureless, spherically symmetric cloud of uniform density ρ that starts from rest and a spherical shell that is initially at radius r_0 . By Newton's theorem, only the mass enclosed within that shell contributes to the gravitational force. Since shells do not cross during the collapse, the enclosed mass remains constant and is given by

$$M = \frac{4\pi}{3} \rho r_0^3. \quad (344)$$

The radial equation of motion is therefore

$$\ddot{r} = -\frac{GM}{r^2}. \quad (345)$$

Because the shell starts from rest at $r = r_0$, its specific energy is

$$E = -\frac{GM}{r_0}. \quad (346)$$

At a later radius $r(t)$, energy conservation gives

$$\frac{1}{2} \dot{r}^2 - \frac{GM}{r} = -\frac{GM}{r_0}, \quad (347)$$

so that

$$\dot{r} = -\sqrt{2GM \left(\frac{1}{r} - \frac{1}{r_0} \right)}, \quad (348)$$

where the minus sign is chosen because the shell is collapsing inward.

The free-fall time is the time required for the shell to move from r_0 to the origin. Rearranging Eq. (348) gives

$$dt = \frac{dr}{-\sqrt{2GM\left(\frac{1}{r} - \frac{1}{r_0}\right)}}, \quad (349)$$

and hence

$$t_{\text{ff}} = \int_0^{r_0} \frac{dr}{\sqrt{2GM\left(\frac{1}{r} - \frac{1}{r_0}\right)}}. \quad (350)$$

This integral is evaluated by the substitution

$$r = r_0 \sin^2 \theta. \quad (351)$$

Substituting into Eq. (350) yields

$$t_{\text{ff}} = 2\sqrt{\frac{r_0^3}{2GM}} \int_0^{\pi/2} \sin^2 \theta \, d\theta. \quad (352)$$

One finds

$$t_{\text{ff}} = \frac{\pi}{2\sqrt{2}} \sqrt{\frac{r_0^3}{GM}}. \quad (353)$$

Finally, substituting the enclosed mass from Eq. (344),

$$M = \frac{4\pi}{3} \rho r_0^3, \quad (354)$$

into Eq. (353) gives

$$t_{\text{ff}} = \frac{\pi}{2\sqrt{2}} \sqrt{\frac{1}{G(4\pi/3)\rho}} = \sqrt{\frac{3\pi}{32G\rho}}. \quad (355)$$

It depends only on the initial density and is independent of the initial radius of the shell.

B Origin of the Extrapolated Charge Estimate

In the main text we showed that the ordinary accretion-based saturation estimate leads to charges many orders of magnitude below the value usually quoted in the original electromagnetic accelerating-universe scenario. It is therefore useful to explain explicitly how that larger benchmark charge is obtained in Ref. [1]. As discussed in the main paper, that result does not follow from a local collapse or accretion calculation, but from an extrapolation of the charge-to-mass ratio Q/M inferred from two lower-mass benchmark points.

The crucial input is an assumed scaling of the charge-to-mass ratio Q/M with mass. In the original argument, two benchmark values were taken from the PBH-charging analysis of Ref. [35]. Expressed in kilograms, these are

$$\frac{Q}{M} \sim 10^{-32} \text{ C kg}^{-1} \quad \text{at} \quad M \sim 10^{20} \text{ kg}, \quad (356)$$

and

$$\frac{Q}{M} \sim 10^{-22} \text{ C kg}^{-1} \quad \text{at} \quad M \sim 10^{30} \text{ kg}. \quad (357)$$

Using $M_\odot \simeq 2 \times 10^{30}$ kg, these correspond roughly to

$$M \sim 5 \times 10^{-11} M_\odot, \quad M \sim 5 \times 10^{-1} M_\odot, \quad (358)$$

respectively. Thus, in solar-mass units, the two anchor points are approximately

$$\frac{Q}{M} \sim 10^{-32} \text{ C kg}^{-1} \quad \text{at} \quad M \sim 5 \times 10^{-11} M_{\odot}, \quad (359)$$

and

$$\frac{Q}{M} \sim 10^{-22} \text{ C kg}^{-1} \quad \text{at} \quad M \sim 5 \times 10^{-1} M_{\odot}. \quad (360)$$

The next step is to assume that these two points define a straight line in logarithmic variables. Writing

$$M = 10^m \text{ kg}, \quad (361)$$

the two benchmarks correspond to

$$(m, \log_{10}(Q/M)) = (20, -32), \quad (30, -22). \quad (362)$$

The straight line through them is

$$\log_{10}(Q/M) = m - 52, \quad (363)$$

which is equivalent to the log-linear ansatz

$$\frac{Q}{M} = 10^{m-52} \text{ C kg}^{-1}. \quad (364)$$

Multiplying by M gives

$$Q = M \frac{Q}{M} = 10^m \cdot 10^{m-52} = 10^{2m-52} \text{ C}, \quad (365)$$

so the charge scales quadratically with the mass,

$$Q \propto M^2. \quad (366)$$

To rewrite this in solar masses, one sets

$$M = 10^p M_{\odot} \simeq 2 \times 10^{p+30} \text{ kg}, \quad (367)$$

which implies

$$m = p + 30 + \log_{10} 2. \quad (368)$$

Hence

$$q = 2m - 52 = 8 + 2p + \log_{10} 4, \quad (369)$$

where $Q = 10^q \text{ C}$. For

$$p = 12, \quad M_A = 10^{12} M_{\odot}, \quad (370)$$

one obtains

$$q = 32 + \log_{10} 4, \quad (371)$$

and therefore

$$Q_A \simeq 4 \times 10^{32} \text{ C}. \quad (372)$$

In this way the large astron charge is obtained not from a local accretion or collapse calculation, but from extrapolating in log-log space a trend inferred from the two much lower-mass benchmark points listed above.

C Debye Screening

We derive here the formula quoted in the main text. Consider a plasma with species s , charge q_s , unperturbed density n_{s0} , and temperature T_s . In a weak electrostatic potential Φ , local thermal equilibrium gives the Boltzmann response

$$n_s(\Phi) = n_{s0} \exp\left(-\frac{q_s \Phi}{k_B T_s}\right). \quad (373)$$

For

$$\left|\frac{q_s \Phi}{k_B T_s}\right| \ll 1, \quad (374)$$

this becomes

$$n_s(\Phi) \simeq n_{s0} \left(1 - \frac{q_s \Phi}{k_B T_s}\right) = n_{s0} - \frac{n_{s0} q_s}{k_B T_s} \Phi. \quad (375)$$

The plasma charge density is therefore

$$\rho_{\text{pl}} = \sum_s q_s n_s(\Phi) \simeq \sum_s q_s n_{s0} - \Phi \sum_s \frac{n_{s0} q_s^2}{k_B T_s}. \quad (376)$$

For a quasi-neutral background,

$$\sum_s q_s n_{s0} = 0, \quad (377)$$

so the linearized charge density reduces to

$$\rho_{\text{pl}} \simeq -\Phi \sum_s \frac{n_{s0} q_s^2}{k_B T_s}. \quad (378)$$

Poisson's equation for the plasma response alone is

$$\nabla^2 \Phi = -\frac{\rho_{\text{pl}}}{\epsilon_0}, \quad (379)$$

hence

$$\nabla^2 \Phi = \left(\sum_s \frac{n_{s0} q_s^2}{\epsilon_0 k_B T_s}\right) \Phi. \quad (380)$$

Writing this as

$$\nabla^2 \Phi = \frac{\Phi}{\lambda_D^2} \quad (381)$$

identifies the multicomponent Debye length,

$$\frac{1}{\lambda_D^2} = \sum_s \frac{n_{s0} q_s^2}{\epsilon_0 k_B T_s}. \quad (382)$$

For a symmetric electron–proton plasma with $n_{e0} = n_{p0} = n_0$ and $T_e = T_p = T$, this gives

$$\frac{1}{\lambda_D^2} = \frac{n_0 e^2}{\epsilon_0 k_B T} + \frac{n_0 e^2}{\epsilon_0 k_B T} = \frac{2n_0 e^2}{\epsilon_0 k_B T}, \quad (383)$$

or

$$\lambda_D^2 = \frac{\epsilon_0 k_B T}{2n_0 e^2}. \quad (384)$$

If one instead defines $n_{\text{tot}} = n_{e0} + n_{p0} = 2n_0$, the same result may be written as

$$\lambda_D^2 = \frac{\epsilon_0 k_B T}{2n_0 e^2} = \frac{\epsilon_0 k_B T}{n_{\text{tot}} e^2}. \quad (385)$$

This last form is only a notation change in the quasi-neutral symmetric case. It is not the electron-only formula, and it is not a general expression for an uncompensated non-neutral plasma.

Now add a point charge Q at the origin. The total charge density is

$$\rho_{\text{tot}} = Q\delta^{(3)}(\mathbf{r}) + \rho_{\text{pl}}. \quad (386)$$

Using the linearized plasma response, Poisson's equation becomes

$$\nabla^2 \Phi - \frac{\Phi}{\lambda_D^2} = -\frac{Q}{\epsilon_0} \delta^{(3)}(\mathbf{r}). \quad (387)$$

For $r > 0$, the delta function is absent and spherical symmetry gives

$$\frac{1}{r^2} \frac{d}{dr} \left(r^2 \frac{d\Phi}{dr} \right) = \frac{\Phi}{\lambda_D^2}. \quad (388)$$

Let

$$\Phi(r) = \frac{u(r)}{r}. \quad (389)$$

Then, for $r > 0$,

$$\nabla^2 \Phi = \frac{u''(r)}{r}, \quad (390)$$

and the radial equation becomes

$$u'' = \frac{u}{\lambda_D^2}. \quad (391)$$

Thus

$$u(r) = Ae^{-r/\lambda_D} + Be^{r/\lambda_D}. \quad (392)$$

The growing exponential is excluded by the condition $\Phi \rightarrow 0$ at infinity, so $B = 0$. Therefore

$$\Phi(r) = \frac{A}{r} e^{-r/\lambda_D}. \quad (393)$$

The constant A is fixed by the singularity at the origin. Integrating Eq. (387) over a small sphere gives

$$\oint \nabla \Phi \cdot d\mathbf{S} = -\frac{Q}{\epsilon_0}, \quad (394)$$

because the volume integral of Φ/λ_D^2 vanishes as the sphere shrinks. Since $\Phi \simeq A/r$ near the origin, the flux is $-4\pi A$, so

$$A = \frac{Q}{4\pi\epsilon_0}. \quad (395)$$

The Debye-screened potential is therefore

$$\Phi(r) = \frac{Q}{4\pi\epsilon_0 r} e^{-r/\lambda_D}. \quad (396)$$

It is useful to verify the exponential directly. For

$$\Phi(r) = A \frac{e^{-r/\lambda_D}}{r}, \quad (397)$$

one has

$$\frac{d\Phi}{dr} = -Ae^{-r/\lambda_D} \left(\frac{1}{\lambda_D r} + \frac{1}{r^2} \right), \quad (398)$$

and therefore

$$\frac{d}{dr} \left(r^2 \frac{d\Phi}{dr} \right) = Ae^{-r/\lambda_D} \frac{r}{\lambda_D^2}. \quad (399)$$

Hence, for $r > 0$,

$$\nabla^2 \Phi = \frac{1}{r^2} \frac{d}{dr} \left(r^2 \frac{d\Phi}{dr} \right) = \frac{Ae^{-r/\lambda_D}}{\lambda_D^2 r} = \frac{\Phi}{\lambda_D^2}, \quad (400)$$

which proves that the Yukawa form solves the screened equation away from the source.

C.1 Debye Screening Beyond a Maxwellian Plasma

In the main text we used the Debye length only as a benchmark and emphasized that its derivation assumes a locally Maxwellian plasma. In this appendix we make explicit why departures from Maxwellian equilibrium can modify the screening length, and why suprathermal plasmas described by Kappa distributions generally exhibit weaker screening, corresponding to a larger effective Debye length. A common parametrization of non-Maxwellian space plasmas is provided by the isotropic Kappa distribution, which replaces the exponential high-energy decay of a Maxwellian by a power-law suprathermal tail. For a species s , it may be written in the form

$$f_{\kappa,s}(\mathbf{v}) = n_{0s} \left(\frac{m_s}{\pi \kappa_s \theta_s^2} \right)^{3/2} \frac{\Gamma(\kappa_s + 1)}{\Gamma(\kappa_s - \frac{1}{2})} \left(1 + \frac{m_s v^2}{\kappa_s \theta_s^2} \right)^{-(\kappa_s + 1)}, \quad \kappa_s > \frac{3}{2}, \quad (401)$$

where κ_s controls the strength of the suprathermal tail and θ_s is a characteristic thermal speed. In the limit $\kappa_s \rightarrow \infty$, the distribution reduces to the ordinary Maxwellian. Such distributions are widely used in space and astrophysical plasmas precisely because tenuous collisionless environments often fail to relax to local thermal equilibrium [46, 47].

The relevance for Debye screening is that the Debye length is derived from the linear response of a Maxwellian plasma. Once the equilibrium distribution acquires a suprathermal tail, the plasma susceptibility changes, and so does the screening scale. In particular, non-Maxwellian plasmas modeled by Kappa distributions can exhibit an effective Debye length different from, and in the conventions of Ref. [48] larger than, the classical Maxwellian value. Physically, the presence of a larger population of energetic particles makes the charge redistribution less efficiently localized, so that the screening cloud becomes more diffuse.

The derivation above shows that the Debye length is controlled by the linear susceptibility, namely by the coefficient of Φ in the density response. If the plasma is non-Maxwellian, this coefficient changes. For a Kappa plasma the equilibrium density in a weak electrostatic potential is often written in the schematic form

$$n_s(\Phi) = n_{0s} \left(1 - \frac{q_s \Phi}{(\kappa_s - \frac{3}{2}) k_B T_s} \right)^{-\kappa_s + \frac{1}{2}}, \quad (402)$$

which reduces to the ordinary Boltzmann relation in the limit $\kappa_s \rightarrow \infty$. Expanding Eq. (402) for small Φ gives

$$n_s(\Phi) \simeq n_{0s} \left[1 + \frac{\kappa_s - \frac{1}{2}}{\kappa_s - \frac{3}{2}} \frac{q_s \Phi}{k_B T_s} \right]. \quad (403)$$

Hence the linear density response is larger by the factor

$$\alpha_\kappa = \frac{\kappa_s - \frac{1}{2}}{\kappa_s - \frac{3}{2}}. \quad (404)$$

The corresponding screening wavenumber becomes

$$k_{D,\kappa}^2 = \alpha_\kappa k_D^2, \quad (405)$$

so that the effective screening length is

$$\lambda_{D,\kappa} = \frac{\lambda_D}{\sqrt{\alpha_\kappa}} = \lambda_D \sqrt{\frac{\kappa_s - \frac{3}{2}}{\kappa_s - \frac{1}{2}}}. \quad (406)$$

Different conventions for the definition of T_s and for the normalization of the Kappa distribution lead to slightly different prefactors in the literature, but the physical conclusion is the same: the screening length is modified once the plasma departs from a Maxwellian. In the conventions adopted by Ref. [48], the effective Debye length is enhanced relative to the standard Maxwellian value when the suprathermal tail becomes important. The enhancement arises because a substantial fraction of the particles occupies high-energy states and is therefore less efficiently rearranged by the electrostatic potential. The screening cloud then becomes more diffuse and the effective screening scale increases.

The significance of this observation for the astron problem is not that Kappa plasmas solve the screening issue by themselves, but that they show explicitly that the Debye expression is not universal. Once local Maxwellian equilibrium is abandoned, even the screening length itself becomes model dependent. This reinforces the broader point made in the main text: in the strong-field and potentially nonthermal astron environment, the classical Debye–Hückel length should be regarded only as a benchmark rather than as a definitive prediction.

D A Nonlinear and Kinetic Framework for Screening

The screening analysis in the main text shows that the standard Debye–Hückel derivation cannot be applied without qualification in the astron regime. The next step is therefore not to assert either complete screening or no screening, but to formulate the correct self-consistent plasma problem. The aim of this appendix is to define that problem in a form suitable for future analysis.

We consider an ion–electron plasma in the vicinity of a compact charged source with charge Q_A . On scales small compared with the Hubble radius, and neglecting magnetic fields for simplicity, the electrostatic response is described by phase-space distribution functions $f_s(\mathbf{x}, \mathbf{v}, t)$ for species $s = e, p$, together with the electrostatic potential $\Phi(\mathbf{x}, t)$. The natural kinetic equations are

$$\frac{\partial f_s}{\partial t} + \mathbf{v} \cdot \nabla_x f_s + \frac{q_s}{m_s} \mathbf{E} \cdot \nabla_v f_s = C_s[f_e, f_p], \quad \mathbf{E} = -\nabla\Phi, \quad (407)$$

supplemented by Poisson’s equation

$$\nabla^2\Phi = -\frac{1}{\epsilon_0} \sum_s q_s \int f_s(\mathbf{x}, \mathbf{v}, t) d^3v. \quad (408)$$

Here C_s denotes a collision operator. In the collisionless limit one has $C_s = 0$, so the problem reduces to the Vlasov–Poisson system. In a weakly collisional medium one should instead retain an effective Fokker–Planck operator.

The usual Debye result is recovered only after a further hierarchy of assumptions. One expands around a spatially uniform Maxwellian background,

$$f_s = f_s^{(0)} + \delta f_s, \quad \left| \frac{q_s \Phi}{k_B T} \right| \ll 1, \quad (409)$$

and assumes that the perturbation remains local and near thermal equilibrium. Under those conditions the densities respond approximately as Boltzmann factors, the equations linearize, and one obtains the

standard screening length λ_D . This derivation therefore identifies very clearly what fails in the astron problem: the source potential is large enough that the small-perturbation expansion is not justified near the object.

The nonlinear problem is most transparent under the assumption of spherical symmetry. For a stationary configuration, the distribution functions depend on integrals of motion rather than on a local Boltzmann factor. A convenient parametrization is

$$f_s = f_s(E_s, L_s), \quad (410)$$

where

$$E_s = \frac{1}{2}m_s v^2 + q_s \Phi(r), \quad L_s = m_s r v_\perp. \quad (411)$$

The corresponding number densities are

$$n_s(r) = \int f_s(E_s, L_s) d^3v, \quad (412)$$

and the potential must satisfy the radial Poisson equation

$$\frac{1}{r^2} \frac{d}{dr} \left(r^2 \frac{d\Phi}{dr} \right) = -\frac{1}{\epsilon_0} \sum_s q_s n_s(r). \quad (413)$$

This system is nonlinear and nonlocal, since the density at a given radius depends on the set of orbits accessible in the full potential and not only on the local value of $\Phi(r)$. The breakdown of linear Debye theory close to the source therefore does not by itself prove the absence of screening at large distances. If the potential eventually becomes weak and the distribution functions relax toward a near-Maxwellian form, a linearized screened tail may still emerge asymptotically. Conversely, if the plasma remains far from local equilibrium or if transport is too inefficient, the asymptotic behaviour may differ substantially from the linear Debye form. The physically relevant question is therefore whether the self-consistent kinetic solution approaches an exponentially screened regime on inter-astron scales, not simply whether the linear approximation fails near the astron.

The dynamical accessibility of such a regime introduces a second timescale problem. Even if a static screened solution exists mathematically, the plasma must rearrange charge over a macroscopic distance L . Depending on the regime, one may estimate the relaxation time schematically as

$$t_{\text{relax}}(L) \sim \begin{cases} L^2/D, & \text{diffusive regime,} \\ L/v_{\text{th}}, & \text{ballistic regime,} \end{cases} \quad (414)$$

where D is an effective diffusion coefficient and v_{th} is a thermal speed. In a weakly collisional plasma one must also compare these scales with the collision time $t_{\text{coll}} \sim \nu_{\text{coll}}^{-1}$. A cosmologically relevant screening mechanism would require not only a screened static profile, but also a relaxation time that is short compared with the Hubble time on the scales of interest.

The nonlinear kinetic problem therefore requires initial and boundary data of the form

$$f_s(r, \mathbf{v}, t_0) \rightarrow f_{s,\infty}(\mathbf{v}), \quad \Phi(r) \rightarrow 0 \quad \text{as } r \rightarrow \infty, \quad (415)$$

together with an inner boundary condition determined by the source charge Q_A and the characteristic source radius. The task is then to solve for the self-consistent f_s and Φ , determine whether the asymptotic field behaves as

$$\Phi(r) \sim \frac{Q_{\text{eff}}}{4\pi\epsilon_0 r} e^{-r/\lambda_{\text{eff}}}, \quad \text{or} \quad \Phi(r) \sim \frac{Q_{\text{eff}}}{4\pi\epsilon_0 r}, \quad (416)$$

or in some intermediate partially screened form, and finally compare the corresponding relaxation timescale with the cosmological expansion time.

Although a complete analytic solution of this nonlinear kinetic system is beyond the scope of the appendix, the formulation above identifies the conditions that must be established before screening can be used either as a constraint on the model or as a mechanism that removes the long-range field. Cosmological viability of the astron scenario requires a demonstration that the asymptotic electric field is not exponentially suppressed on inter-astron scales, or equivalently that the plasma response cannot assemble such a screened configuration within a Hubble time under the relevant initial and boundary conditions. This is a dynamical kinetic problem involving transport, relaxation and the asymptotic phase-space distribution; it cannot be inferred from the linear Debye estimate alone.

E Comparison Naked-Singularity Metrics

This appendix collects a few standard naked-singularity geometries that are useful as comparison cases. They are not used as dynamical models for astrons in the main text. The reason is simple: the astron exterior, under the assumptions of spherical symmetry and no rotation, belongs to the Einstein–Maxwell Reissner–Nordström class, whereas the examples below are sourced either by a scalar field or by vacuum multipole deformations. We write all line elements in the mostly-minus convention used throughout the paper.

E.1 Janis–Newman–Winicour Geometry

The Janis–Newman–Winicour solution, also known as the Fisher–Wyman solution, is a static, spherically symmetric, asymptotically flat solution of Einstein gravity coupled to a massless scalar field [50, 51]. In units $G = c = 1$, one convenient form is

$$ds^2 = \left(1 - \frac{b}{r}\right)^\nu dt^2 - \left(1 - \frac{b}{r}\right)^{-\nu} dr^2 - r^2 \left(1 - \frac{b}{r}\right)^{1-\nu} d\Omega^2, \quad 0 < \nu \leq 1. \quad (417)$$

The Schwarzschild limit is $\nu = 1$, for which $b = 2M$. For $0 < \nu < 1$, the surface $r = b$ is not a regular event horizon. The scalar field and curvature invariants diverge there, so $r = b$ is a naked curvature singularity. The control parameter is a scalar charge, not an electric charge. JNW is therefore a useful comparison geometry for horizonless singular behaviour, but it is not an Einstein–Maxwell astron exterior.

E.2 Zipoy–Voorhees Geometry

The Zipoy–Voorhees metric, often called the γ -metric, is a static, axisymmetric, asymptotically flat vacuum deformation of Schwarzschild [57, 58]. In prolate spheroidal coordinates (x, y) , with

$$x \geq 1, \quad -1 \leq y \leq 1, \quad \rho = \sigma \sqrt{(x^2 - 1)(1 - y^2)}, \quad z = \sigma xy, \quad (418)$$

define

$$F(x) = \left(\frac{x-1}{x+1}\right)^{\gamma_Z}, \quad H(x, y) = \left(\frac{x^2-1}{x^2-y^2}\right)^{\gamma_Z^2}. \quad (419)$$

The line element may be written as

$$ds^2 = F dt^2 - \sigma^2 F^{-1} \left[H(x^2 - y^2) \left(\frac{dx^2}{x^2 - 1} + \frac{dy^2}{1 - y^2} \right) + (x^2 - 1)(1 - y^2) d\phi^2 \right]. \quad (420)$$

The ADM mass is $M = \gamma_Z \sigma$. For $\gamma_Z = 1$, this reduces to the Schwarzschild solution. For $\gamma_Z \neq 1$, the would-be Schwarzschild horizon at $x = 1$ is replaced by a naked singular structure associated with

a vacuum quadrupolar deformation. Thus the singularity is not produced by charge: it is produced by departing from spherical symmetry within the vacuum Weyl class.

E.3 Tomimatsu–Sato Geometry

The Tomimatsu–Sato solutions are stationary, axisymmetric, asymptotically flat vacuum metrics labelled by an integer deformation parameter δ [59, 60]. The $\delta = 1$ member is Kerr. The first genuinely non-Kerr member is $\delta = 2$, which is sufficient for showing explicitly how the family differs from Kerr. Let $p^2 + q^2 = 1$, where q is the dimensionless rotation parameter of this vacuum solution, not an electric charge. In prolate spheroidal coordinates $\xi \geq 1$, $-1 \leq \eta \leq 1$, the $\delta = 2$ metric can be written as

$$ds^2 = \frac{A}{B} dt^2 - \frac{4Mq(1-\eta^2)C}{B} dt d\phi - \frac{M^2 B}{4p^2(\xi^2 - \eta^2)^3} \left(\frac{d\xi^2}{\xi^2 - 1} + \frac{d\eta^2}{1 - \eta^2} \right) - \frac{M^2(1-\eta^2)}{A} \left[\frac{p^2}{4}(\xi^2 - 1)B - 4q^2(1-\eta^2)\frac{C^2}{B} \right] d\phi^2. \quad (421)$$

The functions A , B , and C are polynomials:

$$A = [p^2(\xi^2 - 1)^2 + q^2(1 - \eta^2)^2]^2 - 4p^2q^2(\xi^2 - 1)(1 - \eta^2)(\xi^2 - \eta^2)^2, \quad (422)$$

$$B = [q^2\eta^4 + p^2\xi^4 + 2p\xi(\xi^2 - 1) - 1]^2 + 4q^2\eta^2 [p\xi^3 - p\xi\eta^2 + (1 - \eta^2)]^2, \quad (423)$$

and

$$C = q^2(1 - \eta^2)^3(1 + p\xi) - p^2(\xi^2 - 1)(1 - \eta^2)(p\xi^3 + 3\xi^2 + 3p\xi + 1) - 2p^2\xi(\xi^2 - 1)^2(p\xi^2 + 2\xi + p). \quad (424)$$

The metric coefficient $g_{tt} = A/B$ shows explicitly why the zero sets of these polynomials control the causal and singular structure. In the $\delta = 2$ case the spacetime contains a ring-like naked curvature singularity in the equatorial plane, together with regions in which the azimuthal Killing direction can become timelike. Higher- δ Tomimatsu–Sato solutions have analogous but increasingly complicated polynomial forms and carry higher multipole moments beyond mass and angular momentum. They are therefore useful reference metrics for naked singularities generated by vacuum multipole structure, not by the electromagnetic mechanism relevant for astrons.

F Matching a Charged Interior to a Reissner–Nordström Exterior

In the main text we state that a regular charged interior may be matched to an exterior Reissner–Nordström geometry either smoothly or through a thin shell. Here we spell out the corresponding junction conditions. The word “smooth” is used here in the standard Darmois sense: the intrinsic geometry of the matching hypersurface and its extrinsic curvature must agree when computed from the two sides. These are the continuity conditions for the first and second fundamental forms [8–10]. In ordinary Einstein gravity this is precisely the no-thin-shell condition. If the first fundamental form is continuous but the second is not, the joined spacetime is still meaningful, but the Einstein tensor contains a distributional term supported on the hypersurface. Israel’s junction condition then identifies that term with a surface stress-energy tensor [10, 11].

We use the mostly-minus signature convention of this paper and denote the interior by “−” and the exterior by “+”. Near the surface $r = R$, write

$$ds_{\pm}^2 = A_{\pm}(r)c^2 dt_{\pm}^2 - \frac{dr^2}{F_{\pm}(r)} - r^2 d\Omega^2, \quad (425)$$

with

$$A_-(r) = e^{2\Psi(r)}, \quad F_-(r) = 1 - \frac{2Gm(r)}{c^2 r} + \frac{Gk_e q(r)^2}{c^4 r^2}, \quad (426)$$

and

$$A_+(r) = F_+(r) = f_{\text{RN}}(r) = 1 - \frac{2GM}{c^2 r} + \frac{Gk_e Q^2}{c^4 r^2}. \quad (427)$$

The hypersurface Σ is described intrinsically by $\xi^a = (\tau, \theta, \phi)$, where τ is the proper time measured by an observer comoving with the surface. The embedding of Σ into either spacetime region is

$$x_{\pm}^{\mu}(\tau, \theta, \phi) = (t_{\pm}(\tau), R, \theta, \phi). \quad (428)$$

The tangent vectors to the hypersurface are therefore

$$e_{\tau, \pm}^{\mu} = \frac{\partial x_{\pm}^{\mu}}{\partial \tau} = \left(\frac{dt_{\pm}}{d\tau}, 0, 0, 0 \right), \quad e_{\theta}^{\mu} = (0, 0, 1, 0), \quad e_{\phi}^{\mu} = (0, 0, 0, 1). \quad (429)$$

Since $d\theta = d\phi = dr = 0$ along a static observer on the surface, the metric gives

$$c^2 d\tau^2 = A_{\pm}(R) c^2 dt_{\pm}^2, \quad \frac{dt_{\pm}}{d\tau} = \frac{1}{\sqrt{A_{\pm}(R)}}. \quad (430)$$

The first fundamental form is the induced metric

$$h_{ab}^{(\pm)} = g_{\mu\nu}^{(\pm)} e_{a, \pm}^{\mu} e_{b, \pm}^{\nu}. \quad (431)$$

Continuity of the first fundamental form is the first junction condition,

$$[h_{ab}] \equiv h_{ab}^{(+)} - h_{ab}^{(-)} = 0. \quad (432)$$

For a static spherical surface this induced metric is

$$ds_{\Sigma}^2 = c^2 d\tau^2 - R^2 d\Omega^2, \quad d\tau = \sqrt{A_{\pm}(R)} dt_{\pm}. \quad (433)$$

Thus the matching fixes the normalization of the interior time coordinate. If one uses the same time normalization on both sides of the boundary, this is written as

$$e^{2\Psi(R)} = f_{\text{RN}}(R). \quad (434)$$

The corresponding electromagnetic matching condition is simply Gauss' law. If the enclosed interior charge at the surface differs from the exterior charge, the difference is a surface charge,

$$\sigma_Q = \frac{Q - q(R)}{4\pi R^2}. \quad (435)$$

The choice $q(R) = Q$ therefore corresponds to no charged surface layer.

The second fundamental form is the extrinsic curvature. Geometrically, it measures how the hypersurface bends inside the surrounding spacetime. Equivalently, it measures how the induced metric changes when the hypersurface is displaced infinitesimally in the normal direction. If n^{μ} is the unit normal and $e_a^{\mu} = \partial x^{\mu} / \partial \xi^a$ are tangent vectors to the hypersurface, the extrinsic curvature is defined by projecting the covariant derivative of the normal onto the hypersurface,

$$K_{ab} = e_a^{\mu} e_b^{\nu} \nabla_{\mu} n_{\nu}. \quad (436)$$

With the sign convention used here, this is equivalently

$$K_{ab} = \frac{1}{2} \mathcal{L}_n h_{ab}, \quad (437)$$

where \mathcal{L}_n is the Lie derivative along the normal. Thus continuity of K_{ab} means that the intrinsic metric does not develop a kink as one crosses the surface. If such a kink is present, the curvature contains a delta-function piece and the surface must carry stress-energy.

We now derive K_{ab} explicitly for the spherical matching surface. The unit normal to the surface is orthogonal to the three tangent vectors and is normalized as $n_\mu n^\mu = -1$, because the hypersurface is timelike. With the normal chosen to point from the interior toward increasing r , one may take

$$n_{\mu,\pm} = \left(0, -\frac{1}{\sqrt{F_\pm(R)}}, 0, 0\right), \quad n_\pm^\mu = \left(0, \sqrt{F_\pm(R)}, 0, 0\right). \quad (438)$$

The sign of n_μ is conventional, but it must be used consistently on the two sides. With our convention the extrinsic curvature is

$$K_{ab}^{(\pm)} = e_{a,\pm}^\mu e_{b,\pm}^\nu \nabla_\mu n_{\nu,\pm}. \quad (439)$$

Because the surface is static and n_μ has only a radial component, this reduces to

$$K_{ab}^{(\pm)} = -n_{r,\pm} \Gamma_{\mu\nu,\pm}^r e_{a,\pm}^\mu e_{b,\pm}^\nu. \quad (440)$$

The only Christoffel symbols needed are obtained directly from the metric:

$$\Gamma_{tt,\pm}^r = \frac{1}{2} F_\pm(r) A_\pm'(r) c^2, \quad \Gamma_{\theta\theta,\pm}^r = -F_\pm(r) r, \quad \Gamma_{\phi\phi,\pm}^r = -F_\pm(r) r \sin^2 \theta. \quad (441)$$

Substituting these expressions and using $dt_\pm/d\tau = 1/\sqrt{A_\pm(R)}$ gives

$$K_{\tau\tau,\pm} = c^2 \sqrt{F_\pm(R)} \frac{A_\pm'(R)}{2A_\pm(R)}, \quad K_{\theta\theta,\pm} = -R \sqrt{F_\pm(R)}, \quad K_{\phi\phi,\pm} = -R \sqrt{F_\pm(R)} \sin^2 \theta. \quad (442)$$

Raising one index with the induced metric

$$h^{ab} = \text{diag} \left(\frac{1}{c^2}, -\frac{1}{R^2}, -\frac{1}{R^2 \sin^2 \theta} \right), \quad (443)$$

one obtains the nonzero mixed components

$$K^\tau_{\tau,\pm} = \sqrt{F_\pm(R)} \frac{A_\pm'(R)}{2A_\pm(R)}, \quad K^\theta_{\theta,\pm} = K^\phi_{\phi,\pm} = \frac{\sqrt{F_\pm(R)}}{R}. \quad (444)$$

For the exterior RN region this gives

$$K^\tau_{\tau,+} = \frac{f'_{\text{RN}}(R)}{2\sqrt{f_{\text{RN}}(R)}}, \quad K^\theta_{\theta,+} = \frac{\sqrt{f_{\text{RN}}(R)}}{R}, \quad (445)$$

whereas for the interior one has

$$K^\tau_{\tau,-} = \sqrt{F_-(R)} \Psi'(R), \quad K^\theta_{\theta,-} = \frac{\sqrt{F_-(R)}}{R}. \quad (446)$$

A smooth Darmois matching therefore means imposing continuity of both fundamental forms. Since continuity of the induced metric has already been imposed, the additional no-shell condition is

$$[K^a_b] = 0. \quad (447)$$

The angular component is the simplest one. It gives

$$0 = [K^\theta_\theta] = \frac{\sqrt{F_+(R)} - \sqrt{F_-(R)}}{R}. \quad (448)$$

Since the surface is timelike, both square roots are real and positive, so

$$F_-(R) = F_+(R). \quad (449)$$

Substituting the definitions of F_- and F_+ gives

$$1 - \frac{2Gm(R)}{c^2 R} + \frac{Gk_e q(R)^2}{c^4 R^2} = 1 - \frac{2GM}{c^2 R} + \frac{Gk_e Q^2}{c^4 R^2}. \quad (450)$$

Equivalently,

$$M - m(R) = \frac{k_e}{2c^2 R} [Q^2 - q(R)^2]. \quad (451)$$

If there is no charged surface layer, $q(R) = Q$, this reduces to the usual mass matching condition

$$m(R) = M. \quad (452)$$

The time-time component similarly gives

$$0 = [K^\tau{}_\tau] = \frac{f'_{\text{RN}}(R)}{2\sqrt{f_{\text{RN}}(R)}} - \sqrt{F_-(R)} \frac{A'_-(R)}{2A_-(R)}. \quad (453)$$

Because $A_-(r) = e^{2\Psi(r)}$, one has

$$\frac{A'_-(R)}{2A_-(R)} = \Psi'(R). \quad (454)$$

Thus the smooth matching condition gives the boundary condition on the redshift function,

$$\sqrt{F_-(R)} \Psi'(R) = \frac{f'_{\text{RN}}(R)}{2\sqrt{f_{\text{RN}}(R)}}. \quad (455)$$

When $F_-(R) = f_{\text{RN}}(R)$, this may also be written as

$$\Psi'(R) = \frac{1}{2} \frac{f'_{\text{RN}}(R)}{f_{\text{RN}}(R)}. \quad (456)$$

Therefore a smooth boundary does more than identify the induced metric: it also fixes how the interior redshift function approaches the exterior RN redshift at the surface.

If the induced metric is continuous but the extrinsic curvature is not, the surface carries a stress-energy tensor. With $[X] \equiv X_+ - X_-$, the Israel junction condition in the present sign convention is

$$S^a{}_b = \frac{c^4}{8\pi G} ([K^a{}_b] - \delta^a{}_b [K]), \quad [K] = [K^a{}_a], \quad (457)$$

following the standard thin-shell formalism of Israel [11]. For a spherical shell we write

$$S^a{}_b = \text{diag}(\Sigma_s, -\mathcal{P}_s, -\mathcal{P}_s), \quad (458)$$

where Σ_s is the surface energy density and \mathcal{P}_s is the tangential surface pressure. It is useful to denote

$$\kappa_{\tau,\pm} = K^\tau{}_{\tau,\pm}, \quad \kappa_{\theta,\pm} = K^\theta{}_{\theta,\pm} = K^\phi{}_{\phi,\pm}. \quad (459)$$

Then

$$[K] = [\kappa_\tau] + 2[\kappa_\Omega]. \quad (460)$$

The surface energy density follows from the τ - τ component:

$$\Sigma_s = S^\tau{}_\tau = \frac{c^4}{8\pi G} ([\kappa_\tau] - [\kappa_\tau] - 2[\kappa_\Omega]) = -\frac{c^4}{4\pi G} [\kappa_\Omega]. \quad (461)$$

Using $\kappa_{\Omega,\pm} = \sqrt{F_{\pm}(R)}/R$, one obtains

$$\Sigma_s = -\frac{c^4}{4\pi GR} \left[\sqrt{F_+(R)} - \sqrt{F_-(R)} \right], \quad (462)$$

which is an energy per unit area. The tangential pressure follows from the angular component:

$$-\mathcal{P}_s = S^\theta_\theta = \frac{c^4}{8\pi G} ([\kappa_\Omega] - [\kappa_\tau] - 2[\kappa_\Omega]) = -\frac{c^4}{8\pi G} ([\kappa_\tau] + [\kappa_\Omega]). \quad (463)$$

Therefore

$$\mathcal{P}_s = \frac{c^4}{8\pi G} ([\kappa_\tau] + [\kappa_\Omega]). \quad (464)$$

Substituting the explicit interior and exterior curvatures gives

$$\mathcal{P}_s = \frac{c^4}{8\pi G} \left[\frac{f'_{\text{RN}}(R)}{2\sqrt{f_{\text{RN}}(R)}} - \sqrt{F_-(R)} \Psi'(R) + \frac{\sqrt{f_{\text{RN}}(R)} - \sqrt{F_-(R)}}{R} \right]. \quad (465)$$

These formulae make precise the statement in the main text. If both components of K^a_b are continuous, then $\Sigma_s = \mathcal{P}_s = 0$ and the matching is smooth. If K^a_b jumps, the boundary is not a smooth material surface: it is a thin shell whose surface energy density and tangential pressure are given by the jumps above.

G Derivation of the Relativistic and Charged TOV Equations

This appendix records the derivation of the hydrostatic equations used in the main text. When an equation in this appendix reproduces an equation quoted in the main text, its tag is written with the main equation number and a prime. We use the mostly-minus convention and homogeneous coordinates $x^0 = ct$. Thus, in a local inertial frame,

$$\eta_{\mu\nu} = \text{diag}(1, -1, -1, -1), \quad u^\mu u_\mu = c^2, \quad u^\mu = \frac{dx^\mu}{d\tau}. \quad (466)$$

For a perfect fluid,

$$T^{\mu\nu} = \frac{\epsilon + P}{c^2} u^\mu u^\nu - P g^{\mu\nu}, \quad \epsilon = \rho c^2, \quad (467)$$

where ρ is the rest-mass density and ϵ is the proper energy density. Lowering one index gives

$$T^\mu_\alpha = \frac{w}{c^2} u^\mu u_\alpha - P \delta^\mu_\alpha, \quad w \equiv \epsilon + P. \quad (468)$$

The Euler equation follows from local conservation,

$$\nabla_\mu T^\mu_\alpha = 0. \quad (469)$$

Expanding the derivative,

$$0 = \frac{u_\alpha}{c^2} \nabla_\mu (w u^\mu) + \frac{w}{c^2} u^\mu \nabla_\mu u_\alpha - \nabla_\alpha P. \quad (470)$$

Define the four-acceleration

$$a_\alpha = u^\mu \nabla_\mu u_\alpha. \quad (471)$$

It is orthogonal to the four-velocity:

$$u^\alpha a_\alpha = \frac{1}{2} u^\mu \nabla_\mu (u^\alpha u_\alpha) = \frac{1}{2} u^\mu \nabla_\mu (c^2) = 0. \quad (472)$$

Projecting orthogonally to u^μ with

$$h_\alpha^\beta = \delta_\alpha^\beta - \frac{u_\alpha u^\beta}{c^2} \quad (473)$$

removes the term parallel to u_α and gives

$$\frac{\epsilon + P}{c^2} a_\alpha = \left(\delta_\alpha^\beta - \frac{u_\alpha u^\beta}{c^2} \right) \nabla_\beta P. \quad (474)$$

Raising the acceleration index gives the equivalent form

$$\frac{\epsilon + P}{c^2} a^\alpha = \left(g^{\alpha\beta} - \frac{u^\alpha u^\beta}{c^2} \right) \nabla_\beta P. \quad (475)$$

To display the signs explicitly, evaluate Eq. (475) in a local inertial frame. For a fluid element with ordinary velocity \mathbf{v} ,

$$u^\mu = \gamma(c, \mathbf{v}), \quad \gamma = (1 - v^2/c^2)^{-1/2}, \quad \partial_0 P = \frac{1}{c} \frac{\partial P}{\partial t}. \quad (476)$$

The time component is

$$\begin{aligned} \frac{w}{c^2} a^0 &= \left(g^{00} - \frac{u^0 u^0}{c^2} \right) \partial_0 P + \left(g^{0i} - \frac{u^0 u^i}{c^2} \right) \partial_i P \\ &= (1 - \gamma^2) \partial_0 P - \gamma^2 \frac{v^i}{c} \partial_i P \\ &= -\frac{\gamma^2}{c} \left(\mathbf{v} \cdot \nabla P + \frac{v^2}{c^2} \frac{\partial P}{\partial t} \right). \end{aligned} \quad (477)$$

The spatial components are

$$\begin{aligned} \frac{w}{c^2} a^i &= \left(g^{i0} - \frac{u^i u^0}{c^2} \right) \partial_0 P + \left(g^{ij} - \frac{u^i u^j}{c^2} \right) \partial_j P \\ &= -\partial_i P - \gamma^2 \frac{v^i}{c^2} \left(\frac{\partial P}{\partial t} + \mathbf{v} \cdot \nabla P \right). \end{aligned} \quad (478)$$

In the instantaneous rest frame, $\mathbf{v} = 0$, and the equations reduce to

$$\frac{\epsilon + P}{c^2} a^0 = 0, \quad \frac{\epsilon + P}{c^2} \mathbf{a} = -\nabla P. \quad (479)$$

Thus the inertial density of a relativistic fluid is

$$\frac{\epsilon + P}{c^2} = \frac{\rho c^2 + P}{c^2} = \rho + \frac{P}{c^2}. \quad (480)$$

In the Newtonian limit $P \ll \rho c^2$, this becomes the ordinary Euler equation

$$\rho \mathbf{a} = -\nabla P. \quad (481)$$

For a static Newtonian spherical configuration,

$$\mathbf{a} = -\frac{Gm(r)}{r^2} \hat{\mathbf{r}}, \quad \nabla P = \frac{dP}{dr} \hat{\mathbf{r}}, \quad (482)$$

and therefore

$$\frac{dP}{dr} = -\rho \frac{Gm(r)}{r^2}. \quad (483)$$

For the relativistic static spherical metric

$$ds^2 = e^{2\Psi(r)}(dx^0)^2 - e^{2\Lambda(r)}dr^2 - r^2d\Omega^2, \quad x^0 = ct, \quad (138')$$

the static fluid four-velocity is

$$u^\mu = (ce^{-\Psi}, 0, 0, 0). \quad (484)$$

The radial covariant acceleration is

$$a_r = u^\mu \nabla_\mu u_r = u^0 \nabla_0 u_r. \quad (485)$$

Since $u_r = 0$,

$$\nabla_0 u_r = -\Gamma^\lambda_{0r} u_\lambda = -\Gamma^0_{0r} u_0. \quad (486)$$

Moreover

$$\Gamma^0_{0r} = \frac{1}{2}g^{00}\partial_r g_{00} = \frac{d\Psi}{dr}, \quad u_0 = g_{00}u^0 = ce^\Psi. \quad (487)$$

Therefore

$$a_r = -c^2 \frac{d\Psi}{dr}. \quad (488)$$

The radial component of Eq. (474) gives

$$\frac{\epsilon + P}{c^2} \left(-c^2 \frac{d\Psi}{dr} \right) = \frac{dP}{dr}, \quad (489)$$

or

$$\frac{dP}{dr} = -(\rho c^2 + P) \frac{d\Psi}{dr}. \quad (490)$$

For an uncharged star one writes

$$ds^2 = e^{2\Psi(r)}c^2dt^2 - \left(1 - \frac{2Gm(r)}{c^2r} \right)^{-1} dr^2 - r^2d\Omega^2. \quad (491)$$

The tt Einstein equation gives

$$\frac{dm}{dr} = 4\pi r^2 \rho, \quad (492)$$

while the rr equation gives

$$\frac{d\Psi}{dr} = \frac{Gm(r)}{c^2r^2} + \frac{4\pi G}{c^4} rP. \quad (493)$$

$$1 - \frac{2Gm(r)}{c^2r}$$

Substitution in Eq. (490) yields the neutral TOV equation,

$$\frac{dP}{dr} = - \frac{G \left(\rho + \frac{P}{c^2} \right) \left(m + \frac{4\pi r^3 P}{c^2} \right)}{r^2 \left(1 - \frac{2Gm}{c^2r} \right)}. \quad (494)$$

For a charged regular interior, introduce the enclosed charge $q(r)$. The proper charge density ρ_e is measured in the fluid rest frame. Maxwell's equation implies the curved-space Gauss law

$$q(r) = 4\pi \int_0^r \rho_e(\bar{r}) e^{\Lambda(\bar{r})} \bar{r}^2 d\bar{r} \quad (139')$$

and hence

$$\frac{dq}{dr} = 4\pi r^2 \rho_e e^{\Lambda(r)}. \quad (142')$$

The factor e^Λ appears because the proper radial length of a shell is $e^\Lambda dr$. The charged mass function is defined so that the radial metric coefficient has the Reissner–Nordström form with M, Q replaced by $m(r), q(r)$:

$$e^{-2\Lambda(r)} = 1 - \frac{2Gm(r)}{c^2 r} + \frac{Gk_e q(r)^2}{c^4 r^2}. \quad (140')$$

For $q = 0$ this is the usual neutral interior parametrization. Outside the surface, where $m = M$ and $q = Q$, it becomes the exterior Reissner–Nordström factor

$$f_{\text{RN}}(r) = 1 - \frac{2GM}{c^2 r} + \frac{Gk_e Q^2}{c^4 r^2}. \quad (495)$$

The corresponding interior metric is therefore

$$ds^2 = e^{2\Psi(r)} c^2 dt^2 - \left(1 - \frac{2Gm(r)}{c^2 r} + \frac{Gk_e q(r)^2}{c^4 r^2}\right)^{-1} dr^2 - r^2 d\Omega^2. \quad (141')$$

The Einstein–Maxwell equations give

$$\frac{dm}{dr} = 4\pi r^2 \rho + \frac{k_e q}{c^2 r} \frac{dq}{dr}, \quad (143')$$

where the second term is the electrostatic contribution to the mass function, and

$$\frac{d\Psi}{dr} = \frac{\frac{Gm(r)}{c^2 r^2} + \frac{4\pi G}{c^4} r P - \frac{Gk_e q(r)^2}{c^4 r^3}}{1 - \frac{2Gm(r)}{c^2 r} + \frac{Gk_e q(r)^2}{c^4 r^2}}. \quad (144')$$

Hydrostatic equilibrium includes the Lorentz force density:

$$\frac{dP}{dr} = -(\rho c^2 + P) \frac{d\Psi}{dr} + \rho_e E e^\Lambda. \quad (145')$$

Using $E = k_e q/r^2$ and Eq. (142),

$$\rho_e E e^\Lambda = \frac{k_e q(r)}{4\pi r^4} \frac{dq}{dr}. \quad (496)$$

Thus

$$\frac{dP}{dr} = -(\rho c^2 + P) \frac{d\Psi}{dr} + \frac{k_e q(r)}{4\pi r^4} \frac{dq}{dr}. \quad (146')$$

Substituting Eq. (144') gives the charged TOV equation,

$$\frac{dP}{dr} = -(\rho c^2 + P) \frac{\frac{Gm(r)}{c^2 r^2} + \frac{4\pi G}{c^4} r P - \frac{Gk_e q(r)^2}{c^4 r^3}}{1 - \frac{2Gm(r)}{c^2 r} + \frac{Gk_e q(r)^2}{c^4 r^2}} + \frac{k_e q(r)}{4\pi r^4} \frac{dq}{dr}. \quad (147')$$

Together with an equation of state $P = P(\rho)$, a charge-density prescription, and the regular central conditions $m(0) = q(0) = 0$, this is the interior system used for regular charged astron models.

H Hamilton–Jacobi Separation in the Kerr–Newman Geometry

This appendix gives the Carter separation used in the rotating discussion. We work in geometrized units $G = c = k_e = 1$ and use the mostly-minus convention. The Kerr–Newman line element in Boyer–Lindquist coordinates is Eq. (159), namely

$$ds^2 = \frac{\Delta}{\Sigma} (dt - a \sin^2 \theta d\phi)^2 - \frac{\Sigma}{\Delta} dr^2 - \Sigma d\theta^2 - \frac{\sin^2 \theta}{\Sigma} [(r^2 + a^2)d\phi - a dt]^2, \quad (159')$$

with

$$\Sigma = r^2 + a^2 \cos^2 \theta, \quad \Delta = r^2 - 2Mr + a^2 + Q^2. \quad (160')$$

The electromagnetic potential is

$$A_\mu dx^\mu = -\frac{Qr}{\Sigma} (dt - a \sin^2 \theta d\phi), \quad (162')$$

so that

$$A_t = -\frac{Qr}{\Sigma}, \quad A_\phi = \frac{aQr \sin^2 \theta}{\Sigma}. \quad (497)$$

For a particle of rest mass μ and charge e , the gauge-covariant kinetic momentum is

$$\Pi_\mu = \partial_\mu S - eA_\mu. \quad (498)$$

The Hamilton–Jacobi equation is

$$g^{\mu\nu} \Pi_\mu \Pi_\nu = \mu^2. \quad (499)$$

Stationarity and axisymmetry imply two Killing constants, the energy E and azimuthal angular momentum L . One therefore writes the action as

$$S = -Et + L\phi + S_r(r) + S_\theta(\theta). \quad (500)$$

Thus

$$\partial_t S = -E, \quad \partial_\phi S = L, \quad \partial_r S = S'_r(r), \quad \partial_\theta S = S'_\theta(\theta). \quad (501)$$

The inverse metric may be written in the useful form

$$\begin{aligned} g^{tt} &= \frac{(r^2 + a^2)^2 - a^2 \Delta \sin^2 \theta}{\Sigma \Delta}, & g^{t\phi} &= \frac{a(r^2 + a^2 - \Delta)}{\Sigma \Delta}, \\ g^{\phi\phi} &= -\frac{\Delta - a^2 \sin^2 \theta}{\Sigma \Delta \sin^2 \theta}, & g^{rr} &= -\frac{\Delta}{\Sigma}, & g^{\theta\theta} &= -\frac{1}{\Sigma}. \end{aligned} \quad (502)$$

Substituting Eq. (500) into Eq. (499) and multiplying by Σ , the t, ϕ part combines into two squares:

$$\begin{aligned} \Sigma g^{\mu\nu} \Pi_\mu \Pi_\nu &= \frac{1}{\Delta} [(r^2 + a^2)E - aL - eQr]^2 \\ &\quad - \frac{1}{\sin^2 \theta} [L - aE \sin^2 \theta]^2 - \Delta (S'_r)^2 - (S'_\theta)^2. \end{aligned} \quad (503)$$

The nontrivial point is the cancellation of the apparent mixed r, θ dependence from A_t and A_ϕ . Since

$$\Pi_t = -E + \frac{eQr}{\Sigma}, \quad \Pi_\phi = L - \frac{aeQr \sin^2 \theta}{\Sigma}, \quad (504)$$

the same linear combination that appears in the metric squares gives

$$(r^2 + a^2)(-\Pi_t) - a\Pi_\phi = (r^2 + a^2)E - aL - eQr. \quad (505)$$

The charge coupling therefore enters only the radial square. This is why the charged Kerr–Newman Hamilton–Jacobi equation remains separable.

Using $\Sigma = r^2 + a^2 \cos^2 \theta$, Eq. (499) becomes

$$\begin{aligned} &\frac{[(r^2 + a^2)E - aL - eQr]^2}{\Delta} - \Delta (S'_r)^2 - \mu^2 r^2 \\ &= (S'_\theta)^2 + \frac{(L - aE \sin^2 \theta)^2}{\sin^2 \theta} + \mu^2 a^2 \cos^2 \theta. \end{aligned} \quad (506)$$

The left-hand side depends only on r , and the right-hand side depends only on θ . Both sides must therefore equal the same separation constant. It is conventional to define the Carter constant K by writing

$$K = (S'_\theta)^2 + \frac{(L - aE \sin^2 \theta)^2}{\sin^2 \theta} + \mu^2 a^2 \cos^2 \theta. \quad (507)$$

A closely related constant, used in the main text, is

$$\mathcal{K} = K - (L - aE)^2. \quad (508)$$

With this convention the angular potential becomes

$$\Theta(\theta) = \mathcal{K} - \cos^2 \theta \left[a^2(\mu^2 - E^2) + \frac{L^2}{\sin^2 \theta} \right]. \quad (509)$$

The radial potential is

$$\mathcal{R}(r) = [(r^2 + a^2)E - aL - eQr]^2 - \Delta [\mu^2 r^2 + (L - aE)^2 + \mathcal{K}]. \quad (510)$$

Finally, Hamilton's equations identify the first-order equations of motion. Since

$$p^r = \frac{dr}{d\lambda} = g^{rr} \Pi_r = -\frac{\Delta}{\Sigma} S'_r, \quad p^\theta = \frac{d\theta}{d\lambda} = g^{\theta\theta} \Pi_\theta = -\frac{1}{\Sigma} S'_\theta, \quad (511)$$

squaring gives

$$\Sigma^2 \dot{r}^2 = \mathcal{R}(r), \quad \Sigma^2 \dot{\theta}^2 = \Theta(\theta), \quad (174')$$

where the dot denotes differentiation with respect to the affine parameter λ , which may be chosen as proper time divided by μ for a massive particle.

For the notation used in the main text, set

$$\varepsilon_i = \frac{E_i}{m_i}, \quad \ell_i = \frac{L_i}{m_i}, \quad \alpha_i = \frac{q_i}{m_i}, \quad \mathcal{K}_i = \frac{\mathcal{K}}{m_i^2}, \quad (512)$$

and choose $\mu = m_i$. Dividing Eqs. (510) and (509) by m_i^2 gives exactly the potentials quoted in the rotating section:

$$\mathcal{R}_i(r) = [(r^2 + a^2)\varepsilon_i - a\ell_i - \alpha_i Qr]^2 - \Delta [r^2 + (\ell_i - a\varepsilon_i)^2 + \mathcal{K}_i], \quad (175')$$

and

$$\Theta_i(\theta) = \mathcal{K}_i - \cos^2 \theta \left[a^2(1 - \varepsilon_i^2) + \frac{\ell_i^2}{\sin^2 \theta} \right]. \quad (176')$$

In the equatorial plane, $\theta = \pi/2$, the angular equation is consistently satisfied by $\mathcal{K}_i = 0$. The capture boundary used in the main text is the usual unstable spherical-orbit condition

$$\mathcal{R}_i(r_c) = 0, \quad \frac{d\mathcal{R}_i}{dr}(r_c) = 0, \quad \frac{d^2\mathcal{R}_i}{dr^2}(r_c) < 0. \quad (177')$$

These equations determine the critical impact parameters separating scattering from capture. The dependence on ℓ_i , \mathcal{K}_i , a , and $\alpha_i Q$ is the origin of the anisotropic capture cross section in the rotating charged case.

References

- [1] P. H. Frampton, “Electromagnetic accelerating universe,” *Phys. Lett. B* **835** (2022) 137480, arXiv:2210.10632.
- [2] P. H. Frampton, “A model of dark matter and energy,” *Mod. Phys. Lett. A* **38** (2023) 2350032, arXiv:2301.10719.
- [3] C. Bambi, “Astrophysical Black Holes: A Review,” arXiv:1906.03871 [astro-ph.HE].
- [4] M. Zajacek and A. Tursunov, “Electric charge of black holes: Is it really always negligible?,” arXiv:1904.04654 [astro-ph.GA].
- [5] M. Zajacek, A. Tursunov, A. Eckart and S. Britzen, “On the charge of the Galactic centre black hole,” *Mon. Not. Roy. Astron. Soc.* **480** (2018) 4408–4423.
- [6] J. D. Bekenstein, “Hydrostatic equilibrium and gravitational collapse of relativistic charged fluid balls,” *Phys. Rev. D* **4** (1971) 2185–2190, doi:10.1103/PhysRevD.4.2185.
- [7] S. Ray, A. L. Espindola, M. Malheiro, J. P. S. Lemos and V. T. Zanchin, “Electrically charged compact stars and formation of charged black holes,” *Phys. Rev. D* **68** (2003) 084004, doi:10.1103/PhysRevD.68.084004.
- [8] G. Darmois, *Les équations de la gravitation einsteinienne*, Mémorial des Sciences Mathématiques, Fascicule **25**, Gauthier–Villars, Paris, 1927, https://www.numdam.org/item/MSM_1927__25__1_0/.
- [9] M. Mars and J. M. M. Senovilla, “Geometry of general hypersurfaces in spacetime: Junction conditions,” *Class. Quantum Grav.* **10** (1993) 1865–1897, doi:10.1088/0264-9381/10/9/026.
- [10] E. Poisson, *A Relativist’s Toolkit: The Mathematics of Black-Hole Mechanics*, Cambridge University Press, Cambridge, 2004, doi:10.1017/CBO9780511606601.
- [11] W. Israel, “Singular hypersurfaces and thin shells in general relativity,” *Nuovo Cim. B* **44** (1966) 1–14, doi:10.1007/BF02710419; erratum *Nuovo Cim. B* **48** (1967) 463, doi:10.1007/BF02712210.
- [12] Z. Bogorad, P. W. Graham and H. Ramani, “Constraints on Long-Ranged Interactions Between Dark Matter and the Standard Model,” arXiv:2410.07324 [hep-ph].
- [13] M. V. Medvedev and A. Loeb, “Plasma Constraints on the Cosmological Abundance of Magnetic Monopoles and the Origin of Cosmic Magnetic Fields,” arXiv:1704.05094 [astro-ph.CO].
- [14] E. Alonso-Monsalve and D. I. Kaiser, “Debye screening of non-Abelian plasmas in curved spacetimes,” *Phys. Rev. D* **108** (2023) 125010.
- [15] R. Bibi, T. Clifton and J. Durk, “Cosmological solutions with charged black holes,” *Gen. Relativ. Gravit.* **49** (2017) 98.
- [16] T. Buchert, “On Average Properties of Inhomogeneous Fluids in General Relativity: Dust Cosmologies,” *Gen. Relativ. Gravit.* **32** (2000) 105–125, arXiv:gr-qc/9906015.
- [17] C. Clarkson, G. F. R. Ellis, J. Larena and O. Umeh, “Does the Growth of Structure Affect Our Dynamical Models of the Universe? The Averaging, Backreaction and Fitting Problems in Cosmology,” *Rep. Prog. Phys.* **74** (2011) 112901.
- [18] S. R. Green and R. M. Wald, “A new framework for analyzing the effects of small scale inhomogeneities in cosmology,” *Phys. Rev. D* **83** (2011) 084020, arXiv:1011.4920 [gr-qc].

- [19] S. Navas *et al.* (Particle Data Group), “Review of Particle Physics,” *Prog. Theor. Exp. Phys.* **2024** (2024) 083C01.
- [20] S. Weinberg, “Cosmology,” Oxford University Press, Oxford, 2008.
- [21] S. Dodelson and F. Schmidt, “Modern Cosmology,” 2nd ed., Academic Press, London, 2020.
- [22] F. Becerra, T. H. Greif, V. Bromm, M. A. Klessen and R. S. Somerville, “The formation of supermassive black holes in rapidly rotating discs,” *Mon. Not. Roy. Astron. Soc.* **476** (2018) 3523–3544.
- [23] S. Chon, K. Omukai and V. Bromm, “The formation of supermassive stars by rapid mass accretion in the early Universe,” *Mon. Not. Roy. Astron. Soc.* **475** (2018) 4104–4121.
- [24] S. Navas *et al.* (Particle Data Group), “Review of Particle Physics,” *Phys. Rev. D* **110** (2024) 030001.
- [25] Particle Data Group, “Astrophysical Constants and Parameters,” 2025 online update, <https://pdg.lbl.gov/2025/reviews/rpp2025-rev-astrophysical-constants.pdf>.
- [26] Particle Data Group, “Astrophysical Constants and Parameters,” 2024 review update, <https://pdg.lbl.gov/2024/download/db2024.pdf>.
- [27] M. Rauch, “The Lyman Alpha Forest in the Spectra of QSOs,” *Ann. Rev. Astron. Astrophys.* **36** (1998) 267–316, doi:10.1146/annurev.astro.36.1.267, arXiv:astro-ph/9806286.
- [28] B. T. Draine, *Physics of the Interstellar and Intergalactic Medium*, Princeton University Press, Princeton, 2011.
- [29] A. A. Meiksin, “The Physics of the Intergalactic Medium,” *Rev. Mod. Phys.* **81** (2009) 1405–1469, doi:10.1103/RevModPhys.81.1405.
- [30] M. McQuinn, “The Evolution of the Intergalactic Medium,” *Ann. Rev. Astron. Astrophys.* **54** (2016) 313–362, doi:10.1146/annurev-astro-082214-122355.
- [31] R. Davé, R. Cen, J. P. Ostriker, G. L. Bryan, L. Hernquist, N. Katz, D. H. Weinberg, M. L. Norman and B. O’Shea, “Baryons in the Warm-Hot Intergalactic Medium,” *Astrophys. J.* **552** (2001) 473–483, doi:10.1086/320548.
- [32] J. Tumlinson, M. S. Peeples and J. K. Werk, “The Circumgalactic Medium,” *Ann. Rev. Astron. Astrophys.* **55** (2017) 389–432, doi:10.1146/annurev-astro-091916-055240.
- [33] Center for Astrophysics — Harvard & Smithsonian, “Intergalactic Medium,” <https://pweb.cfa.harvard.edu/research/topic/intergalactic-medium>.
- [34] COSMOS Encyclopedia, “Intergalactic Medium,” <https://astronomy.swin.edu.au/cosmos/I/Intergalactic+Medium>.
- [35] I. J. Araya, N. D. Padilla, M. E. Rubio, J. Sureda, J. Magaña and L. Osorio, “Dark matter from primordial black holes would hold charge,” *JCAP* **02** (2023) 030, arXiv:2207.05829 [astro-ph.CO].
- [36] K. Inayoshi, E. Visbal and K. Kashiyama, “Direct collapse black hole formation via high-velocity collisions of protogalaxies,” *Mon. Not. Roy. Astron. Soc.* **453** (2015) 1692–1700.
- [37] S. Chon, T. Hosokawa and N. Yoshida, “Radiation hydrodynamics simulations of the formation of direct-collapse supermassive stellar systems,” *Mon. Not. Roy. Astron. Soc.* **475** (2018) 4104–4121.
- [38] Y. Luo, K. Ardaneh, I. Shlosman, K. Nagamine, J. H. Wise and M. C. Begelman, “Direct Collapse to Supermassive Black Hole Seeds with Radiative Transfer: Isolated Halos,” *Mon. Not. Roy. Astron. Soc.* **476** (2018) 3523–3539.

- [39] I. Labbé, P. van Dokkum, E. Nelson *et al.*, “A population of red candidate massive galaxies ~ 600 Myr after the Big Bang,” *Nature* **616** (2023) 266–269.
- [40] B. J. Carr and S. W. Hawking, “Black holes in the early Universe,” *Mon. Not. Roy. Astron. Soc.* **168** (1974) 399–415.
- [41] N. Sabti, J. B. Muñoz and M. Kamionkowski, “Insights from HST into Ultramassive Galaxies and Early-Universe Cosmology,” *Phys. Rev. Lett.* **132** (2024) 061002, arXiv:2305.07049 [astro-ph.CO].
- [42] A. Adamo, H. Atek, M. B. Bagley *et al.*, “The first billion years according to JWST,” *Nat. Astron.* **9** (2025) 1134–1147, doi:10.1038/s41550-025-02624-5.
- [43] S. Carniani, K. Hainline, F. D’Eugenio *et al.*, “Spectroscopic confirmation of two luminous galaxies at a redshift of 14,” *Nature* **633** (2024) 318–322, doi:10.1038/s41586-024-07860-9.
- [44] M. Xiao, P. A. Oesch, D. Elbaz *et al.*, “Accelerated formation of ultra-massive galaxies in the first billion years,” *Nature* **635** (2024) 311–315, doi:10.1038/s41586-024-08094-5.
- [45] A. Leauthaud and A. G. Riess, “Looking beyond lambda,” *Nat. Astron.* **9** (2025) 1123–1128.
- [46] V. Pierrard and M. Lazar, “Kappa distributions: theory and applications in space plasmas,” *Sol. Phys.* **267** (2010) 153–174, arXiv:1003.3532 [physics.space-ph].
- [47] G. Livadiotis and D. J. McComas, “Understanding Kappa Distributions: A Toolbox for Space Science and Astrophysics,” *Space Sci. Rev.* **175** (2013) 183–214.
- [48] H. J. Fahr and M. Heyl, “Debye screening under non-equilibrium plasma conditions,” *Astron. Astrophys.* **589** (2016) A85.
- [49] P. O. Mazur and E. Mottola, “Gravitational vacuum condensate stars,” *Proc. Natl. Acad. Sci. USA* **101** (2004) 9545–9550, doi:10.1073/pnas.0402717101, arXiv:gr-qc/0407075.
- [50] A. I. Janis, E. T. Newman and J. Winicour, “Reality of the Schwarzschild Singularity,” *Phys. Rev. Lett.* **20** (1968) 878–880.
- [51] M. Wyman, “Static Spherically Symmetric Scalar Fields in General Relativity,” *Phys. Rev. D* **24** (1981) 839–841.
- [52] R. P. Kerr, “Gravitational Field of a Spinning Mass as an Example of Algebraically Special Metrics,” *Phys. Rev. Lett.* **11** (1963) 237–238.
- [53] E. T. Newman, E. Couch, K. Chinnapared, A. Exton, A. Prakash and R. Torrence, “Metric of a Rotating, Charged Mass,” *J. Math. Phys.* **6** (1965) 918–919.
- [54] B. Carter, “Global structure of the Kerr family of gravitational fields,” *Phys. Rev.* **174** (1968) 1559–1571, doi:10.1103/PhysRev.174.1559.
- [55] C. Corianò, A. Costantini, M. Dell’Atti and L. Delle Rose, “Neutrino and Photon Lensing by Black Holes: Radiative Lens Equations and Post-Newtonian Contributions,” *JHEP* **07** (2015) 160, doi:10.1007/JHEP07(2015)160, arXiv:1504.01322 [hep-ph].
- [56] C. Corianò, L. Delle Rose, M. M. Maglio and M. Serino, “Electroweak Corrections to Photon Scattering, Polarization and Lensing in a Gravitational Background and the Near Horizon Limit,” *JHEP* **01** (2015) 091, doi:10.1007/JHEP01(2015)091, arXiv:1411.2804 [hep-ph].
- [57] D. M. Zipoy, “Topology of Some Spheroidal Metrics,” *J. Math. Phys.* **7** (1966) 1137–1143.
- [58] B. H. Voorhees, “Static Axially Symmetric Gravitational Fields,” *Phys. Rev. D* **2** (1970) 2119–2122.

- [59] A. Tomimatsu and H. Sato, “New Exact Solution for the Gravitational Field of a Spinning Mass,” *Phys. Rev. Lett.* **29** (1972) 1344–1345.
- [60] A. Tomimatsu and H. Sato, “New Series of Exact Solutions for Gravitational Fields of Spinning Masses,” *Prog. Theor. Phys.* **50** (1973) 95–110.